Investigating Novel Therapeutic Strategies in Liver Cancer

Dissertation

der Mathematisch-Naturwissenschaftlichen Fakultät

der Eberhard Karls Universität Tübingen

zur Erlangung des Grades eines

Doktors der Naturwissenschaften

(Dr. rer. nat.)

vorgelegt von

Louise Gaëlle Kaldjob-Heinrich

aus Duala/Kamerun

Tübingen

2022

Gedruckt mit Genehmigung der Mathematisch-Naturwissenschaftlichen Fakultät der Eberhard Karls Universität Tübingen.

Tag der mündlichen Qualifikation:	26.04.2023
Dekan:	Prof. Dr. Thilo Stehle
1. Berichterstatter/-in:	Prof. Dr. Alfred Nordheim
2. Berichterstatter/-in:	Prof. Dr. Michael Bitzer

HANNAH

Table of Contents

Collaborators

My gratitude to all collaborators who worked and helped to fulfill this project.

Department	Institute/Company	Experiment/Contribution	People
Quantitative Biology Center (QBIC)	University of Tuebingen	Bioinformatic support RNA sequencing and Data analysis	Dr. Nahnsen Dr. Czemmel Dr. Peltzer Steffen Lemke
Medical Genetics and Applied Genomics	University Hospital Tuebingen	RNAseq measurement	Prof. Dr. Rieß Dr. Casadei Sven Poths
Pathology	University Hospital Tuebingen	TMA staining and analysis	Dr. Bösmüller Dr. Menendez
Clinical Bioinformatics, Internal Medicine I	University Hospital Tuebingen	GSEA analysis and enrichment plots	Prof. Dr. Claassen Dr. Babaei
Biomedicine	University of Basel	Organoid handling	Prof. Dr. Heim Dr. Nuciforo Dr. Wieland Lauriane Marie-Anne
Internal Medicine I	University Hospital Tuebingen	TMA generation	Dr. Veit Scheble
Internal Medicine VIII	University of Tuebingen	Cell Lines	Dr. Dauch

My research stay in Basel in the group of Prof. Dr. Heim was from December 2019 – April 2020.

Declaration / Contributions

The following study was performed under the supervision of Prof. Dr. Michael Bitzer and Prof. Dr. Alfred Nordheim from December 2017 to January 2022 at the University Hospital of Tübingen. Following data from collaborators are included in this thesis.

1) RNAseq analysis was performed by Dr. Casadei and Sven Poth at the Department of Medical Genetics and Applied Genomics, University Hospital Tuebingen.
2) Dr. Stefan Czemmel and Steffen Lemke, Quantitative Biology Center (QBIC), University of Tuebingen, assisted with downstream bioinformatic analysis of the RNAseq data. Steffen Lemke generated figure 7A.
3) HCC TMAs were generated by Dr. Veit Scheble from the University Hospital Tübingen and CCA TMAs were generated by Dr. Hans Bösmüller from the Department of Pathology, University Hospital Tuebingen.
4) Dr. Hans Bösmüller stained all HCC and CCA TMAs, and Dr. Menendez took pictures for figure 5 at the Department of Pathology.
5) Dr. Hans Bösmüller performed the semi-quantitative analysis of the TMA stains. I did the subsequent data mining (Fig. 6).
6) The transcriptome dataset of the HCC biopsy samples were generated by Prof. Dr. Markus Heim and Dr. Sandro Nuciforo at the Department of Biomedicine, University of Basel. Subsequent data analysis was performed by myself (Fig. 7B).
7) Gene Set Enrichment Analysis (GSEA) and enrichment plots were generated by Dr. Sepideh Babaei at the Department of clinical bioinformatics of the Internal Medicine I, University Hospital Tuebingen. Subsequent Data miming was performed by myself (Table 8 Fig. 16).

All remaining work presented in this thesis was performed by myself.

Abstract

Liver Cancer is the sixth leading cause of cancer death worldwide. Over 80 % of all diagnosed liver cancer types are Hepatocellular carcinoma (HCC) or Cholangiocarcinoma (CCA). Both tumors are often diagnosed in an advanced disease stage with a poor prognosis. The increasing prevalence of HCC and CCA, including the challenges surrounding their diagnosis, management, and limited treatment options, have increased the urgency first to find additional molecular targets, and secondly, to develop novel therapeutic strategies.

This study explored two novel therapeutic concepts for the systemic treatment of HCC and CCA. For the first concept, we investigated the stimulation of adenosine receptor 3 (ADORA3). We could show that an antiproliferative effect of tumor cells after stimulation of ADORA3 was directly dependent on the presence of the receptor. Preliminary published data stated an overexpression of ADORA3 in HCC. In contrast to these data, we found a heterogenous expression level, comparable to non-malignant tissue samples, which might be important in the decision, which patients are suited for treatment strategies including ADORA3 activation. Furthermore, we could show that ADORA3 agonist Namodenoson induces the alteration of epigenetic modifying factors, including a broad downregulation of different histone deacetylases (HDACs).

Supporting these observations, we further show, that the co-treatment using ADORA3 agonists and different histone deacetylase inhibitors (HDACi) led to a synergistic inhibition of HCC or CCA cell proliferation. Additionally, this effect could also be shown in ex vivo cultured patient-derived organoids. These results suggest that combining an ADORA3 agonist with an HDACi may be a promising new treatment option for a selected group of patients.

In the second set of experiments, we targeted direct AKT and HDAC inhibition as a novel therapeutic strategy and investigated the effect of the cotreatment against three significant hallmarks of HCC and CCA: unrestrained proliferation, invasion and metastasis, and cell death resistance. In cell lines from both tumor entities, we observed that the combination with different HDACi, compared to the mono-treatments, showed an increased inhibition of cell proliferation, a reduction in the

ability of the cells to migrate and an induction of apoptosis. We also observed that our combination treatment simultaneously inhibited the AKT dependent PI3K/AKT/mTOR pathway and as a new observation the AKT independent PI3K/SGK1/mTOR pathway. The combinations were observed to be synergistic in defined settings.

The present study has identified two promising new combination strategies for the treatment of HCC and CCA and provided preliminary evidence for carrying out further investigations in preclinical and clinical studies.

Zusammenfassung

Über 80 % aller an primärem Leberkrebs erkrankten Menschen haben ein hepatozelluläres (HCC) oder ein cholangiozelläres (CCA) Karzinom. Die weltweit steigende Prävalenz des HCCs und des CCAs, die Herausforderungen rund um ihre Diagnose sowie die eingeschränkten Therapiemöglichkeiten, haben die Dringlichkeit erhöht, neue molekulare Angriffspunkte zu erforschen und neue Therapieansätze zu entwickeln.

Die vorliegende Dissertation untersucht zwei neue systemische Therapiekonzepte zur Behandlung des HCCs und CCAs.

Im ersten Konzept wird die Adenosin Rezeptor 3 (ADORA3) Aktivierung im HCC und CCA näher untersucht. Dazu wurde im ersten Schritt erarbeitet, dass die tumorhemmende Wirkung der ADORA3 Aktivierung rezeptorabhängig ist. Veröffentlichte Daten weisen auf eine Überexpression von ADORA3 im HCC hin. Im Gegensatz dazu zeigt die vorliegende Arbeit eine heterogene Expression des Rezeptors in tumoralem Gewebe verglichen mit nicht-malignen Gewebeproben. Diese Beobachtung könnte in Zukunft von entscheidender Bedeutung sein, bei der Beantwortung der Frage, welche Patienten für die vorgeschlagene Behandlung geeignet sind. Des Weiteren wird dargestellt, dass der ADORA3-Agonist Namodenoson zu einer Veränderung epigenetische Modulatoren führt und insbesondere eine breite Herunterregulierung verschiedener Histon-Deacetylasen (HDACs) induziert. Basierend auf diesen Beobachtungen wird weiter aufgezeigt, dass die Kombination eines ADORA3-agonisten mit verschiedene Histon-Deacetylase-Inhibitoren (HDACis) zu einer synergistischen Hemmung der untersuchten HCC und CCA-Zelllinien führt. Die erhöhte Anti-Tumor-Wirkung, der ADORA3-Agonist/HDACi Kombination, wird abschließend in von HCC-Patienten stammenden Organoiden untersucht. Zusammenfassend deuten die Ergebnisse darauf hin, dass die Kombination eines ADORA3-Agonisten mit einem HDACi eine erfolgsversprechende neue Behandlungsoption für eine ausgewählte Patientengruppe mit HCC oder CCA sein könnte.

Im zweiten Therapiekonzept wird die kombinierte Hemmung der Proteinkinase B (AKT) und die Hemmung der HDACs untersucht. Hierbei wird der Fokus auf die

Veränderungen in drei entscheidende Tumormerkmale im HCC und CCA gelegt: ungehemmte Proliferation, Migration/Invasion und Metastasierung sowie die Resistenz gegen Zelltod. In beiden Tumortypen wird veranschaulicht, dass die Kombination verglichen zur Monotherapie, eine stärkere Hemmung der Zellproliferation, eine Verringerung der Migrationsfähigkeit der Zellen und eine Induktion von Apoptose bewirkt. Darüber hinaus wird verdeutlicht, dass die Kombinationen synergistisch sind. Im Gegensatz zur Monotherapie wird veranschaulicht, dass die Kombinationen gleichzeitig sowohl den AKT-abhängigen PI3K/AKT/mTOR Signalweg als auch den AKT-unabhängigen PI3K/SGK1/mTOR Signalweg hemmen. Abschließend wird mit aus Patienten stammenden Organoiden die tumorhemmende Wirkung der AKTi/HDACi Kombination untersucht.

Zusammenfassend erschließt die vorliegende Dissertation zwei potenzielle Kombinationstherapien gegen HCC und CCA und liefert erste vielversprechende Ergebnisse und eine Evidenz für weitere präklinische und klinische Studien.

1. Introduction

1.1. Primary Liver Cancer

Primary liver cancer (PLC) remains one of the most frequently diagnosed malignant tumors globally. Slung and colleagues reported that PLC is the sixth leading cause of cancer mortality worldwide, with over 905.000 new cases and 830.000 deaths in 2020 (1, 2). Looking at the global burden of liver cancer in the last three decades, Lin and colleagues reported an increasing trend with nearly twice the number of incident cases and death cases (from 452.688; 1990 to over

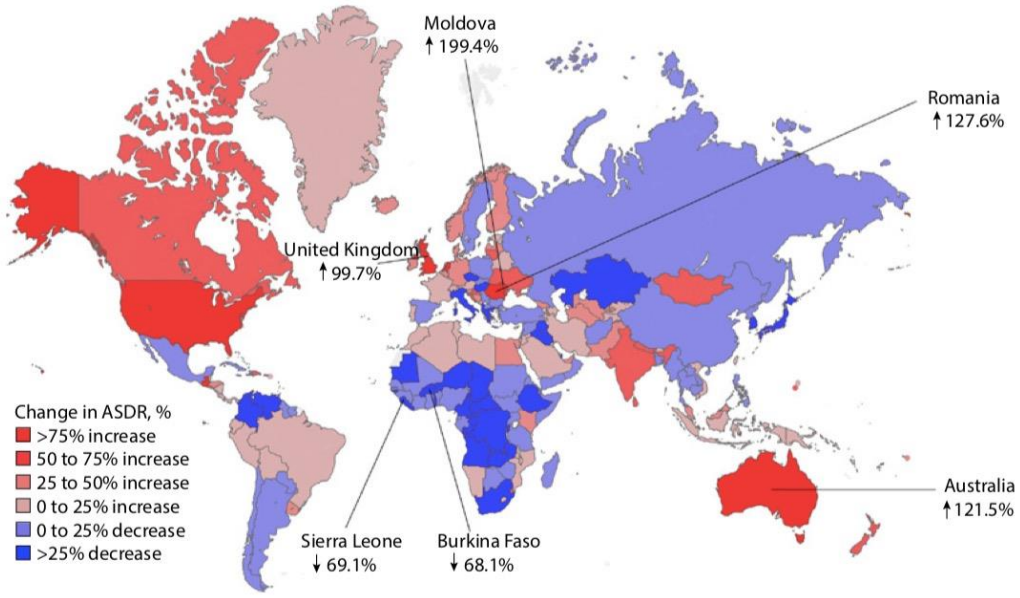

Figure 1. Changes in PLC incidence and in death rate (ASDR: Age standardize death rate) from 1990 to 2017 (Figure adopted from Lin et al. 2020).

Figure 2. Changes in PLC incidence and in death rate (ASDR: Age standardize death rate) from 1990 to 2017 (Figure adopted from Lin et al. 2020).

800.000; 2017) (Fig. 1) (3). Along with other studies (1, 4) projecting the development of PLC until 2030, Valery et al. recently predicted increasing rates of PLC predominantly among men, in the western countries (5). In this pursuit, there is a continuous need to investigate the causes and treatment options of the disease. PLC summarizes a heterogeneous group of malignant tumors, each based on the type of cells that become cancerous. The most common (75%) primary malignant liver tumor is hepatocellular carcinoma (HCC). HCC arises

from hepatocytes in the liver or progenitor cells, albeit the latter to a lesser extent (6, 7). The second most diagnosed form of PLC is cholangiocarcinoma (CCA, 12%). CCA arises from cholangiocytes, which line the bile duct (8). Other Forms of PLC, including hepatic hemangiosarcoma and mixed HCC-CCA, account for less than 1 percent of all cases (6, 9). Two other rather sporadic kinds of PLC are fibrolamellar HCC and Hepatoblastoma. The last one is the most common primary liver cancer in children, accounting for only about 1% of pediatric cancer types (10).

1.2. Hepatocellular Carcinoma

HCC is the most common form of primary liver cancer. Summarizing publications around HCC from the last decade, there has been remarkable progress in understanding its epidemiology, risk factors, and molecular profiles. Further, there is an ongoing effort to translate research outcomes and implicate programs around HCC prevention, detection, diagnosis, surveillance, and treatment.

1.2.1. Epidemiology and Etiology of HCC

HCC incidences remain high with nearly 800.000 new cases per year worldwide (11). Recent predictions show that more than 1 million patients will die per year from liver cancer by 2030 (2, 5, 12). HCC is progressively prevalent in the older population (> 60 years) after longstanding chronic liver disease, with men being disproportionally more affected than women (2). Regional and ethnical variations of HCC mortality are dependent on the level of exposure to environmental and infectious risk factors, the accessibility to healthcare resources, the ability to detect HCC at an early stage and provide the appropriate curative treatment. The leading causes of HCC are hepatitis B or C (HBV, HCV) viral infections, coinfection with hepatitis D (HDV), alcohol abuse, smoking, nonalcoholic fatty liver disease in patients with metabolic syndrome, and diabetes (11). Other (co)factors such as aflatoxin B1, contaminated water with hepatotoxic microcystins, and betel nut contribute to HCC development and increase the disease's incidence if other common risk factors are present (13, 14). Patients with chronic hepatitis of any cause or cryptogenic cirrhosis have an increased risk of developing HCC.

1.2.2. HCC Molecular Pathogenesis

HCC is a quite heterogeneous cancer with a solid relationship between molecular and pathological features. Hepatocarcinogenesis is a complex multistep biological process that can either arise in the presence of underlying chronic liver disease and cirrhosis or as a malignant transformation of hepatic adenomas. In

cirrhosis, up to 32% of dysplastic nodules transform to HCC over time. Hepatic adenomas can be grouped into HNF1A, CTNNB1, JAK/STAT, Sonic Hedgehog mutation-driven, and unclassified adenomas (15). Whole exome and genome sequencing have highlighted some of the most important signaling pathways frequently altered in HCC, such as telomere maintenance, Wnt/ß-catenin, P53/cell cycle regulation, MAP kinase and AKT/mTOR regulated pathways as well as pathways modulated by epigenetic modifiers (15).

1.2.3. Diagnosis and management of HCC

HCC mainly progresses silently, especially in cases where there is still sufficient liver function. Impaired liver function, which is a sign of an underlining advanced-stage disease, accumulates various symptoms such as upper right abdominal pain, hepatomegaly, or jaundice (16). Imaging studies (ultrasonography, computed tomography scanning, and magnetic resonance imaging) and laboratory tests for immunohistochemical markers (alpha-fetoprotein (AFP)-level, HepPar1, albumin, fibrinogen, a1-antitrypsin, glypican-3) are tools that are applied for HCC diagnosis. Based on the HCC stage, the liver function, the patient's performance status, physical abilities, and environmental conditions, guidelines recommend different treatment options. A diagnosis at an early stage allows curative treatments such as resection, liver transplantation, or local ablation, which lead to an extended survival (>6 years) and a recurrence rate of about 70% (17). Patients diagnosed with an intermediate stage HCC and Child-Pugh class A graded liver function are candidates to receive transarterial chemoembolization (TACE), which can prolong survival for about 2- 3 years (18). Advance stage HCC or patients who progress after TACE receive systemic therapies (molecular targeted therapies, immune checkpoint inhibitor or a combination of both) with an overall survival of more than two years.

1.2.4. Treatment of HCC

Sorafenib, an angiogenic receptor tyrosine kinase (RTK) inhibitor, was the standard first-line treatment of choice for over one decade. A significant overall survival benefit could be shown compared to a placebo group (10.7 months

versus 7.9 months) (19). Most first-line therapeutic options tested in numerous clinical trials remained inferior to sorafenib for a long time. Lenvatinib however, a small molecule type V tyrosine kinase inhibitor was found to be non-inferior to sorafenib with a median overall survival of 13.6 months versus 12.3 months for sorafenib (11). Beside targeting tyrosine kinases other molecular target were poor in the context of HCC treatment. This lack of diverse molecular targeted treatment options summarizes a long-lasting gap in the management of advanced HCC (20). Only recently, the introduction of immune checkpoint inhibitors has revolutionized the management of HCC. Immune tolerance in HCC generally occurs due to myeloid-derived suppressor cells (MDSCs), alterations of immune checkpoint molecules such as cytotoxic T-lymphocyte antigen 4 (CTLA-4), programmed cell death protein 1 (PD-1) and an enrichment of T-regulatory cells (Tregs). Agents against CTLA-4 (tremelimumab), PD-1 (nivolumab, pembrolizumab) or its ligand PD-L1 (atezolizumab, durvalumab) have been investigated in HCC (21). The combination of atezolizumab, an anti PD-L1 antibody, and bevacizumab, an anti-VEFG antibody in a study, improved overall survival from 13.4 to 19.2 months compared to sorafenib (22) and was approved as a new first-line therapy by the European Commission in November 2020. In later stages, after progression during the treatment with sorafenib, the multi-kinase inhibitors regorafenib, cabozantinib, as well was the anti-VEGFR2-antibody ramucirumab (the latter only for patients with >400ng/ml AFP) are approved drugs (11, 18). Although all available approved tyrosine kinases, antiangiogenic molecules and immune checkpoint inhibitors have improved HCC treatment, not all patients with HCC can benefit from these therapies. The molecular heterogeneity that contributes to the development of HCC is not sufficiently targeted to date. It is therefore inevitable for future therapeutic options to identify and investigate on novel targets and promising compounds for future treatment. Further, taking into consideration that the recent breakthrough in the treatment of advanced HCC was accomplished with the combination of the compounds atezolizumab and bevacizumab it seems that a single drug may not be sufficient for the treatment of HCC. Therefore, future investigations for the systemic treatment of advanced HCC focus on combination therapies.

1.3. Cholangiocarcinoma

Cholangiocarcinoma comprises a heterogeneous group of biliary adenocarcinomas. It accounts for about 20 % of the primary hepatobiliary malignancies and is thus the second most common cancer found in the liver behind HCC. With a consistently increasing incidence worldwide and despite the advances in knowledge, diagnosis, and therapy, CCA remains a challenging disease with poor prognostic outcomes.

1.3.1. Epidemiology and Etiology of CCA

Globally, with about 0.3 - 6 incidences per 100.000 inhabitants per year and 1 - 6 death cases per 100.000 inhabitants per year, there is an increasing trend in CCA occurrence. In general, CCA mortality was higher in men than women comparing countries in Asia versus western countries (23). Several risk factors are associated with CCA development. Variations in incidence reflect changes in local risk factors. Risk factors are alcohol abuse, smoking, infection with HBV or HCV, liver cirrhosis, obesity, diabetes mellitus, congenital hepatic fibrosis. Exposure to toxic agents such as dioxin and thorothrast and infections caused by liver flukes such as *Clonorchis sinensis* or *O. viverrini*. as well as genetic predisposition plays an increasing role in CCA development (8, 24, 25). Khan and colleagues described that polymorphism in genes involved in xenobiotic detoxification, DNA repair, multidrug resistance, immune response, and folate metabolism increase CCA initiation (24).

1.3.2. CCA Development and molecular pathogenesis

CCA can be subdivided into three main variants depending on where they anatomically originated: intrahepatic (iCCA), perihilar (pCCA), and distal (dCCA) cholangiocarcinoma (Fig. 2). pCCA and dCCA are also referred to as extrahepatic CCA (eCCA). Intrahepatic CCA can form at any intrahepatic biliary tree and subdivides into small-duct iCCA and large-duct iCCA. Small duct iCCA characteristics are isocitrate dehydrogenase (IDH1, IDH2) mutations or fibroblast growth factor receptor 2 (FGFR2) fusions. Large duct iCCA, and eCCA demonstrate a high frequency of KRAS, TP53, and ILF3 mutations. pCCA

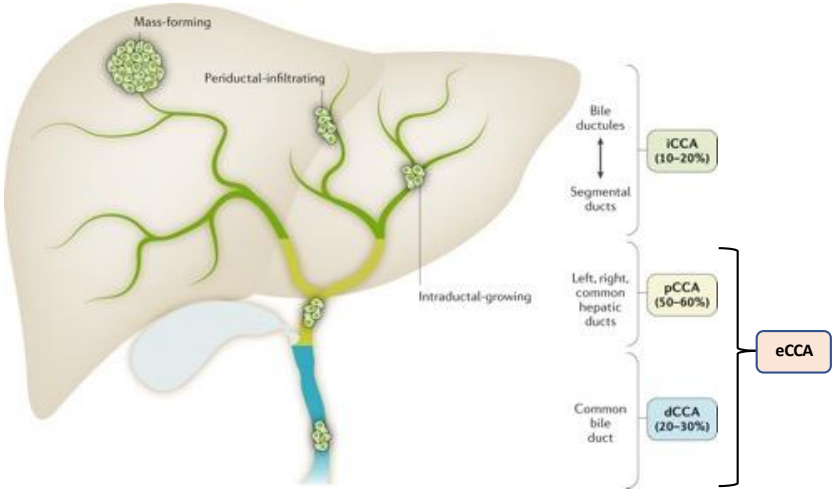

Figure 3 Different location of Cholangiocarcinoma (CCA) on the biliary tree (Figure adopted from Banales et al. 2020).

Figure 4 Different location of Cholangiocarcinoma (CCA) on the biliary tree (Figure adopted from Banales et al. 2020).

emerges at both hepatic duct sites, and dCCA arises at the common bile duct. Cells of origin are tissue-specific stem and progenitor cells, giving rise to different subtypes of cancer. CCA's three main growth patterns are mass-forming, referring to a mass lesion in the hepatic parenchyma, periductal-infiltrating iCCA, which grows alongside the duct wall, and intraductal-growing CCA that growths inside the duct lumen (Fig. 2) (8, 25).

CCA carcinogenesis depends on the cancer type background, which includes its genetic, epigenetic, histological, morphological, biological, and clinical features. CCA mainly arises after excessive exposure to mediators of biliary inflammation and cholestasis such as interleukin-6 (IL-6), Tumour Necrosis Factor-α(TNF-α),

Cyclo-oxygenase-2 (COX2) and Wnt. Prolonged exposure to these mediators results in progressive mutations of tumor-associated suppressor genes, proto-oncogenes, DNA mismatch-repair genes, the modulation of several signaling pathways, and subsequently cholangiocyte transformation (26). Further, accumulating bile acids from cholestasis and, consequently, the reduced pH leads to activation of the RAS-MAPK, PI3K-AKT-mTOR, and NF-κB pathways that encourage cell proliferation, migration, and survival (8, 26).

1.3.3. Diagnosis and management of CCA

CCA at an early stage is mostly asymptomatic. eCCA frequently shows jaundice, weight loss, pale stools, and dark urine as symptoms. iCCA, on the other hand, is mostly accidentally diagnosed since it appears with relatively nonspecific symptoms such as malaise, abdominal pain, nausea, and weight loss. Currently, there is no standard guideline for the early detection of CCA. Its diagnosis is managed by combining different tools: first, the clinical presentation of tumor markers (Carbohydrate antigen 19-9, circulating nucleic acid found in biofluids) or frequently found mutations (KRAS, IDH1, FGFR2). Second, imaging information using US, contrast-enhanced US (CEUS), CT, and MRI. Third, histopathological or cytological analysis are implied (8, 27). CCA shows various differentiation grades: poor, moderate, and well. Those with low-grade or well-differentiated type have a better prognosis and lower incidence of distal metastases than with high-grade carcinomas. Surgical resection combined with adjuvant treatment is currently the only curative option for early staged CCA. Since CCA diagnosis mainly occurs at an advanced stage, metastasis presentation and disease progression only enable 25% of patients to undergo surgical treatment (28-30). Patients with advanced CCA have limited options regarding systemic treatments.

1.3.4. Treatment of CCA

The first-line treatment of choice for an advanced and unresectable cholangiocarcinoma is based on the combination of gemcitabine and cisplatin (31). The FOLFOX (folonic acid, fluorouracil, and oxaliplatin) therapy is recommended as a second-line treatment. Studies around the FOLFOX treatment regime have improved the survival outcome of patients progressing on cisplatin/gemcitabine (32). A variety of studies are currently focusing on novel targeted therapies. Promising targets are the JAK/STAT3 pathway, inhibition of IDH1/2 mutation or targeting cancer-associated fibroblast (27). Only recently, the FGFR-selective TKIs pemigatinib and infigratinib were approved by the Food and Drug Administration (FDA) for a subgroup of patients with a fibroblast growth factor receptor 2 (FGFR2) fusion gene (33-35).

Additionally, other studies favor combined therapeutic approaches (36). To conclude, current management of CCA is constantly improving, however, long-term outcomes are still limited. Novel insights and new emerging molecular targeted therapies are therefore urgently needed.

1.4. Identifying future molecular targeted therapies for HCC and CCA

Next-generation sequencing (NGS) studies have emphasized HCC and CCA molecular heterogeneity (37, 38). Currently only two targeted therapies have been approved for the treatment of advanced CCA and at present, approved molecular targeted therapies in HCC mainly include multikinase inhibitors, antiangiogenic, and immunotherapy agents. There is therefore an unmet need to develop additional novel therapeutic agents which could potentially augment the presently available options, with the goal of improving the survival of more patients with advanced HCC or CCA. Scientific investigations should therefore address this gap and identify promising new targets or find applicable novel treatment regimens.

In this pursuit, first approaches were already made. The need for alternative targets is being addressed in several preclinical and clinical studies. Targeting HCC with combination therapies, such as the combination of antiangiogenic agents with immune-checkpoint inhibitors (ICIs), the combination of two ICIs and the combination of targeted agents in conjunction with surgery or other loco-regional therapies, have been extensively investigated and have proved to show satisfactory treatment results than monotherapies (39). Other therapeutic combinations such as durvalumab with tremelimumab (40) used against melanoma or Lenvatinib with pembrolizumab (41) used against renal cell carcinoma are approaches that were recently published to be promising for HCC.

1.4.1. Epigenetics and HDAC inhibition in HCC and CCA

Epigenetic changes are heritable changes of the chromatin structure, but not in the DNA sequence, that influence the accessibility of the transcriptional machinery to DNA and thereby affecting transcription, DNA repair, or replication. Histone acetylation and deacetylation play an important role in HCC and CCA. Histone acetylation regulates the activation of a gene by transferring an acetyl group (–CH3CO) from the acetyl-coenzyme A (acetyl-CoA) to the amino group of a lysine residue. Three types of histone acetyltransferases (HATs) mediate acetylation. They belong to the Gcn5-related N-acetyltransferase (GNAT), MYST and CREB-binding protein (CBP)/p300 family (42). Acetylation affects the interaction between DNA and histone by changing the positive charge on the lysine residue and thus promoting structural changes of chromatin. The acetyl group added can further be recognized by bromodomain (BRD)-containing proteins (acetyl-lysine binding proteins) such as the bromodomain and extra terminal domain (BET) bromodomain proteins BRD2, BRD3, and BRD4, which also promotes open chromatin (42, 43). The counterpart of HATs are histone deacetylases (HDACs) which remove acetyl groups from lysine residues. There are four classes of HDACs (I, II, III, and IV) known to date. Their classification depends on sequence similarities and cofactor dependency. Class I, II, and IV HDACs are Zn+-dependent. HDACs 1, 2, 3, and 8 are expressed in the nucleus of all cells and belong to Class I. Class II HDACs can be subdivided into IIA

(HDACs 4, 5, 7, and 9) and IIB (HDACs 6 and 10). They move between cytoplasm and nucleus, and whereas HDAC IIA is primarily expressed in the brain and heart, HDAC IIB is mainly found in the testis, liver, and kidney. Class III encompasses the so-called Sirtuins (SIRT 1-7), which are NAD+ dependent and have a very distinct catalytic mechanism for deacetylation compared with other classes of HDACs. Class IV has only one identified member, HDAC11. Its expression was reported in the smooth muscle, heart, kidney, and brain (44-46). Of note, HATs and HDACs were also described to interact with non-histone proteins, including tumor suppressors and oncogenes such as p53, Rb, and Myc. They hereby regulate protein stability, DNA binding, protein-protein interaction, enzymatic activity, or protein localization (45).

Epigenetic modulations through various mechanisms are frequent events in HCC and correlate with poor patient prognosis (47). The underpinnings behind HDAC contribution to hepatocarcinogenesis or cholangiocarcinogenesis are highly complex and not fully understood. Different HDACs (SIRT1, 2, 7 and HDAC 1, 2, 4, 5) have been reported to be significantly overexpressed in HCC and to correlate with a poor disease outcome by promoting pro-oncogenic events such as cell cycle progression, apoptosis evasion, adaptation to hypoxia and metabolic reprogramming (48). HDAC8 overexpression was reported to promote proliferation in HCC (49). HDAC11 was found to regulates glycolysis through the LKB1/AMPK signaling pathway and thus maintain HCC stemness (50).

Alterations in key oncogenes of CCA such as KRAS, TP53, IDH1/2 were shown to trigger the activation of epigenetic modifiers (writer, readers, and erasers), leading to changes in the expression of mediator genes involved in stemness or survival (51-53). Two preclinical studies of HDACs in CCA tumorigenesis state that overexpression of Class 1 HDACs correlates with advanced tumor staging, increased lymph node metastases, and increased microscopic vascular tumor infiltration and thus with a poor prognosis (54, 55).

The majority of currently approved HDAC inhibitors (HDACis) are for the treatment of cutaneous T-cell lymphoma and peripheral T-cell lymphoma (HDACi: Vorinostat, Romidepsin). As single agents, histone deacetylases inhibitors (HDACis) have demonstrated to be well-tolerated depending on the

doses applied and not toxic to normal tissues in preclinical studies (56, 57). Phase I clinical studies with Romidepsin (58), Belinostat (59) and Panobinostat (60, 61) in different solid cancer types showed encouraging anticancer activity. Subsequent evaluation as monotherapies in phase II trials against solid tumors however, demonstrated modest responses in a negligible number of patients and most importantly they inhibitors induced severe side effects (62-65). In HCC preclinical models, Pan-HDAC inhibitor (HDACi) Panobinostat was shown to regulate cell proliferation and angiogenesis and to induce apoptosis (66, 67). Only one clinical trial, which evaluated the effect of HDACi inhibitor Belinostat as a single agent in HCC patients was completed. Yeo et al. demonstrated that, after treating patients with unresectable HCC in a Phase I/II clinical trial, HDACi Belinostat led to a progression-free survival (PFS) and an overall survival (OS) of 2,64 % and 6.6 months respectively. They showed that HR23B expression correlated with disease stabilization (68). For CCA, even though experimental studies on the effect of epigenetic drugs on CCA in vitro exist (69-71), clinical trials are limited. It can be summarized that despite all evidence of benefit in preclinical studies, HDACis as monotherapy have had limited success in clinical trials, showing only modest responses, especially in solid tumors, and they were reported to induce adverse effects. These disadvantages could be resolved, at least in part, by combining HDACis with other anticancer drugs. Successful examples of HDAC inhibitors in the treatment of solid tumors when combined with other agents exist. Dizon et al., Bitzer et al., and other studies have demonstrated that HDACis in combinations enhanced the therapeutic efficacy compared to their effect as monotherapy, and fewer adverse effects, were observed (72-76).This approach appeared to substantially improve the conventional treatment effect in many cancer studies because of synergistic or additive anti-tumor effects. These studies suggest that HDACis play a key part in inducing clinical response rates in the clinical setting. Novel investigation using HDACis for the treatment of solid tumors such as HCC and CCA should therefore consider combining them to other agents to increase clinical response.

1.4.2. Adenosine receptor signaling

The adenosinergic system is a significant regulator element in various physiological and pathological conditions. Adenosine is an ubiquitous endogenous signaling molecule. Under physiological conditions, adenosine originates intracellularly from the hydrolysis of AMP and S-adenosylhomocysteine (SAH). Extracellular adenosine comes from the external transport of intracellularly generated adenosine or is generated through dephosphorylation of its precursors: ATP, ADP, and AMP. This transport is mediated by concentrative nucleoside transporter (CNTs) and equilibrative

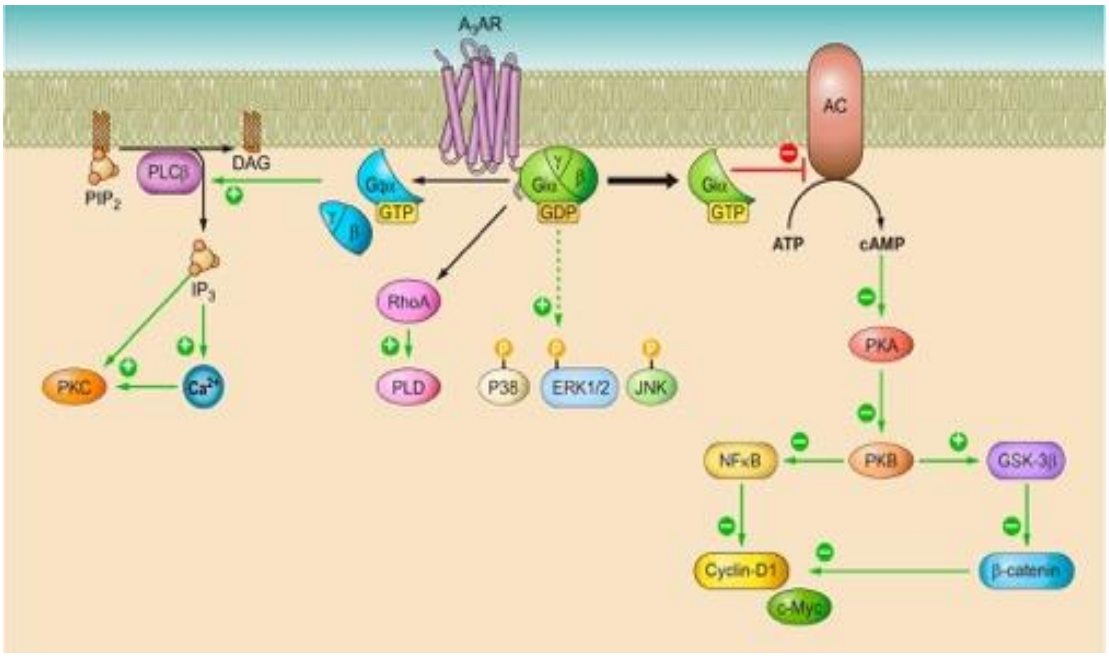

Figure 5 Overview of ADORA3 intracellular signaling. Receptor activation mediates the disassociation of Gi and Gq protein from the Gßγ subunit. The Gi and Gq subunits further regulate the phosphatidylinositol 3-kinase (PI3K) / protein kinase B (AKT), c-Jun N-terminal kinase 1/2 (JNK1/2), mitogen-activated protein kinase (MAPK), nuclear factor-κB (NFκB) / cMyc and glycogen synthase kinase 3β (GSK-3β) / β-catenin pathway (Figure adopted from Borea et al. 2018).

Figure 6 Overview of ADORA3 intracellular signaling. Receptor activation mediates the disassociation of Gi and Gq protein from the Gßγ subunit. The Gi and Gq subunits further regulate the phosphatidylinositol 3-kinase (PI3K) / protein kinase B (AKT), c-Jun N-terminal kinase 1/2 (JNK1/2), mitogen-activated protein kinase (MAPK), nuclear factor-κB (NFκB) / cMyc and glycogen synthase kinase 3β (GSK-3β) / β-catenin pathway (Figure adopted from Borea et al. 2018).

nucleoside transporters (ENTs) (77). Adenosine binds to four subtypes of adenosine receptors (ADORA) of the large G-protein-coupled receptor (GPCR) family, ADORA1, ADORA2A, ADORA2B, and ADORA3. All receptors are expressed in different tissues throughout the body. Structurally, all receptors

possess a seven-helix transmembrane domain which is linked by three intracellular and three extracellular loops. Physiologically ADORA1 and ADORA3 mediate their signaling through Gi and Go members of the GPCR family, which leads to the decrease of adenyl cyclase (AC) activity and cAMP levels. ADORA2A and ADORA2B, on the other hand, stimulate AC activity leading to increasing cAMP activity. Both pathways subsequently activate a plethora of mediators. Different studies on the receptors´ involvement in pathological conditions such as tissue protection, liver fibrosis, anti-inflammation, or cancer exist (78-80). Adenosine receptor 3 (ADORA3) signaling is an essential factor in tumor biology that affects the immune system by modulating the tumor microenvironment and intracellular signaling cascades in tumor cells (81, 82). The gene encoding for ADORA3 is widely expressed in various primary cells, cell lines, and tissues, including the brain, heart, lung, and liver. ADORA3 generally triggers various intracellular signaling events. Receptor stimulation and subsequent reduction in cAMP level can trigger Phospholipase C (PLC), calcium production, and phospholipase D (PLD) production through monomeric G protein RhoA, thus affecting the Mitogen-activated protein kinase (MAPK) and phosphatidylinositol 3-kinase (PI3K)/protein kinase B (AKT) pathway (83). On the other hand, reduction in cAMP also results in protein kinase A (PKA) inhibition, which via protein kinase B (PKB) inhibit nuclear factor (NF)-κB signaling and promotes glycogen synthase kinase (GSK) - 3ß (Fig. 3) (77, 84, 85). ADORA3 has been extensively investigated as a potential drug target during the last decade (77, 84, 86-88). Interestingly, muscle cells secrete natural agonists to ADORA3 with an antitumor effect that seems to account for the rarity of tumor metastases in striated muscles (89). ADORA3 was described to be overexpressed in tumor tissues from small groups of patients with mesothelioma (90), thyroid (91), breast or colon cancer (92, 93).

In HCC several observations concerning ADORA3 have been reported. In a cohort of 21 patients with HCC, the intratumoral ADORA3 mRNA expression was found upregulated compared to adjacent tissue (85), however data on the protein level have not been reported for human-derived tumors before. ADORA3

stimulation with the specific agonist Namodenoson (CF102) in preclinical models accelerated mitosis with an improved regeneration after partial hepatectomy (94). The stimulation of ADORA3 has already reached clinical testing for non-alcoholic steatohepatitis (NASH) and HCC (95, 96). Namodenoson has been applied in a phase II study with 78 patients with Child-Pugh B advanced HCC (96). At first glance, with OS of 4.1 months for patients with Namodenoson compared to 4.3 months with placebo, this study did not reach its primary endpoint of a statistically significant OS difference. Despite this negative result, Namodenoson led to an objective response in single patients and a positive efficacy signal for the group of patients with Child-Pugh B7 with a 12-month survival rate of 44%, compared to 18% in the placebo group (96).

Data on the role of ADORA3 in CCA have not been reported yet.

These early clinical results show that stimulation of ADORA 3 is feasible and safe, even in patients with reduced liver function. However, the further development of this approach requires a more detailed characterization of cellular responses of liver cancer cells to stimulation of ADORA3. These insights could help discriminate between responding and non-responding tumors and could lead to new drug combinations to enhance beneficial antitumor effects in HCC and CCA.

1.4.3. PI3K/AKT/mTOR signaling in HCC and CCA

The PI3K/ AKT/mammalian target of rapamycin (mTOR) pathway is a commonly aberrant signaling pathway in HCC (11) and CCA (97).

AKT, a serine/threonine (Ser/Thr) protein kinase, plays a crucial role as a central regulator in this pathway. It exists in three isoforms: AKT1, 2 and 3 and has three structural relevant domains, the amino-terminal pleckstrin homology (PH) domain, a central domain, and a carboxyl-terminal regulatory domain. The PH domains of each isoform are structurally divergent. Two phosphorylation events are crucial for AKT to attain full function. For AKT1, Phosphorylation at Thr 308, by phosphoinositide-dependent kinase-1 (PDK-1), and at Ser 473, by mammalian target of rapamycin complex 2 (mTORC2) are crucial. All the other isoforms have homologous sites for Ser/Thr phosphorylation. AKT regulates several cellular processes such as cell survival by directly inhibiting pro-apoptotic proteins, cell

growth, proliferation, genome stability, and glucose metabolism. Protein phosphatases such as protein phosphatase 2A (PP2A), PH domain leucine-rich-repeat-containing protein phosphatase 2A (PHLPP2), and phosphatase and tensin homolog (PTEN) mediate the negative feedback regulation of AKT (98).

The importance of AKT in HCC and CCA has been demonstrated in different studies. Boyault et al. and Zhou et al. reported that overexpression of AKT, which was found in two subgroups of HCC, correlated with disease characteristics and poor survival (99, 100). Dysregulations in this pathway were found to mediate resistance to therapeutic agents (101-103). Kunter, Mroweh and colleagues as well as Dokduang et al. have demonstrated that the overactivation of the AKT signaling pathway is crucial in promoting and sustaining a highly proliferative status in HCC (98, 104) and CCA (105), respectively. Positive immunostaining for AKT and its phosphorylated form (p-AKT) has been reported with higher rates in neoplastic cells compared to the surrounding normal and dysplastic epithelium (106). The hyperproliferative stage of tumorigenic cells and the elevated oncogenic signaling is partly responsible for the tumor cell ability to resist cell apoptosis and activate anti-apoptotic mechanisms that contribute to its survival. Frequent mutations found in patients with HCC (PTEN (107)) and CCA (K-Ras (108)) trigger AKT overactivation to support aberrant proliferation and antiapoptotic signaling in tumorigenesis (109). Beside the direct involvement of the AKT signaling pathway in tumor growth, different mechanisms were described to use the AKT signaling axis to promote HCC (110, 111) and CCA (112, 113) progression. Epithelial-mesenchymal transition (EMT) broadly regulates the multistep mechanism of migration, invasion and metastasis in cancer. Yothaisong et al. as well as other studies associated the aberrant activation of AKT signaling to an invasive, metastatic and drug resistant cancer phenotype (97, 114-116).

Evidently, it can be suggested that direct inhibition of AKT may be a promising therapeutic option. Interestingly however, current inhibitors of the PI3K/PTEN/AKT/mTOR pathway focus on PI3K or mTOR as molecular targets. Inhibiting mTOR however, was shown to enhance diverse regulating feedback loops, that reduce its antiproliferative potential (117). One of this feedback loops

is the activation of AKT, which results from the inhibited mTOR dependent negative feedback on AKT (118). In this context most recent studies suggested that a dual AKT/mTOR inhibition may be more favorable (119). MK2206 is an allosteric AKT inhibitor that is correctly evaluated in different clinical trials. Out of 50 clinical trials assessing the effect of MK2206, 21 used MK2206 as a monotherapy. Out of these 21 studies 1 study was withdrawn and 5 terminated due to discouraging results, related toxicity, or limited activity. Out of the 15 remaining studies only 6 studies posted results and discussed them in respective publications. Of note, all 6 published studies reported dose limiting toxicities for MK2206, albeit well tolerated. Further all of them concluded that MK2206 monotherapy only generate modest results mostly due to incomplete or inadequate target inhibition (120-125).

The possibility of directly targeting AKT signaling in HCC and CCA has been addressed in several preclinical studies (126-128). Approaches to translate promising preclinical observations into clinical studies using AKT inhibitors, led to early termination of the studies due to discouraging results and severe adverse effects (NCT01239355) or missing clinical activity (129). After conducting a phase-II study with the AKT Inhibitor MK-2206 in patients with Advanced Biliary Cancer, Ahn et al concluded that further development of AKT inhibitors may need to focus on combinations with other molecular targeted agents, conventional cytotoxic chemotherapy, and prospective patient selection (129).

The combination of AKT inhibitor MK2206 and HDACis was shown effective in different models of solid tumors. Buglio et al. showed that patients with relapsed or refractory Lymphoma could benefit from the combination of MK2206 and HDACi Vorinostat. This combination was associated to an increased PARP cleavage and induction of apoptosis (125, 130). Promising results were observed in pancreatic cancer (131) and Prostate cancer(132). Janku et al. reported in a case study that 2 patients with advanced HCC could benefit from the combinatorial therapy with the PI3K/AKT/mTOR inhibitor sirolimus and Vorinostat(133). To our knowledge there is no report about the efficacy of the combination treatment of a direct AKT inhibitor such as MK2206 and HDACis in HCC and CCA.

1.5. Aim of the study

ADORA3 activation, direct AKT inhibition, and HDAC inhibition have been identified as promising targets and investigated in liver cancer. However, current studies with respective drugs as single agents were disappointing. A recent clinical investigation on ADORA3 activation in HCC patients using the agonist Namodenoson, did not meet its primary endpoint, which was an improved overall survival, even though it was effective in a selected group of patients. This trial and other preclinical studies demonstrated that the underpinnings of ADORA3 stimulation in HCC and CCA still need to be elucidated.

Direct AKT inhibition using the agent MK2206 was repeatedly shown to be promising in vitro, but to date missing clinical activity or discouraging results were stated in two clinical trials in liver cancer, thus arising the need to combine it to another agent. HDAC inhibitors as single agents are generally recognized as effective drugs against hematological tumors, but only modest success has been reported in solid tumors. Bitzer et al. as well as other studies presented evidence that combining HDAC inhibitors to other targets increased the overall success rate. The effect of AKT and HDAC co-inhibition in HCC and CCA has not been investigated so far. In this pursuit, the aim of the presented study was to explore the role of ADORA3 in HCC and CCA and investigate novel combination treatment approaches for the treatment of HCC and CCA. To achieve these aims the following objectives were performed:

1. Explore the role of ADORA3 in HCC and CCA by analyzing and comparing its expression in healthy vs. tumor tissue.
2. Investigate molecular mechanisms triggered after ADORA3 stimulation with the selective agonist Namodenoson.
3. Explore the potential benefit of simultaneous ADORA3 activation and HDAC inhibition as novel treatment strategy for HCC and CCA.
4. Investigate the effect of an AKT/HDAC co-inhibition on three different hallmarks of cancer: sustained proliferation, evaded apoptosis, and promoted cell migration.
5. Explore the molecular underpinnings of AKT/HDAC co-inhibition.

2. Material and Methods

2.1. Material

All mentioned materials were utilized according to the instructions of the manufacturers.

2.1.1. Chemicals and working Material

Chemicals and working materials were purchased from the following companies: AGFA, Amersham, Bioscience, Biozym Scientific, Bio-Rad, Boehringer Mannheim, Falcon™, GE Healthcare, Hycultec, ThermoFischer Scientific, Millipore, Life technologies, Promega, Qiagen, Roche, Carl Roth, Sarstedt, StarLab, Sigma-Aldrich/Merck, Santa Cruz Biotechnology, Selleckchem Tocris, Wertheim. Exceptions will be hinted specifically.

2.1.2. Drugs

All Drugs used are summarized in Table 1.

Table 1. Compounds used in this study.

Name	Provider (Cat. No.)
Namodenoson (CF102)	Hycultec (HY12365)
Piclidenoson (CF101)	Tocris (1066)
MRE3008F20	Hycultec (HY103178)
MK2206	Hycultec (HY10358)
Perifosine	Santa Cruz Technology (sc-364571)
Ipatasertib	Selleckchem (S2808)
Resminostat	Hycultec (HY-14718A)
Vorinostat	Hycultec (HY-15149)
Belinostat	Hycultec (HY-10225)
Romidepsin	Hycultec (HY-15149)

2.1.3. Biological Materials

Cell lines

All Cell lines used in this study are listed in Table 2. Cell lines were purchased at the German Collection of Microorganisms and Cell Culture (DSMZ), the Riken Cell Bank (Riken), the American Type Culture Collection (ATCC) or obtained from laboratories of our cooperation partners (Dr. Daniel Dauch/ Prof. Dr. Lars Zender or Prof. Dr. Nisar Malek).

Table 2. Cell lines

Name	Source
Human Cell lines	
Huh7	Hepatocellular Carcinoma (DSMZ)
HepG2	Hepatoma (DMSZ)
JHH1	Hepatocellular Carcinoma (Prof. Dr. Lars Zender – Cell line was re-authentified)
RBE	Cholangiocarcinoma (Riken)
HUCCT1	Cholangiocarcinoma (Riken)
TFK-1	Cholangiocarcinoma (DSMZ)
SZ1	Cholangiocarcinoma (Prof. Dr. Nisar Malek)

Organoids

The organoids used were generated and established as previously described by the laboratory of Markus Heim, Biomedicine Department Basel (Basel, Switzerland) (134).

2.1.4. Antibodies and Enzymes

All primary and secondary antibody used for Immunoblotting or TMA staining are summarized in Table 3.

Table 3. Antibodies and Enzymes

Primary Antibodies			
Antigen	**Species**	**Dilution (Application)**	**Provider (Name)**
ADORA3	Rabbit	1:500 (WB, IHC)	SAB (Signalway) (35615)
Ac-Histone H3	mouse	1:1000 (WB)	Santa-Cruz sc-56616
PARP	Rabbit	1:500 (WB)	Cell Signaling (9542)
Cleaved PARP (Asp214)	Rabbit	1:1000 (WB)	Cell Signaling (5625)
Phospho-p70 S6 Kinase (Ser371)	Rabbit	1:1000 (WB)	Cell Signaling (9208)
Phospho-mTOR (Ser 2481)	Rabbit	1:1000 (WB)	Cell Signaling (2974)
mTOR	Rabbit	1:1000 (WB)	Cell Signaling (2983)
Phospho-AKT (Ser473)	Rabbit	1:1000 (WB)	Cell Signaling (4060)
Phospho-AKT (Thr308)	Rabbit	1:1000 (WB)	Cell Signaling (4056)
Pan-AKT	Rabbit	1:1000 (WB)	Cell Signaling (4685)
SGK1(Ser78)	Rabbit	1:1000 (WB)	Cell Signaling (12103)
p53	mouse	1:500 (WB)	Santa-Cruz sc-126
Phospho-4E-BP1 (Thr37/46)	Rabbit	1:1000 (WB)	Cell Signaling (2855)
β-Actin	Mouse	1:5000 (WB)	Cell Signaling (3700)

Secondary Antibodies			
Anti-rabbit IgG – HRP	Donkey	1:10000	ThermoScientific
Anti-mouse IgG – HRP	Donkey	1:10000	ThermoScientific
FITC-conjugated anti-Rabbit IgG	Goat	1:1000	ThermoScientific

2.1.5. Nucleotides

All Nucleotides used are summarized in Table 4.

Table 4. Nucleotides

Oligonucleotides for qPCR		
Oligoname	**Sequence (5' – 3')**	**Reference**
HDAC1-F	CATCTCCTCAGCATTGGCTT	**(135)**
HDAC1-R	CGAATCCGCATGACTCATAA	**(135)**
HDAC2-F	ATGAGGCTTCATGGGATGAC	**(135)**
HDAC2-R	ATGGCGTACAGTCAAGGAGG	**(135)**
HDAC3-F	CTGTGTAACGCGAGCAGAAC	**(135)**
HDAC3-R	GCAAGGCTTCACCAAGAGTC	**(135)**
HDAC4-F	CTGGTCTCGGCCAGAAAGT	**(135)**
HDAC4-R	CGTGGAAATTTTGAGCCATT	**(135)**
HDAC5-F	GAACTGGGCATGGCTCTTG	**(135)**
HDAC5-R	GGGAACCATCCTTGGAAATC	**(135)**
HDAC6-F	GCGGTGGATGGAGAAATAGA	**(135)**
HDAC6-R	CCGGAGGGTCCTTATCGTAG	**(135)**
HDAC7-F	CCTGCTGTTGTCACCGC	**(136)**
HDAC7-R	TCCTCTCCAGCTCAGAGACC	**(136)**
HDAC8-F	GCGTGATTTCCAGCACATAA	**(135)**
HDAC8-R	ATACTTGACCGGGGTCATCC	**(135)**
HDAC9-F	GCCCACAGGAACTTCTGACT	**(135)**

HDAC9-R	GAACTCTAAGCCAGATGGGG	**(135)**
HDAC10-F	GAACAGCCACATCCAGGG	**(135)**
HDAC10-R	CCTCTTAGATGGGATGCTGG	**(135)**
HDAC11-F	AAGGAAGTTGGGGAGGAAGA	**(135)**
HDAC11-R	GCACACGAGGCGCTATCTTA	**(135)**
GAPDH-F	AGAAGGCTGGGGCTCATTTG	**(136)**
GAPDH-R	AGGGGCCATCCACAGTCTTC	**(136)**

2.1.6. Media and Buffers

Media

Cell culture media and additives were purchased from Gibco, Invitrogen, Tocris, PeproTech or Sigma unless stated otherwise. Plasticware was obtained from Corning, Falcon, Nunc and PAA.

Organoid Culturing Media

Media used for organoid generation and maintenance are summarized in table 5.

Table 5. Composition of media for human liver cancer organoid generation and culture.

Basal Media	
Substances	**Concentration**
Collagenase V	2.5 mg/ml
DNase	0.1 mg/ml
Earle's Balanced Salt Solution (EBSS)	1x
Human Expansion Medium (HEM)	
Advanced DMEM/F-12	-
B-27	1x
N-2	1x
Nicotinamide	10 mM
N-acetyl-L-cysteine	1.25 mM
Gastrin	10 nM

Forskolin	10 µM
A83-01	5 µM
EGF	50 ng/ml
FGF10	100 ng/ml
HGF	25 ng/ml
Rspo1	1 µg/ml
Penicillin/Streptomycin	50 units/ml

Buffer

Self-made and ready-to-use buffers used in this study are summarized in table. 6.

Table 6. Buffers

Self-Made Buffers	
Name (1 liter)	Composition
1x Tris-buffered saline (TBS)	50 mM Tris, 150 mM NaCl, adjust pH with HCL to pH 7.6
1x Tris-buffered saline + tween20 (TBST)	TBS 1x + 0.1% Tween20
1x Running Buffer	30.3 g TRIS, 144 g Glycine, 10 g SDS Fill with Millipore water and adjust pH to 8.3 – 8.5
1x Transfer Buffer	48 mM Tris-HCl (pH 8.3), 39 mM glycine, 20 % methanol, 0.037 % SDS
Ready-to-use buffers	
Name	Provider
Restore™ Plus Western Blot Stripping Buffer	ThermoScientific
RIPA lysis buffer	Sigma-Aldrich
Clarity™ Western ECL Blotting Substrates	BioRad
NuPage Protein Loading Buffer	ThermoScientific

2.1.7. Kits and Arrays

All kits used in this study are summarized in Table 7.

Table 7. Kits and Arrays

Kits	
Name	Provider
Pierce™ BCA Protein Assay	ThermoScientific
Nucleospin® RNA purification Kit	Machery-Nagel
QuantiTect reverse transcription	QIAGEN
Pierce™ SuperSignal™ West Femto, Rabbit Fast Western Blot Kit	ThermoScientific
Annexin V-FITC/PI staining kit	BD Biosciences
OptiView DAB TMA detection kit	Roche
Arrays	
PI3K/AKT/mTOR RT™ Profiler™ PCR Array	QIAGEN

2.2. Methods

2.2.1. Cell Culture

HepG2, Huh7, HUCCT1, RBE, and JHH1 were cultured in Dulbecco's modified Eagle medium (DMEM, Sigma-Aldrich; Merck KGaA, Darmstadt, Germany) with 10% fetal bovine serum (FBS, Sigma-Aldrich; Merck KGaA, Darmstadt, Germany). TFK1 and SZ1 cells were cultured in RPMI-1640 medium containing 10% FBS. All cells were cultured in a humidified incubator (37°C, 5% CO2) and regularly tested to be negative for mycoplasma contamination.

2.2.2. Generation of human HCC and CCA organoids from human liver biopsy samples

All organoids were generated and established as previously described by the laboratory of Markus Heim, Biomedicine Department Basel (Basel, Switzerland)

(134). Briefly, human tissues were from patients undergoing diagnostic ultrasound-guided needle liver biopsy at the University Hospital Basel. All patients included were informed and signed to an ethically approved consent. Cylindrical biopsies for an organoid generation were collected in advanced DMEM/F-12 (GIBCO) on ice, digested to small cell clusters in digestion solution at 37 °C. Finally, those clusters were embedded in BME2 (Cat. No. 3533-005-02, Trevigen®) droplets and incubated to solidify. Droplets were covered with human expansion/culture medium (HEM). Organoids were cultured in a humidified environment (37°C, 5% CO_2), and media was changed every 3 - 4 days.

2.2.3. Drug's preparation

All substances were dissolved in DMSO at 10 mM stock aliquots and stored at - 20 °C. Working concentrations of the compounds were freshly prepared from the stock for each experiment. Compounds were added to the corner of the well and mixed gently for distribution.

For the experiments on the ability of MRE308F20 a ADORA3 antagonist to reverse observed effects after the incubation with Namodenoson an ADORA3 agonist, cells were pretreated with the antagonist first for 30 min. before adding the agonist.

2.2.4. Cell viability assays

Human cell lines were plated in 24-well plates (3×10^4 cells per well) and adhered for 24 h. After 24 h medium was changed before the addition of any compound. Substances and DMSO control (Ctrl.) were prepared in serum-free DMEM, and cells were treated accordingly. Cell viabilities were determined after an incubation time of 72 h, employing the Sulforhodamine B assay (SRB, which measures the remaining cell mass (137)). For SRB assay, cells were washed twiced with PBS, fixed with cold 10 % trichloroacetic acid (TCA, Cat. No. T6399, Sigma) and dried at 55°C. Fixation solution was collected separately. Thereafter, cells were stained with SRB staining solution (0.4 % Sulforhodamine B; HY-D0974, Hycultec, in 1 %

acetic acid; Cat. No. 1000631011, Sigma). Staining solution was washed out with tap water. After drying overnight, the stain was solubilized in 10 mM Tris base, pH 10.5. The optical density was measured at a wavelength of 550 nm in a microtiter plate reader. Differences in cell mass were obtained by comparing DMSO treated control wells to drug-treated wells. DMSO controls were set to 100 %.

For organoid cultures, cell viability was measured using CellTiter-Glo 3D reagent (Promega). Single-cell suspensions of tumor organoids were plated in 384-well plates at a density of 1000 cells per well. After two days of recovery and formation of 3D structure, drug solution was added to treatment wells, and DMSO was added to controls. After six days of treatment, cell viability was measured using CellTiter-Glo 3D reagent following provider instructions. Luminescence was measured on a Synergy H1 Multi-Mode Reader (BioTek Instruments). Results were normalized to the vehicle (=100 % DMSO). Curve fitting was performed using Prism (GraphPad) software and the nonlinear regression equation. All experiments were performed at least two times in duplicate or as indicated in the figure legends.

2.2.5. Colony formation assay

Cell lines (10×10^3) were suspended and incubated in an upper layer containing 0.35 % agarose (Lonza Rockland, Inc.) in DMEM supplemented with Pen/Strep (Sigma), 20% FBS (Sigma), and the drug used or DMSO as control. The mixture was added on top of a layer of 0.7 % basal agar in DMEM with 20 % FBS, which was added to a six-well plate and placed at room temperature until the agarose solidified. The wells were then overlaid with a solution of 1 ml of DMEM containing 10 % FBS Pen/Strep and Drug without agarose to prevent wells from drying out. The upper medium was changed after ten days. The colonies grew for 21 days and were then stained with NBT (nitrobluetetrazolium, Sigma) for two days, photographed, analyzed, and counted using ImageJ software. Colonies larger than 0.15 mm in diameter were scored.

2.2.6. Cell migration assay

All cells were seeded in 12-well plates for the migration assay and allowed to grow to 80 % confluence, respectively. Initially, the confluent monolayers of the cells were gently scratched alongside the middle line of the well using 200 µl pipette tips under an angle of around 30 degrees. Then, cells were washed briefly with pre-warmed PBS to remove cell debris and dead cell. Fresh media was then added, and cells were treated with the indicated concentrations of Drugs. Wound images were taken using a regular inverted microscope (Carl Zeiss, Göttingen Germany) at 0 h and 48 h, respectively. The migration index was calculated using the following formula: Area migrated by the cells (A) = (Wound Area at 0 h – Wound Area at 48 h), which is then expressed as % wound closure. Three independent repeats were carried out for analysis. Results are shown as mean ± SEM.

2.2.7. Flow Cytometry: detection of Apoptosis by Annexin V Staining

Annexin V-FITC/PI staining assay was performed according to the manufacturer's instructions. Briefly, cells (1.5 x 10^5 per well) were grown in 12-Well Plates and treated as indicated for 48h. After the respective treatments, the supernatant of each well (including floating apoptotic cells) was collected, and the adherent cells were trypsinized and then collected to the same tube. The tubes were centrifuged for 5 mins at 1000 rpm. The supernatant was discarded, the cell pellet was gently washed once with PBS. After another round of centrifugation, the pellet was re-suspended with 1 ml 1X Binding Buffer at a concentration of approximately 1 x 10^6 cells/ml. Cells were then incubated with fluorescein isothiocyanate (FITC)-labeled Annexin V (10 µg/mL) and PI (20 µg/mL) at 37°C for 20 min in the dark, and signal detection was performed using Flow Cytometer FACS Canto II (BD Biosciences, Heidelberg, Germany) of the FACS core facility at the University Hospital in Tuebingen. Result analysis was made with FlowJoTM v.10.7 (FlowJo, LLC, Ashland, USA). Quantification of apoptotic cells was performed using Graphpad Prism.

2.2.8. Immunoblotting

For western blot analysis, treated cells were washed once with PBS lysed on ice with 100 µl RIPA lysis buffer supplemented with 0.1 % Halt™ protease and phosphatase inhibitor cocktail and 0.1 % Phenylmethylsulfonyl fluoride per well. Cell lysates were collected in tubes and sonicated (Bandelin Sonoplus) for 5 seconds at 20 kHz. Cells were then incubated on a rotating wheel for one hour at 4 °C then centrifuged at 12,000 g for 7 min at 4 °C. The supernatants were used for western blot analysis. The protein concentration was determined with the Pierce BCA Protein Assay Kit using BSA at different concentrations as the standard to generate a regression curve. At least 20 µg of protein was mixed with NuPage sample buffer supplemented with 50 µM DTT. Protein lysates including NuPage were boiled at 94 °C for five min. 20 to 40 µg of cooked protein was loaded onto 4-12 % SDS-PAGE gels and then transferred to polyvinylidene difluoride (PVDF) membranes (Millipore). After blotting, membranes were blocked with 5 % nonfat milk in TBST for one hour and incubated with the respective diluted primary antibodies at 4 °C overnight. The membranes were incubated with the appropriate secondary antibodies for one hour the next day. An ECL chemiluminescence detection kit was used to detect signals following the manufacturer's recommendations.

For weak antibodies, the Pierce™ SuperSignal™ West Femto, Rabbit Fast Western Blot Kit was used. Briefly, primary antibodies were diluted with the antibody diluent solution provided which the kit. The solution was added to the membrane directly after blotting without any blocking step. After 24 h of incubation at 4 °C with the primary antibody, the antibody was removed, stored and the prepared Fast Western optimized HRP / Peroxide working mix was directly added to the membrane as recommended by the manufacture. Finally, after incubation with the HRP / Peroxide mix for 30 min, the membrane was washed twice with the provided wash solution and detected using a 1:1 mix of the SuperSignal West Femto Luminol/Enhancer Solution.

The film was exposed to the membrane for 1 – 60 minutes and processed with the AGFA developer solution. Detected signals were fixed using the AGFA

fixation solution. Films were then washed once in tap water and dried for further analysis. The β-actin antibody confirmed equal protein loading.

For testing different Antibodies on one membrane, bound antibodies on the membranes were removed by washing with the Restore™ Plus Western Blot Stripping Buffer twice (10 min each time) and washing with TBS-T twice (10 min each time), then, the blotted membranes were re-blocked and re-probed with other antibodies as previously described.
For quantification, stained band intensities were analyzed and compared using Image Lab software (Bio-Rad Laboratories), Image J and GraphPad Prism version 9.

2.2.9. Quantitative Real-time PCR (qPCR)

To assay gene expression level under different treatment conditions, total RNA was isolated from control and treated cells using the NucleoSpin® RNA purification Kit following the manufacturer's instructions. RNA concentrations were quantified with a Nanodrop spectrophotometer. Samples with a 260 / 280 ratio of about 2.0 were accepted as pure. 1 µg of RNA was reversed transcribed to complementary-DNA using QuantiTect Reverse Transcription Kit following manufacturer's instructions. Selected genes were amplified and analyzed using corresponding oligo (dt) primers, an SYBR™ Select Master Mix (ThermoFisher Scientific), and the LightCycler 480 System (Roche). Amplification was performed after a 10 min. hold stage at 95 °C and 40 cycles of denaturation at 95 °C for 15 s, followed by a 1 min. annealing and elongation phase at 60 °C. The melting curve data were collected to check primer quality and specificity. Each cDNA sample was analyzed as triplicate, the housekeeping gene GAPDH and corresponding samples with no cDNAs were included as controls. Relative quantities of the transcript were determined using GAPDH as a reference and normalized relative to the untreated control using the $2^{-\Delta\Delta Ct}$ method. Results are presented relative to the mean of GAPDH (138, 139).

2.2.10. RT^2-Profiler PCR

RT^2 Profiler^{TM} PCR Array analysis was performed with extracted total RNA from treated cells. Briefly, the total RNA was reverse-transcribed as described above, and the resulting cDNA was analyzed with a 96-well plate RT^2 Profiler^{TM} quantitative PCR array. The array includes 84 critical genes of the pathway of interest. Each gene is prepared in one well. 5 wells are used for housekeeping genes, 1 well for genomic DNA control, 3 wells as reverse transcription controls and another 3 wells as positive PCR controls. Amplification was performed according to the vendor's instructions using the LightCycler 480 System (Roche) and 45 cycles. Gene expression levels were analyzed using the spreadsheet-based tool provided by the vendor. A sum of 12 96-Plates of the PI3K/AKT/mTOR pathway were used. 6 plates for each cell line and 3 replicates for each condition. Two conditions were tested: AKTi alone as control vs. the combination AKTi/HDACi. Data from the combined treatment were collected and normalized based on the Ct values of the housekeeping genes included in the arrays and further normalized to the monotherapy (AKTi) as control. The fold-change of gene expression was calculated using the $2^{-\Delta\Delta Ct}$ method.

2.2.11. Synergy Screening

Two different models were used to assess synergistic interactions.

The first model is the simplified high single agent (HSA) synergy model (140), which is used when two drugs are analyzed at one specific concentration respectively. This model, which is also referred to as the Gaddum's non-interaction model, defines a synergistic combination effect as beneficial outcome on top of what is observed for each individual drug at the dose used in the combination. Briefly, for synergistic interaction the effect of the combination should be more then additive (Fig. 4).

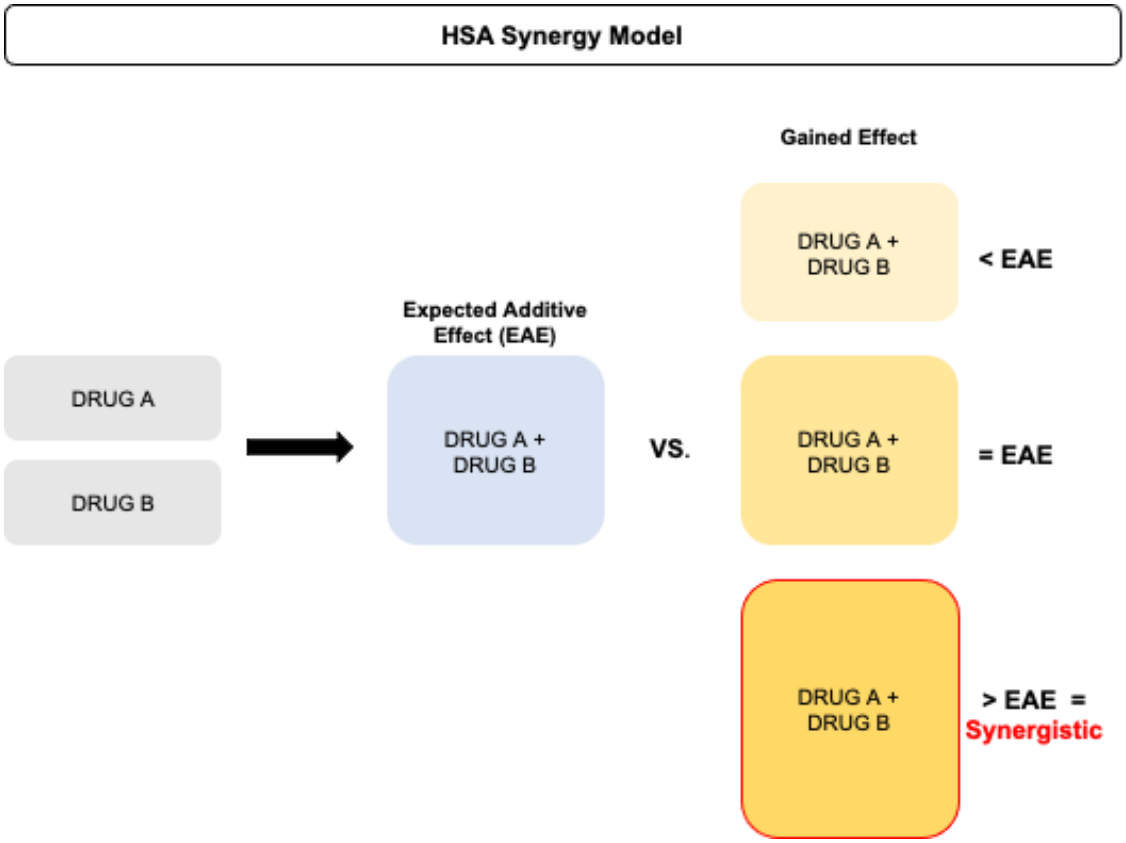

Figure 7. Schematic description of the highest single agent synergy model. The model is based on the comparison of the expected additive effect (EAE) of each individual drug to the gained effect in the experimental setting. The EAE is the sum of the effect observed of each individual drug at the tested concentration. The gained experimental effect can be lower than the expected additive effect (< EAE), the same as the expected additive effect (= EAE), or higher than the expected additive effect (>EAE). A combination is considered synergistic when the gained effect is higher than the EAE.

The second model is the zero-interaction potency (ZIP) model. This model was used when comparing two drugs at different concentrations. Briefly, the model takes into consideration, that two non-interacting drugs acquire changes in their potency (the amount of compound that is needed to produce a certain effect) when combined. This change in the drugs potency is best observed when different concentration of the drugs are tested. In this model synergy is calculated by comparing the changes in potency of the dose-response curves.

Before analysis the optimal dose range and the IC50 values were determined for each cell line individually. ADORA3 agonist or AKT inhibitor (Drug 1) and HDACis (Drug 2) combination screens were performed in 5 × 6 dose-response matrices or as indicated. All tested cell lines were treated with drugs one and two at the indicated concentrations.

Drug synergy scores (δ-scores) were generated using the online version of SynergyFinder 2.0 (141-144). The degree of a drug combination effect or synergy is visualized as an interactive landscape over the dose matrix. To show the average of all δ-scores over the dose-response matrix Δ-values were calculated. An overall synergy score (Δ-value) lower than -10 is considered an antagonistic combination, between -10 and 10 is considered additive and above 10 synergistic. (https://synergyfinder.fimm.fi/synergy/synfin_docs/).

2.2.12. Tissue Microarray Staining

TMA from paraffin blocks was retrieved from the Institute of Pathology archives at the University of Tuebingen as previously described (145). The ethics committee of the Medical Faculty approved this analysis (880/2020BO2). The stainings were performed at the Institute of Pathology in Tuebingen. Briefly, the analysis included samples from 36 patients with HCC and 51 patients with CCA. For each patient, a total of 3 slides representing tumor tissue and three slides with normal liver tissue were investigated. For immunohistochemistry, the primary antibody ADORA3 (Signalway antibody) was applied. Tissue sections were pretreated with EDTA buffer solution (pH 8.6) at 95 °C for 32 min. The detection kit required for staining was the OptiView DAB. The detection of ADORA3 was analyzed per high power field (magnification x400), and for the semi-quantitative evaluation, a score between 0 (no ADORA3 detectable) and 3 (strong ADORA3 signal) was attributed to each evaluable tissue core. In case of a discrepancy between the scores of evaluable slides, the patient sample's highest score was taken.

2.2.13. Immunofluorescence staining of cells

Tumor cells were grown on sterilized coverslips in 12-well plates. For staining, media was removed, and the wells gently washed with prewarmed PBS. The cells were then directly fixed with 70 % ethanol for 15 min. After fixation, cells were permeabilized and blocked with a solution of 10% goat serum and 0.1 % Tween 20 for 20 minutes at RT and then stained at 4 °C overnight with the primary

antibody ADORA3 (rabbit) diluted in blocking buffer. The primary antibody was removed, and the wells were washed thrice. Thereafter, the secondary antibody FITC-conjugated goat anti-rabbit antibody was applied for one hour in the dark at RT. After further washing, DAPI was added for nuclear staining. The images were acquired using the laser scanning confocal microscopy Zeiss LSM 710.

2.2.14. Short Interfering (si-) RNA mediated Gene Knockdown

For si-RNA experiments, cells ($4x10^5$) were seeded in 6-Well-Plate and allowed to grow up to 70 % confluent. After 24 h, cells were transfected using Silencer® Select ADORA3 siRNA (Cat. AM16708, Thermo Fischer Scientific) and Lipofectamine 3000 reagents (Cat. No. L3000015, ThemoFisher Scientific) according to the manufacturer's instructions. Briefly, 7.5 µl Polyfectamine 3000 reagent per well was diluted with 250 µl of serum-free medium for 10 min at room temperature. 100 µM siRNA stock was generated by adding 50 µl RNAse-free H_2O to 5 nmol siRNA. A final concentration of 800 nM siRNA per well was used. siRNA master mix was prepared by diluting siRNA to serum-free medium and P3000™ Reagent (250 µl/well). Polyfectamine solution (250 µl) was added to the diluted siRNA. After incubation for 15 min at room temperature, the DNA-lipid complex was added to each well containing 0.5 ml of complete medium. The final volume was 1 ml. After 48 h of incubation at 37 °C medium was changed, and transfected cells were treated accordingly for another 72 h.

2.2.15. RNA-Seq Analysis and Bioinformatics

Transcriptome analysis was performed after total RNA extraction and purity control as described in the section 6.2.9. Analysis was further performed using the Flow-Cell (400 Clusters, 75 BP, single-ended) reverse transcription technique (146) and Illumina Sequencing on an Illumina MiSeq machine at the Department of Medical Genetics and Applied Genomics, University Hospital Tuebingen, according to the manufacturer's guidelines. Bioinformatic and differential

expression analyses were performed in cooperation with the Quantitative Biology Center (QBIC) at the University of Tuebingen.

The Nextflow-based nf-core RNA-Seq pipeline release 1.3 https://github.com/nf-core/rnaseq1 was used for the bioinformatics analysis. An aggregation of the bioinformatics workflow analysis was conducted by MultiQC v1.72 (147). FASTQC3 (148) was used to determine quality of the FASTQ files. Subsequently, adapter trimming was conducted with Trim Galore v0.5.04 (149). STAR v2.6.1d (150) aligner was used to map the reads that passed the quality control to the human genome GRCh 38 (Ensembl release 92). The evaluation of the RNA-seq experiment was performed with RSeQC v3.0.0 (151) and read counting of the features (e.g. genes) with featureCounts v1.6.4 (152) For differential expression analysis, the raw read count table resulting from featureCounts is processed with the R package DESeq2 v1.22.1 (153). Graphs were also produced in the RStudio v1.1.456 with R version 3.5.1 (2018-07-02) mainly using the R package ggplot2 v3.1.1. Final reports were produced using the R package rmarkdown v1.13, with the knitr v1.22 and DT v0.6 R packages. The sample similarity heatmap was created using the edgeR R package.

Gene set enrichment analysis (GSEA) is a computational tool used to identify functional enrichment by comparing genes of interest with predefined gene sets. A gene set is a group of genes that shares localization, pathways, functions, or other features. Gene set enrichment analysis (GSEA) was performed using the Bioconductor package fgsea (154). All human gene sets from Molecular Signatures Database (MSigDB) gene sets (155) were examined. The p-value (<0.05) and the false discovery rate (FDR) <0.2, were used to select statistically significant gene sets.

The analysis of active transcriptional binding sites was performed as previously described (156, 157). Briefly the g:PROFILER web tool uses regulatory motifs of the TRANSFAC database version 2015.3 and compares it to the input gene list to make computational predictions of binding sites in gene promoters.

2.2.16. TCGA-LIHC RNA-Seq tissue biopsy data

Through the recount2 project portal, gene counts (version 2) of the TCGA-LIHC cohort were obtained (https://jhubiostatistics.shinyapps.io/recount/) (158). Samples from patients were used only when both HCC and adjacent healthy liver tissue samples were available. Thus in total, 50 HCC samples and 50 adjacent healthy tissue samples were included in the analysis. For the differential expression analysis, the R package DESeq2 v1.30.1 with R version 4.0.3 was used. The p-values were corrected for multiple testing using the Benjamini-Hochberg method (159) For the plot, the gene counts were converted to transcript per million (TPM) values by utilizing the median transcript length for each gene, determined using GTFtools (160). The plots were created using the Python package seaborn v0.10.1 with Python version 3.8.3.

2.2.17. Statistical analysis

When comparing multiple groups, p values were calculated with a two-way analysis of variance. An unpaired t-test was used to determine statistical differences between two groups compared once. Other statistical tests used are specified in the Results section and the figure legends. All analyses were performed using GraphPad Prism v.8.0 (GraphPad Software, Inc., La Jolla, CA, USA). Results in the figures are expressed as mean values with their standard errors. In all presented figures, p-values > 0.05 were marked as non-significant (n. s.), and p-values $\leq$ 0.05 were considered as statistically significant differences and indicated accordingly.

3. Results

3.1. Adenosine receptor 3 modulation in liver cancer

3.1.1. Heterogeneous level of ADORA3 in healthy liver, HCC and CCA tissues

To explore the role of ADORA3 in HCC and CCA we investigated its presence in HCC and CCA patient-derived tissue samples by an immunohistochemical analysis.

This experiment was performed in cooperation with the Institute of Pathology at the University Hospital in Tuebingen.

We used tissues microarrays (TMAs) of patients with HCC and CCA and stained them for ADORA3. The semiquantitative analysis comparing triplicates, differentiated between “strong” (3), “moderate” (2), “weak” (1) and “negative” (0) (Fig. 5). Briefly, the highest stain and thus the highest number in the set of 3 replicates was chosen for each patient. Notably, most of the normal 81 liver samples had a “strong” (3) receptor level and no normal liver tissue was graded as “negative” (0). Surprisingly, in contrast to a published assumption, both tumor types, HCC (n=36) and CCA (n=50) showed a heterogeneously distributed level of ADORA3 expression (Fig. 6). Most notably we even found that some HCC and

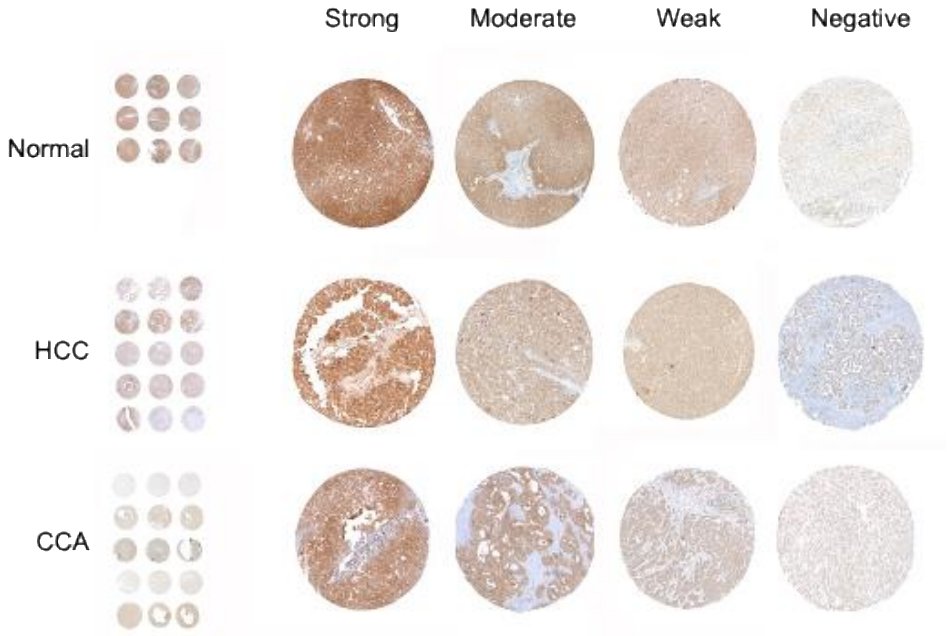

Figure 8 Tissue Microarray (TMA) of patient-derived samples of HCC and CCA tumors. TMA were stained for ADORA3 expression and scored semi quantitatively with negative, weak, moderate, and strong. Representative stains out of triplicates are shown as an example. Pictures for this analysis were taken at the Institute of Pathology of the University Hospital Tübingen.

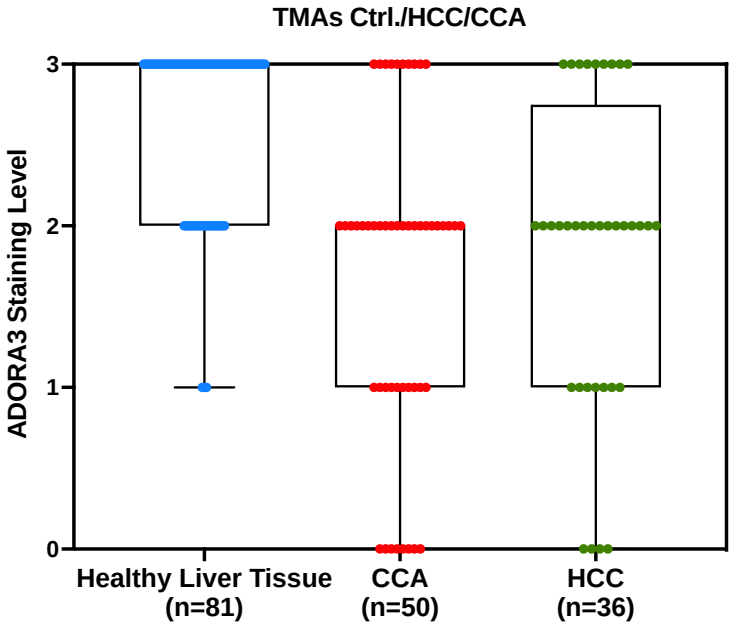

Figure 9 Comparison of semi quantitative stainings for ADORA3 expression between healthy liver tissue, CCA and HCC samples. Data represent the average of individual semiquantitative scores between 0 (negative), 1 (weak), 2 (moderate) and 3 (strong) for ADORA3 staining of normal liver (n=81), CCA (n=50) and HCC (n=36) samples. The result of each sample is shown.

CCA patients did not expressed the receptor at all. Since our observation was in contrast to the hypothesis that ADORA3 is overexpressed in tumors compared to normal tissue (161), we wanted to explore whether we would have similar findings using a different experimental setting. We therefore investigated on the gene

expression of ADORA3 using TCGA patient data and RNA-Seq tissue biopsy data (Fig. 7 A/B).

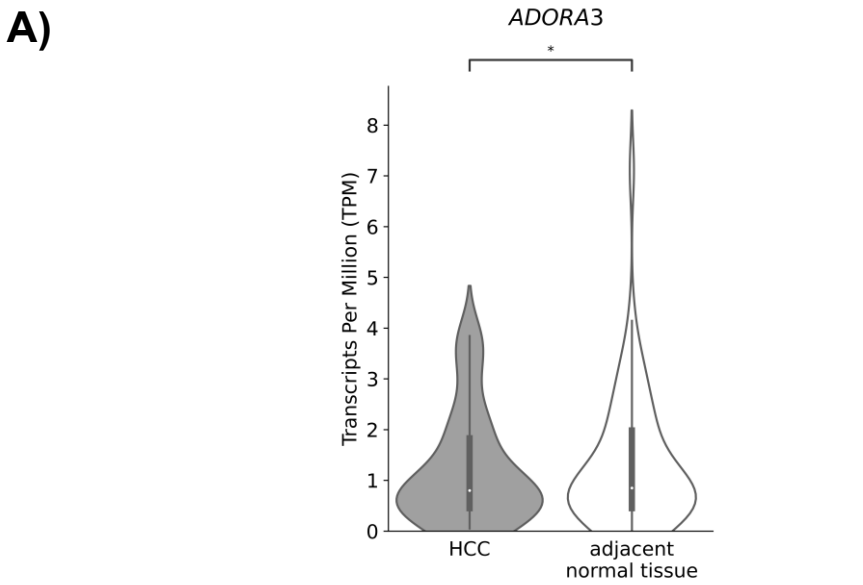

*Figure 10 Comparison of ADORA3 m-RNA expression in different tissue samples. A) TCGA-LIHC cohort violin blot analysis of 50 normal tumor adjacent tissue and 50 tumor tissue samples from HCC patients. Gene counts were exported from the recount2 project portal. For the differential expression analysis, the R package DESeq2 was used. Gene expression data is shown as transcripts per million (TPM). The p-values were corrected for multiple testing using the Benjamini-Hochberg method. Statistical analysis indicate a significant difference between both cohorts ($p < 0.05$ = *) (B) ADORA3 expression in RNA-Seq liver tissue biopsies in normal liver (n=13), tumor adjacent liver tissue (n=117) and tumor (n=121). Gene expression data is shown as TPM. Statistical analysis was performed using one-way ANOVA. Asterisk indicates that the differences are not significant (ns).*

The TGCA-LIHC analysis of a public available data source was performed in collaboration with the quantitative biology center (QBIC) and biopsy data from

patients were generated at the Department for Biomedicine in the group of Prof. Dr. Markus Heim, Basel, Schweiz, and analyzed by myself during my research stay at the laboratory in Basel.

Data are presented as transcripts per million (TPM), which is the relative abundance of a transcript among a population of sequenced transcripts. Figure 7A shows a significant difference between HCC and adjacent tumor tissue. Of note, the gene coding for ADORA3 was observed to be significantly ($p<0.05$) more expressed in the normal adjacent tissue. Figure 7B further shows that there was no significant expression of the ADORA3 gene when comparing normal liver tissue versus tumor samples or tumor adjacent liver tissue versus tumor samples. These results support the observation that the ADORA3 gene is not generally overexpressed in HCC.

3.1.2. ADORA3 is ubiquitously expressed in HCC and CCA derived established cell lines.

The first results indicate that ADORA3 is not generally overexpressed in CCA or HCC tissues. To investigate on the molecular mechanistic trigged after ADORA3 activation we first aimed to test and identify which HCC and CCA cell lines synthesized ADORA3 proteins. Using western blot analysis, we explored ADORA3 protein levels in three different HCC (Huh7, JHH1 and HepG2) and three different CCA (HUCCT1, RBE, TFK1) human derived established cell lines.

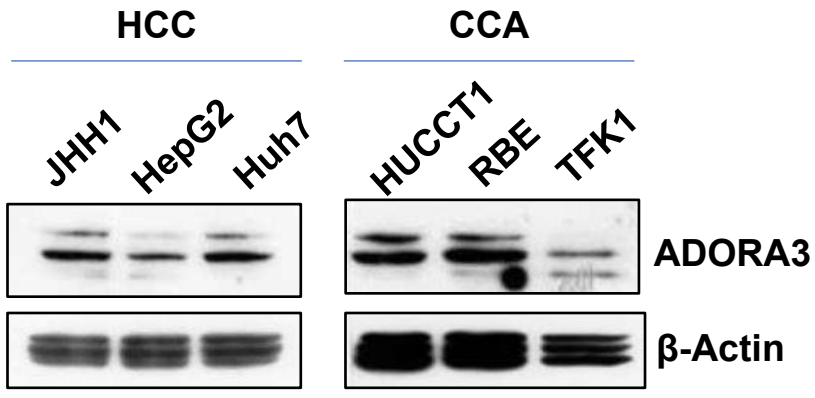

Figure 11 Western Blot analysis of ADORA3 (upper row) in different HCC (JHH1, HepG2, Huh7) and CCA (HUCCT1, RBE, TFK1) cell lines. Cells were grown in dishes then protein extraction and western blot analysis was performed. Equal protein loading was verified by beta actin staining (lower row).

We could demonstrate the presence of ADORA3 in all cells tested (Fig. 8).

We further performed immunocytochemical stains of HepG2 and Huh7 cells (Fig. 9). We could show that both cell lines expressed ADORA3, which supports our previous observation. To sum up, we concluded that all cell lines were suitable models to explore ADORA3 activation.

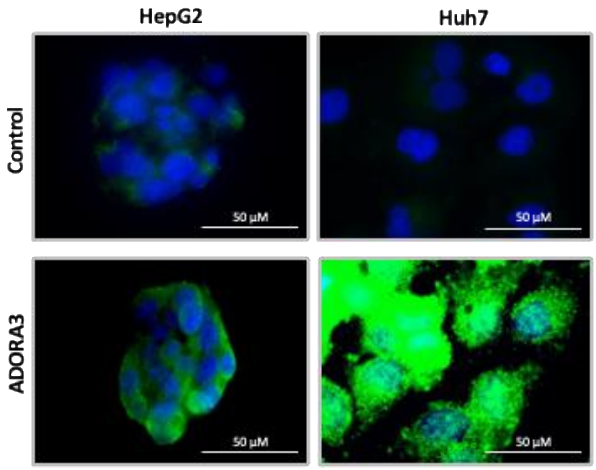

Figure 12 Immunocytochemical analysis of ADORA3 (green) in HCC cell lines HepG2 and Huh7. Cells lines were seeded on coverslips, fixed, blocked and stain with a primary antibody for ADORA3. For controls the primary antibody was omitted. After incubation with the primary antibody and a washing step, the secondary antibody was added to all cells. Thereafter nuclei were stained using DAPI (blue). Pictures were taken using laser scanning confocal microscopy Zeiss LSM 710. Original magnification 40x.

3.1.3. ADORA3-activation mediates antiproliferative effects of Namodenoson in HCC and CCA derived established cell lines.

We next investigated the cellular response to ADORA3 stimulation using the specific ADORA3 activator Namodenoson. To examine the effects of Namodenoson on liver cancer cell proliferation we firstly performed dose-response studies.

A)

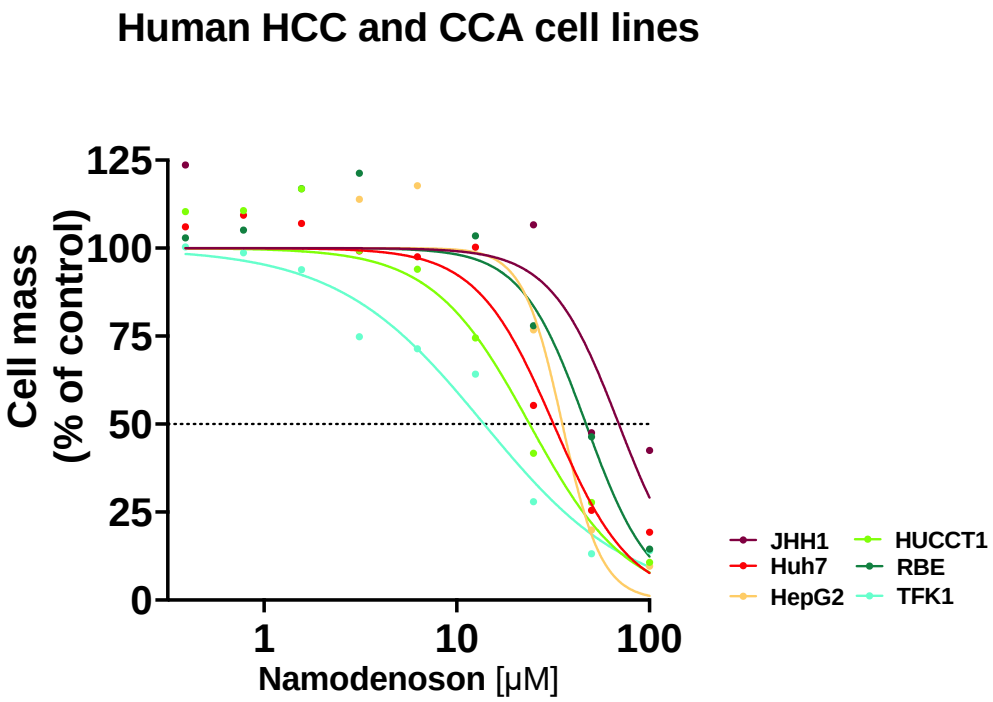

B)

IC50 Value Human HCC and CCA cell line			
HCC (95% CI)		CCA (95% CI)	
JHH1	69.3 (38.9 – 177.5)	HUCCT1	23.9 (17.3 – 33.5)
Huh7	31.8 (25.6 – 40.3)	RBE	46.8 (33.6 – 66.7)
HepG2	35.3 (24.1 – 54.2)	TFK1	13,9 (11.9 – 15.9)

Figure 13 (A) Dose dependent antiproliferative effect of Namodenoson (Namo.) on HCC- (HepG2, Huh7, JHH1) and CCA-derived cell lines (HUCCT1, RBE, TFK1) investigated by SRB assay. Cells were seeded overnight, and varying concentrations (0.39, 0.78, 1.56, 3.12, 6.25, 12.5, 25, 50, and 100 µM) of Namodenoson were added to each well for 72h. The percentage of the cell mass as a surrogate marker for proliferation was determined. The curves were automatically fitted using nonlinear regression with GraphPad Prism. Nonlinear regression was constrained to 100 for the top and 0 for the bottom. Thereafter IC50 values were calculated. The dashed line represents the IC50. The dots represent the average of four independent values gained for each treatment condition. (B) Calculated IC50 values of Namo. treatment.

For these experiments we applied the sulforhodamine B (SRB) assay, which was developed by Skelan and colleages to measure drug-induced cytotoxicity and cell proliferation (137, 162). As a surrogate marker for cellular proliferation, the cell

mass was determined after 72 h of drug treatment and relative to DMSO treated control cells.

As shown in Figure 10 all cell lines showed a concentration dependent decrease in cell mass (Fig. 10A) with IC50 values ranging from 13.9 µM for TFK1 to 69,3 µM for JHH1 (Fig. 10B). Since the presented study aims to combine minimal effect doses of compounds, we defined the minimal concentration range as the minimum drug concentration needed to activate the receptor and generate a cell mass reduction of about 10 – 20 %. The results obtained therefore suggest that for all cell lines, Namodenoson minimal effect concentration ranges between 5 – 20 µM. 10 µM was therefore chosen as a suitable average concentration for the following experiments.

3.1.4. Namodenoson mediated antiproliferative effect in HCC and CCA cell lines is fully receptor dependent

To exclude off target effects, we next investigated whether the observed antiproliferative effect of Namodenoson depended on the receptor. In order to do so, we performed two inhibitory assays in HCC (HepG2) and CCA (HUCCT1) cell lines.

Firstly, we pretreated the cells with MRE3008F20 (MRE.), a specific ADORA3 receptor antagonist. We then added Namodenoson and incubated the cells for 72h. We performed SRB assays and assessed, whether we could inhibit the Namodenoson antiproliferative effect. For this analysis we used MRE. concentrations that did not significantly affected the cell lines proliferation as single treatment: for HepG2 concentrations up to 0.03 µM, and for HUCCT1 concentrations up to 0.1 µM did not influence the SRB results (Fig. 11).

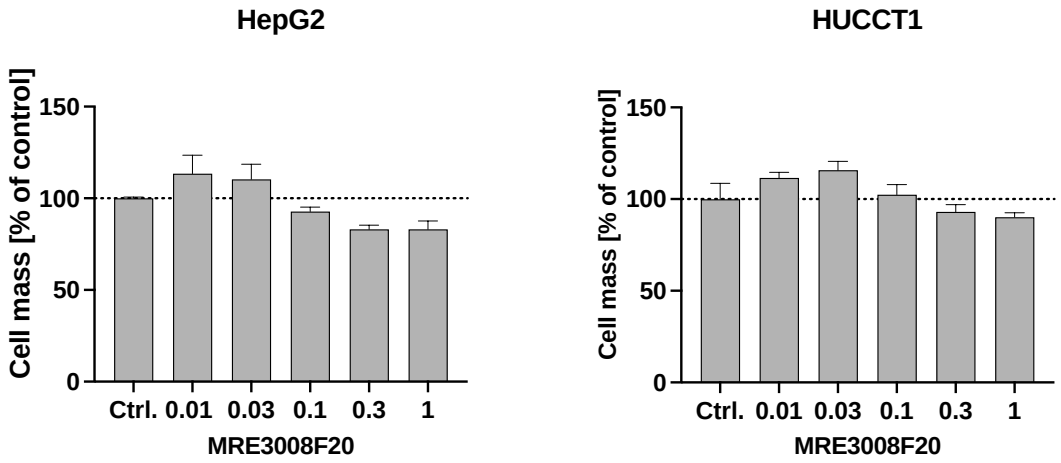

Figure 14 Dose response study with specific ADORA3 antagonist MRE3008F20. HepG2 and HUCCT1 cells were seeded overnight and thereafter treated with different concentrations (0.01, 0.03, 0.1, 0.3, 1 µM) of MRE3008F20 for 72 h. Cell mass was determine via SRB assay. Data represent standard error of the mean of three independent experiments.

As an important result, we found that the antagonist could significantly inhibit the antiproliferative effect observed with 10 µM Namodenoson in HepG2 ($p<0.01$) and HUCCT1 ($p<0.05$) cells (Fig. 12). In both cell lines Namodenoson inhibited cell proliferation up to 30 %. This effect was not observed in the combination with MRE.

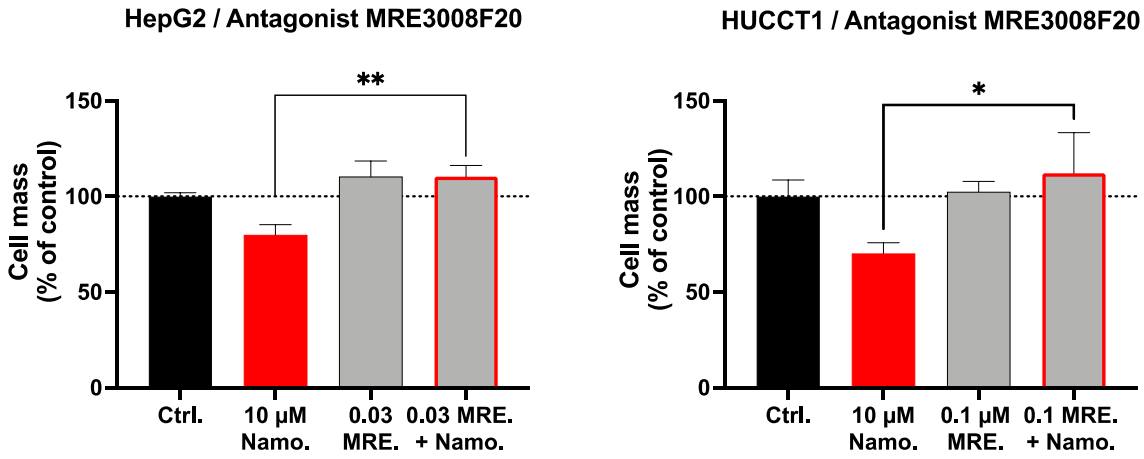

Figure 15 Co-treatment of Namodenoson (Namo.) with the specific ADORA3 antagonist MRE3008F20 (MRE.). For drug combination experiments, cells were pretreated with 0.03 µM (HepG2) and 0.1 µM (HUCCT1) of antagonist MRE3008F20 for 30 minutes before treatment with 10 µM Namo. or solvent as control for 72h. The cell mass as a surrogate marker for proliferation was determined via SRB assay. Data represent standard error of the mean of three independent experiments. Statistical analysis was performed using unpaired t-test comparing Namodenoson to the combination of Namo. + MRE3008F20 (= p <0.05; ** = p<0.01)).*

Secondly, we knocked down the receptor using RNAi technology and assessed whether we could inhibit the antiproliferative effect of Namodenoson.

Of note, ADORA3 siRNA prevented the antiproliferative effect of Namodenoson in both cell lines (Fig. 13). This result supports our first observation. To sum up we presented evidence, that the effect of Namodenoson on cellular proliferation was directly dependent on ADORA3.

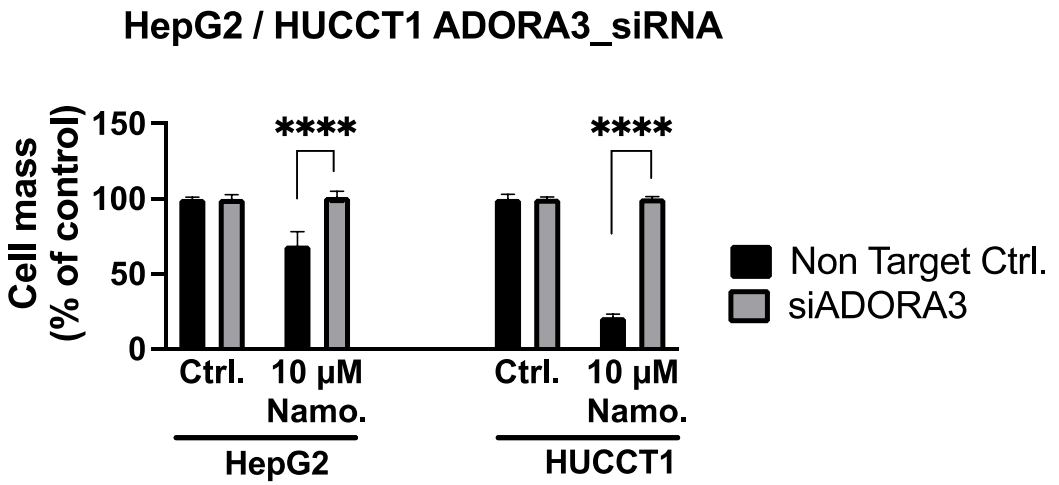

*Figure 16 The antiproliferative effect of Namodenoson (Namo.) can be blocked by silencing ADORA3 using siRNA. HepG2 and HUCCT1 cells were transfected with ADORA3 siRNA (siADORA3) or scrambled control (Non-Target Ctrl). 48 h after transfection, cells were treated with 10 µM Namo. or DMSO solvent as control (Ctrl.) for 72 h. The cell mass as a surrogate marker for proliferation was determined via SRB assay. Data represent standard error of the mean of three independent experiments. Statistical analysis was performed using 2way ANOVA with Šídák's multiple comparisons test (**** = p<0,0001).*

3.1.5. ADORA3 stimulation induces chromatin-modifying events

The mechanism of action of Namodenoson on liver cancer cells is only partly understood so far. To learn more about potential mechanisms, which could help to identify patients that are suited for an ADORA3 stimulatory drug treatment or to identify possible new combination treatments, RNA-Seq was performed. RNA-Seq data on how ADORA3 agonist Namodenoson alter the transcriptome of tumor cells, has not been described yet.

Therefore, we performed a gene expression analysis in HepG2 cells treated with Namodenoson for 24 or 36 hours (Fig. 14A). Of the 36,521 mapped gene tags in HepG2 cells 682 genes (338 genes upregulated and 344 genes downregulated) were differently expressed after 24 h and 940 genes (445 upregulated and 495 downregulated) were differently expressed after 36h when comparing Namodenoson treated cells to DMSO treated controls. Both treatment timepoints shared 525 genes (Fig. 14B). Genes were considered differentially expressed

(DE) when the adjusted p-value was lower than 0.05 (padj < 0.05) and a log2FC of greater than 0.5 or lower then -0.5.

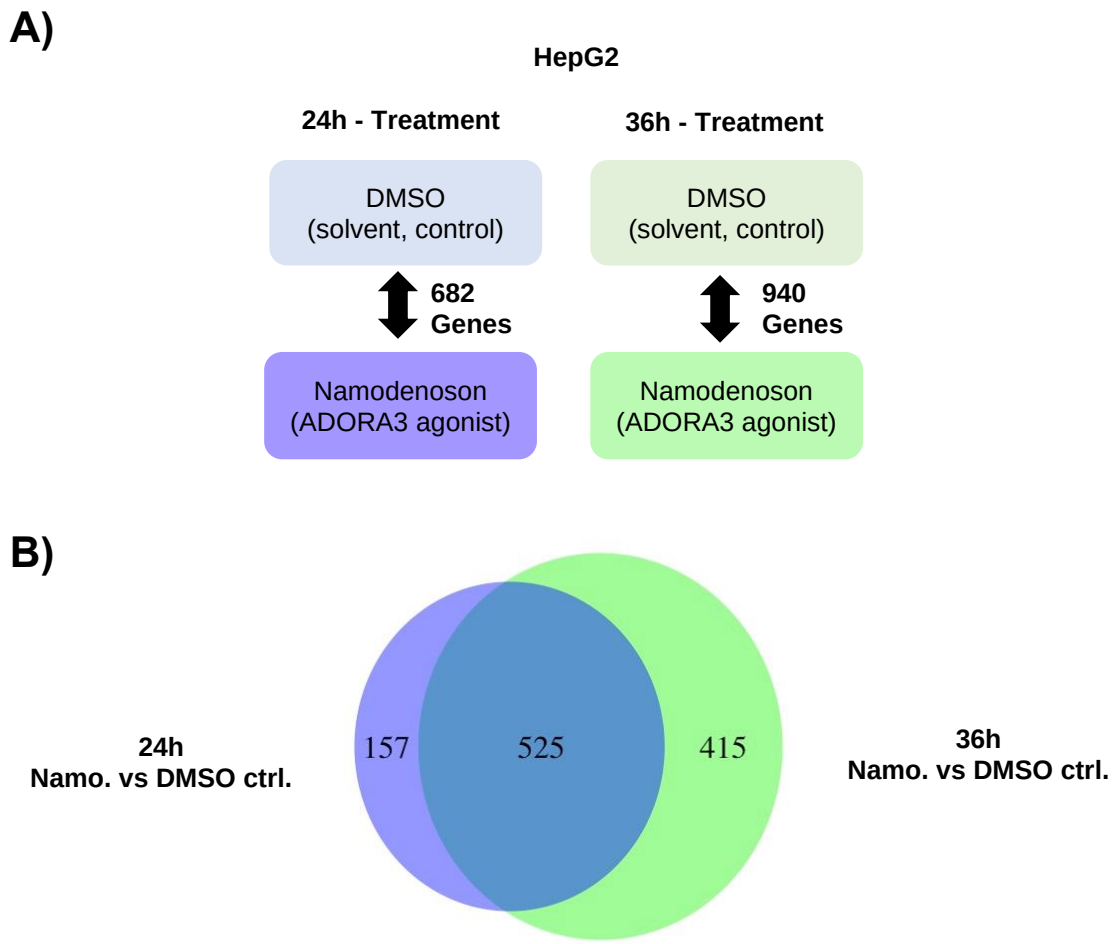

Figure 17 Overview of RNA-Seq analysis in HepG2 cells. (A) Experimental scheme of RNA-Seq analysis and number of deregulated genes; 24h (blue) or 36h (green). (B) Venn diagram showing the amount of differently expressed genes after 24h (682 – blue circle) and 36h (940 - green circle) and the overlapping area, indicating the number of shared genes (525).

Considering the profound alteration in gene expression within the first 24 h after treatment with Namodenoson and the common regulation pattern between the 24 h and 36 h batch, which is assumed due to the high number of shared genes, we postulated that the observed alteration in gene expression may be due to changes in the amount of available transcription factor binding sites (TFBSs). To investigate on this assumption, we performed a computational approach using the g:PROFILER online tool, to predict the changes in TFBSs after the treatment with Namodenoson (156, 157). The differentially expressed genes found after

24 h (682) and 36 h (940) were used as query entry. In our query 84 TFBSs were predicted after the treatment with Namodenoson for 24 h. 209 TFBSs were predicted for the 36 h timepoints. Of note, out of the activated 84 TFBSs found after 24h of treatment 77 were also seen in the 36 h treatment batch (Fig. 15). These results support the assumption that major changes in the transcriptional machinery might be initiated within the first 24 h. In conclusion, the results underscored that the first 24 h are crucial in Namodenoson way of action and further they indicated that Namodenoson triggers remodeling events, that can lead to an increased number of TFBSs.

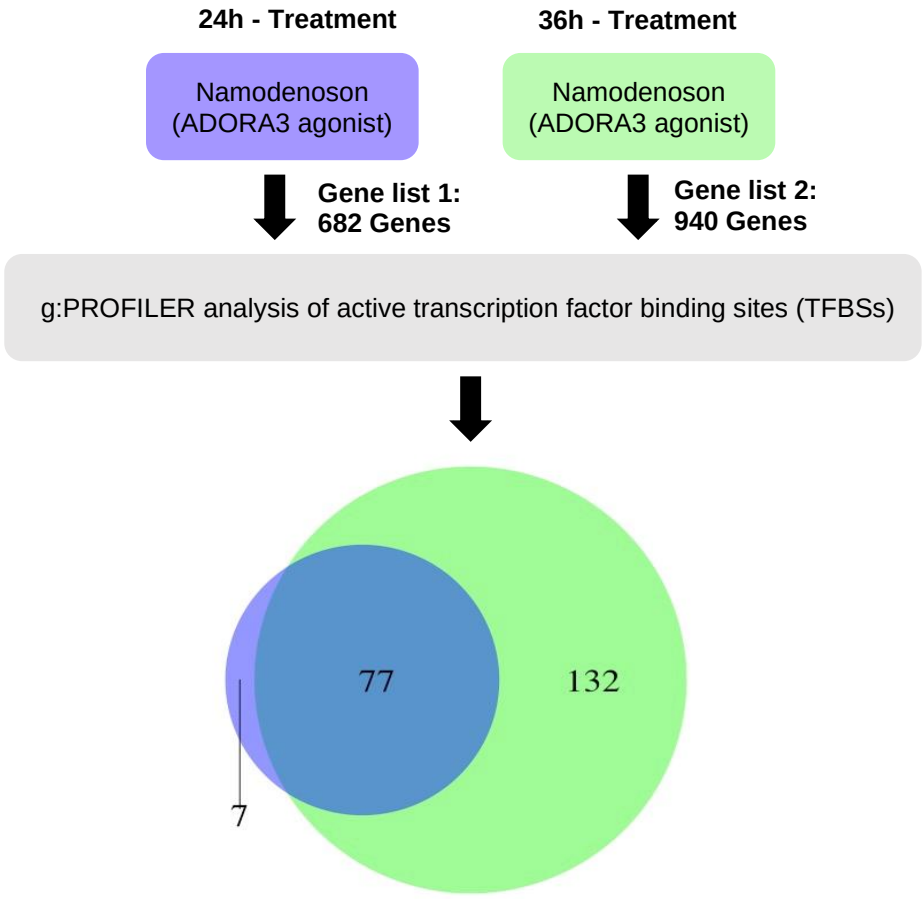

Figure 18 g:PROFILER analysis of active transcription factor binding sites(TFBSs) after treatment with Namodenoson for 24h or 36h. The gene list of differentially expressed genes generated after each treatment timepoints where taken as Input for the g:PROFILER query. Gene list 1 form the 24 h treatment (blue) generated 84 TFBSs and gene list 2 from the 36h treatment (green) generated 209 TFBSs. Both Timepoints had 77 TFBSs in common.

The previous result implied that Namodenoson triggers remodeling events. We therefore postulated that Namodenoson might lead to changes in chromatin state

via epigenetic remodeling events. To assess this assumption, we performed a gene set enrichment analysis (GSEA) (163) of the differentially expressed (DE) genes at 24 h with a focus on epigenetic pathways. Here we investigated the first point in time namely 24 h, since our previous results indicated that within the first 24 h over 500 genes are regulated and TFBS increased, implying a very crucial time for Namodenoson way of action. Considering all analyzed gene sets, our GSEA query revealed 18 functional gene sets associated with epigenetic regulation pattern with p-value of < 0.05, and normalized enrichment score (NES) of < -1.8 or > 1.8 and a false discovery rate of < 0.2. (Table. 8). Interestingly all gene sets had a negative NES which shows their downregulation during the treatment with Namodenoson.

Table 8. Gene set enrichment analysis of hallmark gene sets and curated gene sets for identification of enriched pathways. Query entry was based on all 682 significantly altered genes when comparing Namodenoson treatment versus DMSO after 24 hours. 18 Gene sets were identified. p-value (p-val.), FDR (false Discovery Rate, adjusted p-value) normalized enrichment score (NES).

Gene Set Enrichment Analysis (GSEA) - Significantly regulated gene sets associated with epigenetic events.			
Gene Set Name	**p-val**	**FDR**	**NES**
SENESE_HDAC1_TARGETS_UP	4,32E-07	7,28E-04	-2,75
PASINI_SUZ12_TARGETS_DN	5,01E-06	4,03E-03	-2,61
LU_EZH2_TARGETS_DN	8,32E-05	2,13E-02	-2,33
SENESE_HDAC1_AND_HDAC2_TARGETS_UP	2,35E-04	3,30E-02	-2,30
PRC2_EZH2_UP.V1_UP	5,51E-04	5,57E-02	-2,22
KHETCHOUMIAN_TRIM24_TARGETS_UP	9,26E-04	7,44E-02	-2,12
ACEVEDO_METHYLATED_IN_LIVER_CANCER_DN	1,15E-03	8,11E-02	-2,03
SATO_SILENCED_BY_METHYLATION_IN_PANCREATIC_CANCER_1	1,51E-03	9,44E-02	-2,08
MISSIAGLIA_REGULATED_BY_METHYLATION_UP	1,74E-03	1,02E-01	-2,04
SENESE_HDAC3_TARGETS_UP	1,79E-03	1,03E-01	-2,05
GSE27434_WT_VS_DNMT1_KO_TREG_DN	2,07E-03	1,09E-01	-1,96
LIU_SMARCA4_TARGETS	2,50E-03	1,22E-01	-1,94
WANG_SMARCE1_TARGETS_DN	4,90E-03	1,66E-01	-1,89
HELLER_HDAC_TARGETS_SILENCED_BY_METHYLATION_DN	7,43E-03	1,97E-01	-1,85

GSE26488_WT_VS_HDAC7_KO_DOUBLE_POSITIVE_THYMOCYTE_DN	7,14E-03	1,95E-01	-1,82
HENDRICKS_SMARCA4_TARGETS_UP	9,01E-03	2,11E-01	-1,86
CHICAS_RB1_TARGETS_SENESCENT	3,75E-03	1,47E-01	-1,99
CHICAS_RB1_TARGETS_CONFLUENT	4,89E-03	1,66E-01	-1,87

Four of the identified gene sets were highly significant with an FDR of < 0.05 (Fig. 16, Table 8). The y-axis of the enrichment plots represents the NES. The dashes on the upper x-axis represent the genes included in the respective gene set. Their distribution from left (control site) to the right (Namodenoson site) shows that for SENESE_HDAC1_TARGETS_UP, PASINI_SUZ12_TARGETS_DN, SENESE_HDAC1_AND_HDAC2_TARGETS_UP, most genes are only found at the right site, meaning that the genes in those sets are only regulated in the Namodenoson batch and not in the control. The genes included in the set LU_EZH2_TARGETS_DN were found to be more distributed along the upper x-

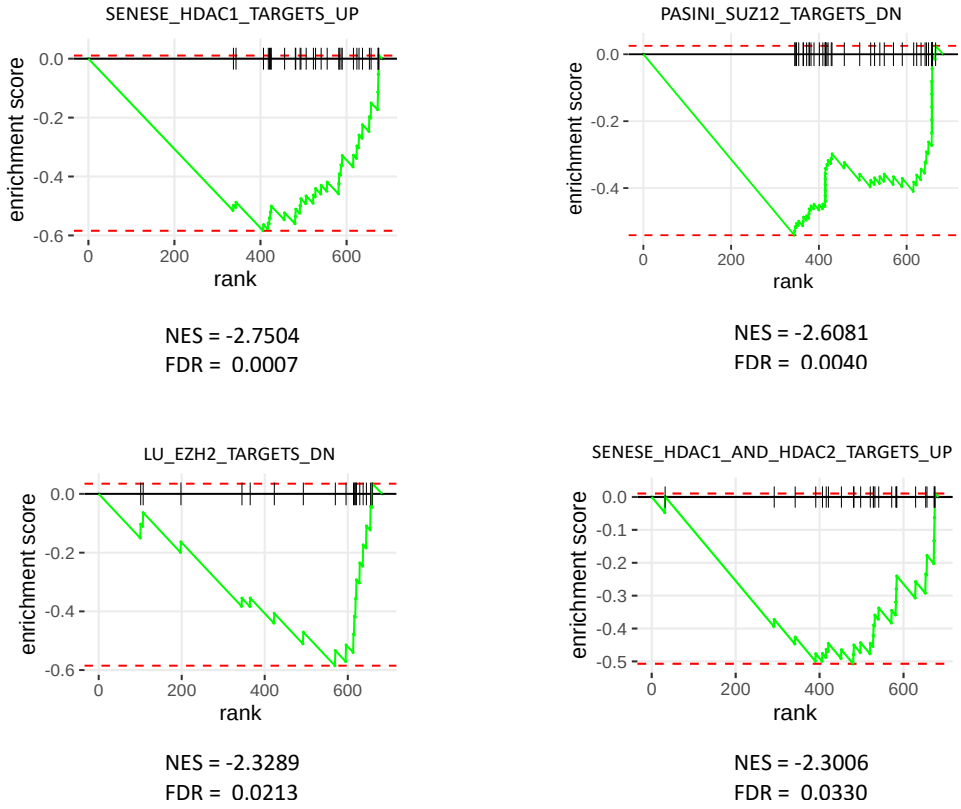

Figure 19 Gene Set Enrichment Analysis (GSEA) of RNASeq analysis after treatment with Namodenoson after 24 h. Shown are enrichment plots of the four significantly downregulated gene sets associated with epigenetic events. Gene sets were considered significant with a false discovery rate (FDR) < 0.05 and a normalized enrichment score (NES) > 1.8.

axis of the enrichment plot. This implies that in in both control and Namodenoson batch genes were found to be downregulated. Nevertheless, when comparing, more genes were only regulated with Namodenoson (Fig. 16). To conclude, the four presented enrichment plots illustrate that most of the genes included in the gene sets are only regulated with Namodenoson. Interestingly the downregulation of those gene sets is associated with an increased transcriptional activity (164-166).To sum up, our GSEA analysis supported the hypothesis that the stimulation of ADORA3 by Namodenoson leads to changes in genes that play a crucial role in the context of epigenetic modifications. Of note, two of the gene set indicate a regulation of histone deacetylases.

Well-known enzymes in epigenetic regulations are histone deacetylases. Since or previous results implied a regulation of histone deacetylases, we wanted to investigate whether Namodenoson has an influence on the cellular expression of HDACs. Therefore, as the next step, we treated HepG2 cells with different concentrations of Namodenoson and analyzed the expression of HDAC1 to HDAC11 using qPCR (Fig. 17).

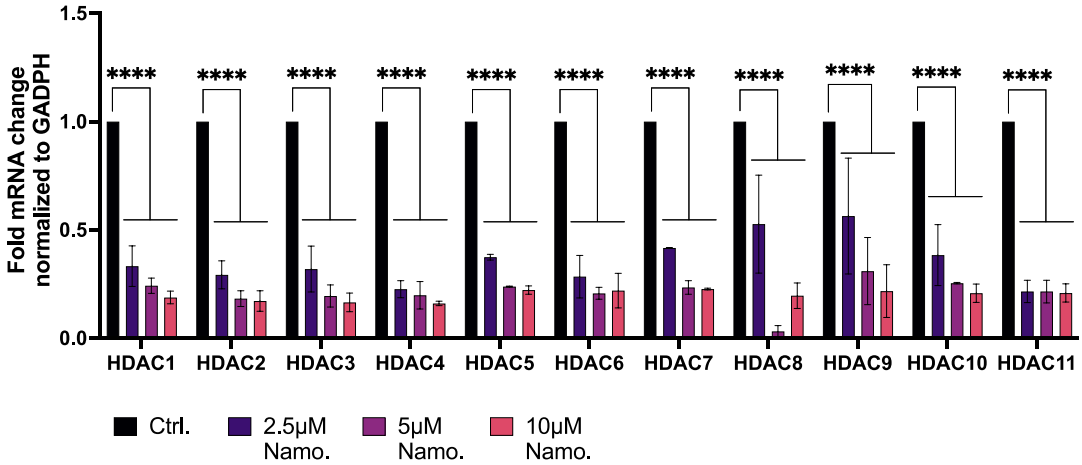

*Figure 20 Real-time PCR analysis of HDAC 1 – 11 mRNA in HepG2 cells treated with rising concentrations of Namodenoson (2.5, 5, 10 µM) for 24 h. Data represent standard error of the mean of three independent experiments. Statistical analysis was performed using 2way ANOVA with Dunnett's multiple comparisons test (**** = p<0,0001).*

Surprisingly, as results, we found a broad regulation pattern that involved all investigated HDACs with a downregulation after Namodenoson treatment independent of its concentration.

One of the mechanisms of action of HDACs is to reverse the acetylation of lysine residues on histones H3, which leads to an inactive or close state of chromatin,

and subsequently prevents transcription factors access to the promoters of target genes.

As a next step, we therefore investigated, whether the observed inhibition of HDACs via Namodenoson is reflected by an increased acetylation of histone H3. We determined the histone-H3 acetylation by Western Blot analysis (Fig. 18) and observed an increased level in histone H3 acetylation after the treatment with increasing concentrations of Namodenoson. In HepG2 cells the level of acetylated H3 proteins already increased during treatment with 5 µM Namodenoson. The same was observed in RBE cells with 10 µM Namodenoson. An increased alteration in H3 acetylation was still observed when the Namodenoson concentration was elevated to 20 µM, even though it did not quantify as significant for HepG2. Overall, we could show that Namodenoson treatment increased histone H3 acetylation, which is in line with a reduced activity of HDACs.

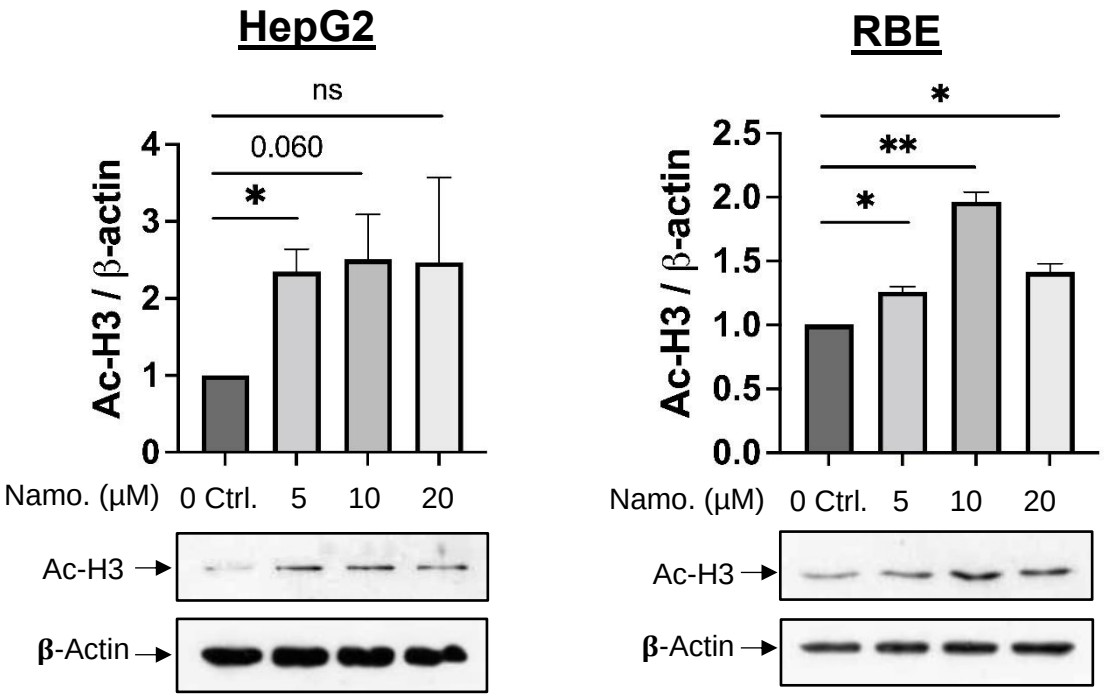

Figure 21 Western blot analysis and quantification of histone 3 acetylation (Ac-H3) in HepG2 and RBE cells after 24 h of treatment with rising concentrations (0, 5, 10,20 µM) Namodenoson. (Upper part) Quantification of three (HepG2) or two (RBE) independent replicates. (Lower part) Representative Western blots. Arrows indicate the protein of interest. Statistical analysis was performed using unpaired t-test comparing treatment to DMSO control (ctrl.) (= p <0.05; ** = p<0.01, ns= not significant).*

To sum up, we found that Namodenoson triggers epigenetic remodeling processes, by inhibiting histone deacetylation, which might primarily lead to an open chromatin state and an increased number of TFBSs, which may in turn play an important role in the observed increased in gene expression.

3.1.6. Inhibition of HDACs and ADORA3 stimulation synergize to inhibit cell growth in HCC and CCA cells

We next explored the effects of Namodenoson co-treatment to approved inhibitors of histone deacetylases (HDACi). Since Namodenoson diminishes HDAC transcription, we assumed that pharmacologically inhibiting HDACs might enhance this effect and therefore HDAC inhibitors could be an interesting co-treatment approach to the stimulation of ADORA3. Several HDAC inhibitors (HDACis) are already approved for the treatment of mainly hematological disorders, therefore a combination treatment could easily be translated to clinical studies.

First, we performed dose-response studies to assess the cellular response of our cells to the treatment with different HDACis (Fig. 19). Four well studied HDACis were chosen: Resminostat (73), Vorinostat (167), Belinostat (68) and Romidepsin (168). All cell lines showed a concentration dependent decrease in cell mass after treatment, independently of the HDACi used. To determine a minimal effective concentration range for further combination experiments, the IC50 values were calculated. The IC50 values ranged between 1.6 – 2.1 µM for Resminostat, 1.1 – 1.5 µM for Vorinostat 0.5 – 0.7 µM for Belinostat and 2.8 – 8 nM for Romidepsin (Fig. 19B). We observed that concentrations of about 1 µM for Resminostat, 1 µM for Vorinostat (Vori.), 0.25 µM for Belinostat and 2 nM for Romidepsin lead to a cell mass reduction of about 20 – 30 %. Consequently, we defined those concentrations as minimal effective and used them for following experiments. Concerning Namodenoson we chose the previously identified minimal concentrations of 10 and 20 µM for combination experiments.

A)

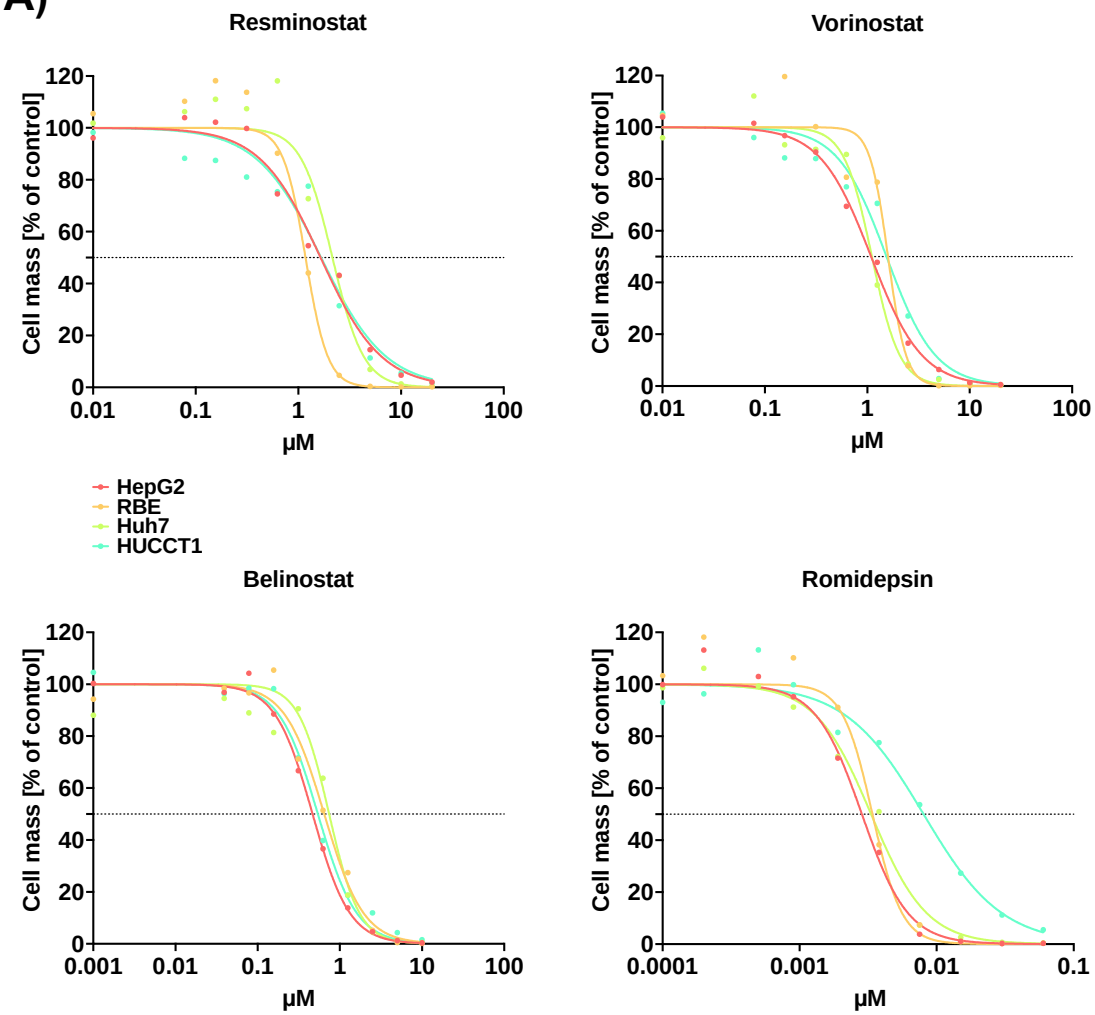

B)

IC50 Value (95% CI) Human HCC and CCA cell line				
Cells	**Resminostat (µM)**	**Vorinostat (µM)**	**Belinostat (µM)**	**Romidepsin (nM)**
HepG2	1.6 (1.3 – 2.1)	1.1 (0.9 – 1.2)	0.5 (0.4 – 0.6)	2.8 (2.3 – 3.3)
RBE	1.2 (1.0 – 1.3)	1.6 (1.3 – 1.9)	0.6 (0.4 – 0.8)	3.4 (2.7 – 4.1)
Huh7	2.1 (1.7 – 2.6)	1.1 (0.9 – 1.3)	0.7 (0.5 – 0.9)	3.3 (2.8 – 3.9)
HUCCT1	1.6 (1.2 – 2.2)	1.5 (1.3 – 1.8)	0.5 (0.4 – 0.6)	8 (6.4 – 9.9)

Figure 22 A) Dose dependent antiproliferative effect of different HDAC inhibitors on HCC cells (HepG2 (red), Huh7 (green)) and CCA cells (RBE (orange), HUCCT1 (light blue)). Cells were seeded overnight, and varying concentrations of the HDACis (20; 10; 5; 2,5; 1,2; 0,6; 0,3; 0,15; 0,07; 0 µM for Resminostat and Vorinostat, 10; 5; 2,5; 1,2; 0,6; 0,3; 0,15; 0,07; 0,03; 0 µM for Belinostat and 60; 30; 15; 7,5; 3,8; 1,9; 0,9; 0,5; 0,2; 0 nM for Romidepsin) were added for 72h. SRB assays were performed, the percentage of the cell mass as a surrogate marker for proliferation was determined. The curves were automatically fitted using nonlinear regression with GraphPad Prism. Nonlinear regression was constrained to 100 for the top and 0 for the bottom. Thereafter IC50 values were calculated. The dashed lines represent the IC50. The dots represent the average of four values gained for each treatment condition. (B) The table shows the calculated IC50 values of each treatment.

As the next step we co-treated different HCC and CCA cell lines with the four different HDCA inhibitors alone or in combination with two different concentrations of Namodenoson for 72 hours.

We observed that for all cell lines tested, independent of the tumor type, the combination affected cell mass more effectively compared to the HDACi treatment alone. In HCC cells a significant ($p<0.05$ – $p<0.0001$) inhibition of cell proliferation in all cell lines was observed when 20 µM Namodenoson was combined to HDACis. Similar results were observed with in both CCA cell lines. Of note, in all cell lines tested 10 µM Namodenoson showed a significant inhibition of cell proliferation when combined to Resminostat ($p<0.05$ – $p<0.001$) or Vorinostat ($p<0.05$, $p<0.001$). The combinations to Romidepsin or Belinostat showed varying results. Even though the treatment with Romidepsin alone, showed a cell mass inhibition of over 50 % in HepG2 and HUCCT1 cells, the

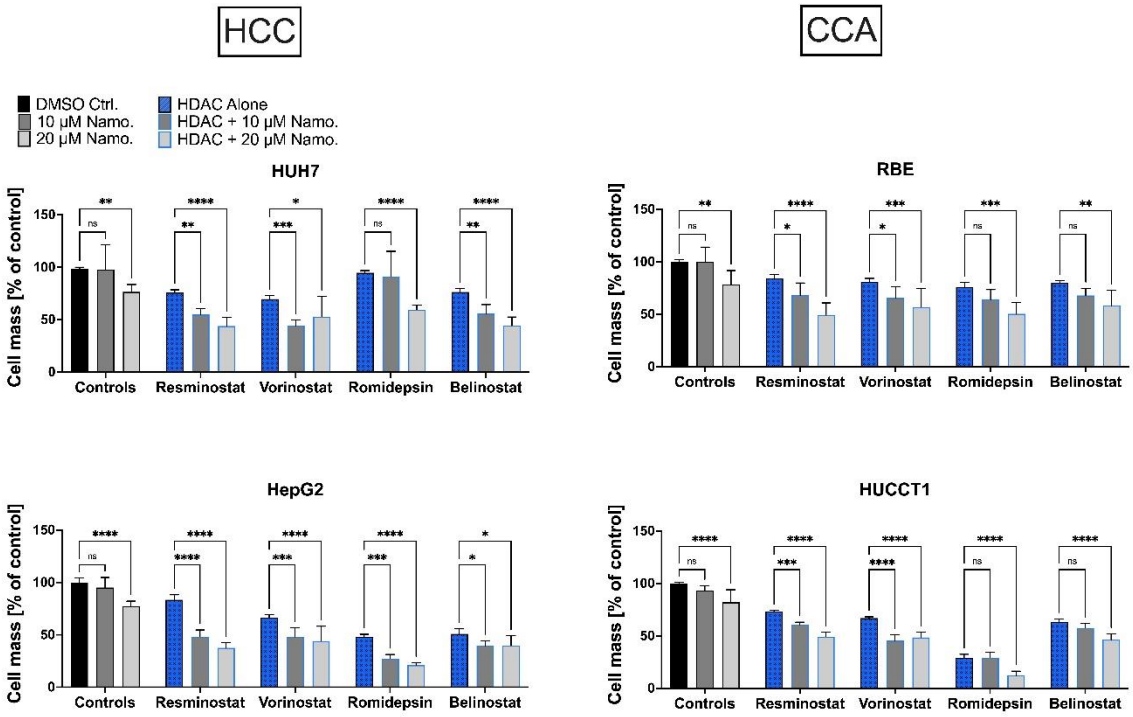

Figure 23 Combination treatment of Namodenoson and different HDACi. HCC cell lines HepG2 and Huh7, and CCA cell lines HUCCT1 and RBE were treated with four different HDAC inhibitors (1 µM Resminostat, 1 µM Vorinostat, 0.25 µM Belinostat and 2 nM Romidepsin) alone or in combination with two different concentrations of Namodenoson (10 µM or 20 µM Namo.). SRB assays were performed, the percentage of the cell mass as a surrogate marker for proliferation, was determined. The effects of the Namodenoson treatment alone were compared to DMSO treated controls. The combination of HDACi and Namodenoson was compared to the incubation with each HDAC inhibitor alone. Data represent three independent experiments. Statistical analysis was performed using a 2way ANOVA with Dunnett's multiple comparison test (= p <0.05; ** = p<0.01, *** = p<0,001, **** = p<0,0001, ns= not significant).*

addition of the ADORA3 agonist Namodenoson could still enhance the observed antiproliferative effect (Fig. 20).

To further evaluate whether the observed inhibition in the combination treatments was synergistic, the simplified highest single agent (HSA) synergy model was used (140). This model, which is also referred to as the Gaddum's non-interaction model, defines a synergistic combination effect as beneficial outcome on top of what is observed for each individual drug at the dose used in the combination. Briefly, the combination should be more then additive to be stated synergistic.

To apply the HSA model for synergistic interactions, we calculated the expected additive effect, which is the sum of the effects observed of each drug alone and compared it to the actually gained effect in our experiment (Fig. 21).

Figure 20 shows the calculated expected additive effects for the HDACi/Namo. combination in black (HDACi+10 µM Namo.) and grey (HDACi + 20 µM Namo) and the gained effect of the combinations in blue (HDACi + 10 µM Namo.) and orange (HDACi + 20 µM Namo.). Compared are black to blue and grey to orange. In all cell lines we found that the gained effects of the combinations with Resminostat was significantly higher than the expected effects independently of the concentration used for Namodenoson, which according to the HSA model are stated synergistic interactions. The combination of 10 µM Namodenoson to Vorinostat was also significantly synergistic throughout all tested cell lines. Varying interactions were observed in der Combinations to Romidepsin or Belinostat in Huh7, HepG2 and RBE cells. In HUCCT1 cells the combinations with Romidepsin and Belinostat were observed to be exclusively additive for the concentrations tested. Of note, none of the gained effects was significantly below the expected additive effect. These results underscore that the co-treatment of an ADORA3 agonist with and HDACi might be a promising approach to enhance antiproliferative effects on HCC and CCA cells in an additive or synergistic way.

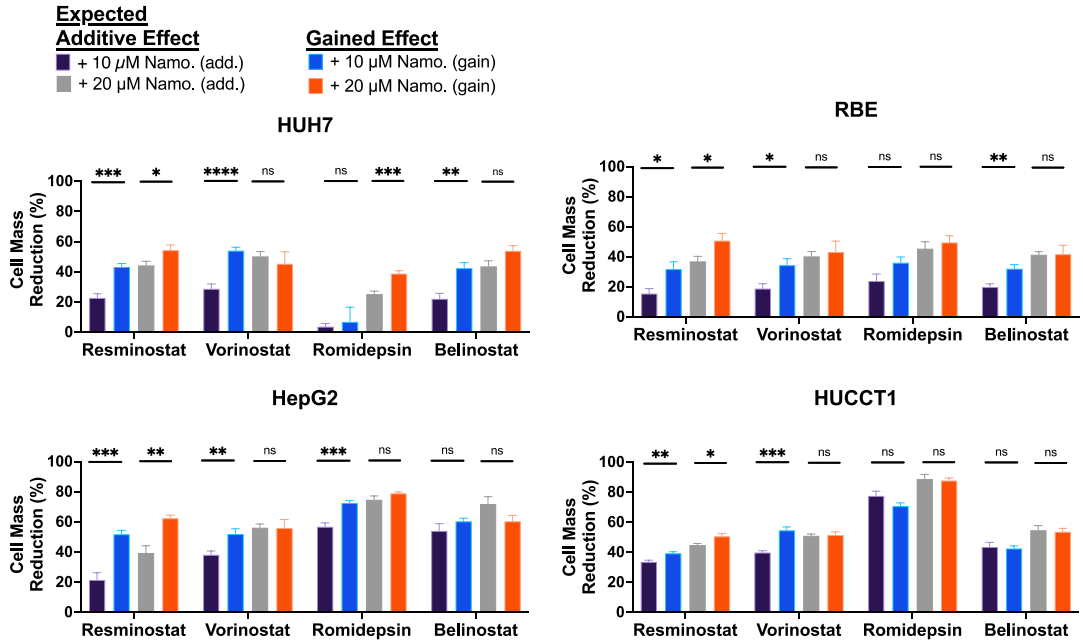

Figure 24 Highest Single Agent (HSA)model-based synergy analysis of HCC cell lines HepG2 and Huh7, and CCA cell lines HUCCT1 and RBE treated with four different HDAC inhibitors (HDACis)(1 µM Resminostat, 1 µM Vorinostat, 0.25 µM Belinostat and 2 nM Romidepsin) in combination with two different concentrations of Namodenoson (10 µM or 20 µM Namo.). The HSA synergy analysis is based on the comparison of the expected additive effect (EAE) (here in black for 10 µM Namo. + HDACi and grey for 20 µM Namo + HDACi) and the gained effect from the experiments (here in blue for 10 µM Namo. + HDACi and orange for 20 µM Namo. + HDACi). The effects were initially measured as the reduction of cell mass in precent compared to DMSO treated control. Statistical analysis was performed using unpaired t-test comparing the EAE to the gained effect (black to blue and grey to yellow) (= p <0.05; ** = p<0.01, *** = p<0,001, **** = p<0,0001, ns= not significant).*

All experiments so far were performed with the clinically most advanced ADORA3 agonist Namodenoson. To investigate, whether the observed results could also be expanded for further ADORA3 agonists, ADORA3 agonists CF101 (Piclidenoson) and MRS5698 were examined as a combination partner to the different HDACis. HepG2 and HUCCT1 were treated with either each HDAC inhibitor alone or in combination with each agonist as previously described for Namodenoson.

The concentrations used for CF101 and MRS5698 showed a maximum reduction in cell mass of about 20 % (± 10 %), which render those concentration as minimal effective. As results in HepG2 cells, CF101 showed significant ($p<0.0001$) inhibition of proliferation when combined to Romidepsin or Belinostat. In contrast to our observation with Namodenoson, the combinations to Resminostat or Vorinostat were not significant. In HUCCT1 cell on the other hand, significant inhibition of proliferation was observed throughout HDACis combined to 20 µM

CF101 (Fig. 22A). Surprisingly, MRS5698 showed significant ($p<0.001$ – $p<0.0001$) downregulation of cell proliferation throughout all combinations tested and in both tumor types (Fig. 22B). In summary, our results firstly support our assumption that a selective activation of ADORA3 is substantial for the observed

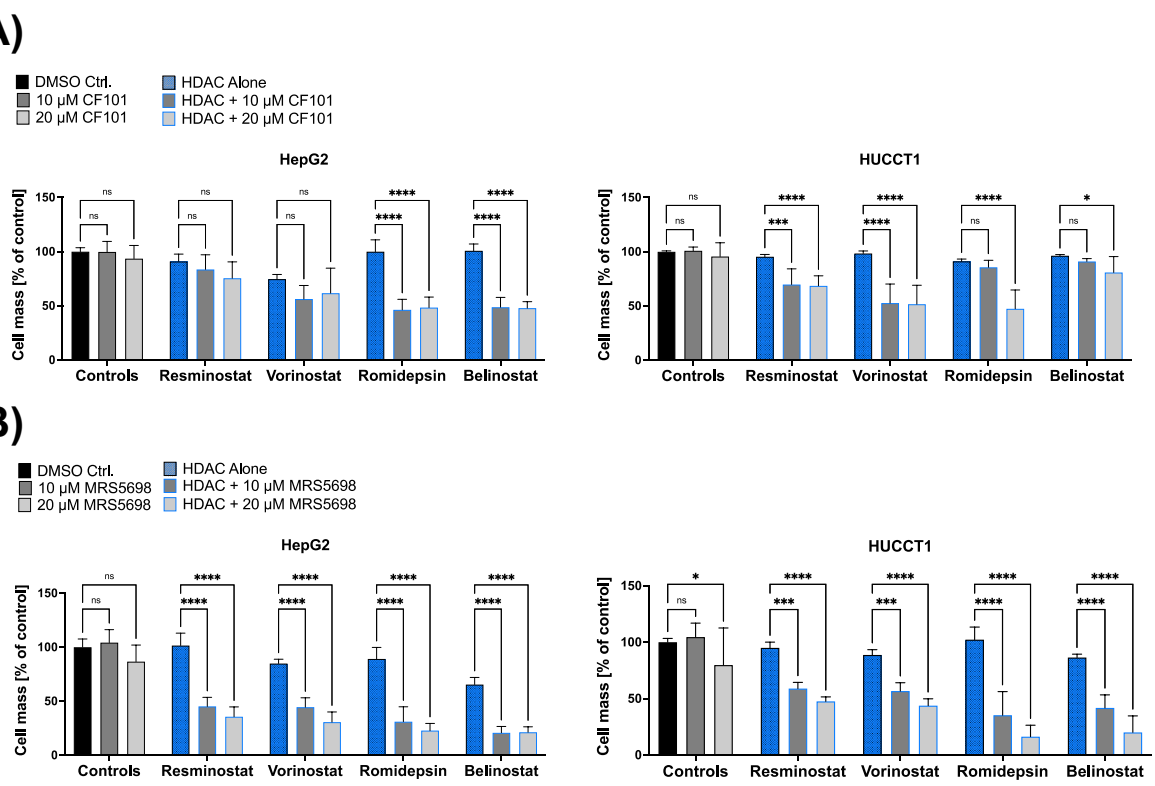

Figure 25 Combination of two different ADORA3 agonists, CF101 and MRS5698, with HDAC inhibitors. HCC cell line HepG2 and CCA cell line HUCCT1 were treated with four different HDAC inhibitors (HDACi) (1 µM Resminostat, 1 µM Vorinostat, 0.25 µM Belinostat and 2 nM Romidepsin) alone or in combination with (A) CF101 (10, 20 µM) and (B) MRS5698 (10, 20 µM). SRB assays were performed, the percentage of the cell mass as a surrogate marker for proliferation was determined. The effects of each agonist treatment on the tested cell lines are summarized in each control group. Here the agonist treatment was compared to DMSO treatment. The combination of HDACi and the respective ADORA3 agonist was compared to the incubation with each HDAC inhibitor alone. Data represent three independent experiments. Statistical analysis was performed using 2way ANOVA with Dunnett's multiple comparison test (= p <0.05; ** = p<0.01, *** = p<0,001, **** = p<0,0001, ns = not significant).*

antiproliferative effect and secondly our results further show that co-targeting HDAC inhibition and ADORA3 activation might be an interesting new combination treatment in liver cancer.

To conclude, we examine, whether the combinations CF101/HDACis or MRS5698/HDACis were synergistic based on the HSA model.

Figure 23A shows the calculated expected additive effects for the HDACi/CF101 combination in black (HDACi+10 µM CF101.) and grey (HDACi + 20 µM CF101)

and the observed effect of the combinations in blue (HDACi + 10 µM CF101) and orange (HDACi + 20 µM CF101.)

Figure 23B shows the same for MRS5698.

For CF101, the interactions observed when combined to Romidepsin or Belinostat in HepG2 cells showed to be synergistic. In contrast to that, In HUCCT1 cell synergistic interaction were observed for the combinations to Resminostat and Vorinostat while the combinations to Romidepsin or Belinostat showed varying results. Interestingly, for MRS5698, throughout all combinations tested the gained effects were significantly higher than the expected effects

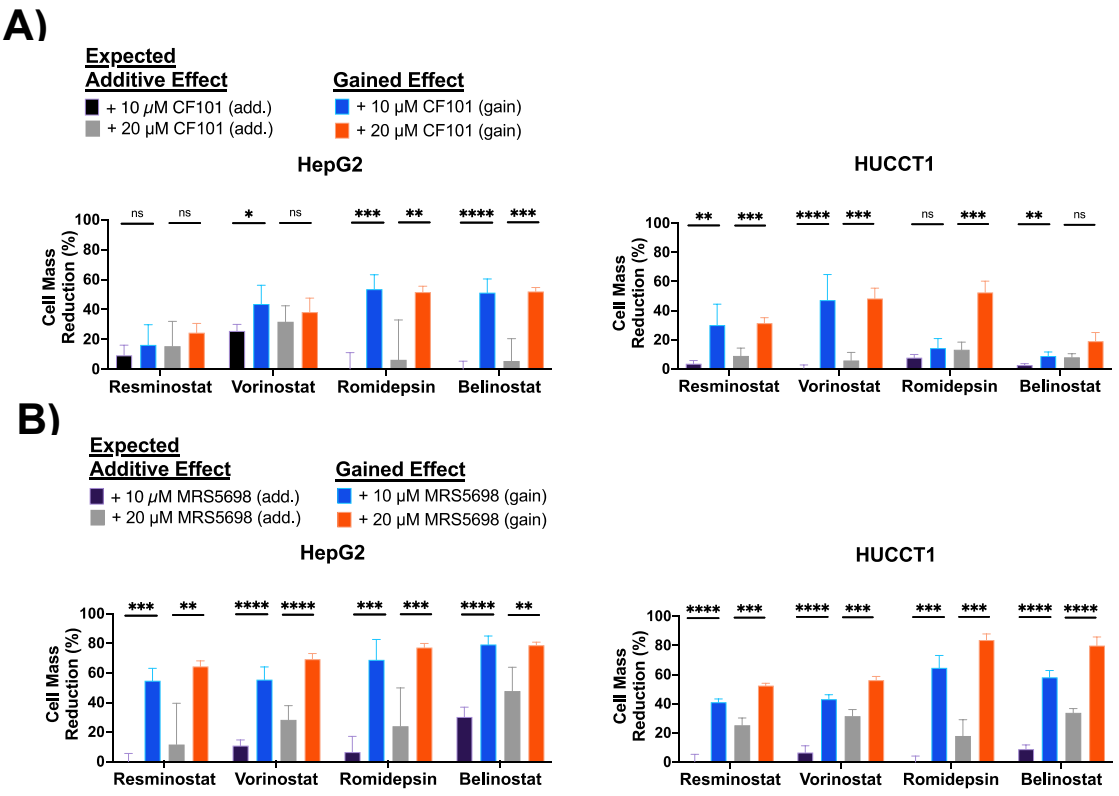

Figure 26. Highest Single Agent (HSA)model-based synergy analysis of HCC cell line HepG2 and CCA cell line HUCCT1 treated with four different HDAC inhibitors (HDACis) (1 µM Resminostat, 1 µM Vorinostat, 0.25 µM Belinostat and 2 nM Romidepsin) in combinations with two different concentrations (10 µM or 20 µM) of the agonists CF101 (A) or MRS5698 (MRS.) (B). The HSA synergy analysis is based on the comparison of the expected additive effect (EAE) (here in black for 10 µM CF101or MRS. + HDACi and grey for 20 µM CF101 or MRS.+ HDACi) and the gained effect from the experiments (here in blue for 10 µM CF101 or MRS. + HDACi and orange for 20 µM CF101 or MRS. + HDACi). The effects were initially measured as the reduction of cell mass in precent compared to DMSO treated control. Statistical analysis was performed using unpaired t-test comparing the EAE to the gained effect (black to blue and grey to yellow) (= p <0.05; ** = p<0.01, *** = p<0,001, **** = p<0,0001, ns= not significant).*

(p<0.01 – p<0.0001). Conclusively all combinations with MRS5698 and HDACis are stated as synergistic according to the HSA model. These results emphasize

the importance of a selective activation and support the assumption that co-targeting of ADORA3 activation and HDAC inhibition is a promising treatment approach.

3.1.7. Namodenoson and HDACi inhibit viability of patient derived HCC and CCA organoids.

With the previous results we have presented evidence that co-targeting ADORA3 activation and HDACi showed synergistic antiproliferative effects in cell lines. We next aimed to explore the combination of Namodenoson and HDACis in patient derived tumor organoids (PDOs).

The following experiments were performed in cooperation with the lab of Prof. Dr. Markus Heim during an exchange period at the Department of Biomedicine in Basel.

A)

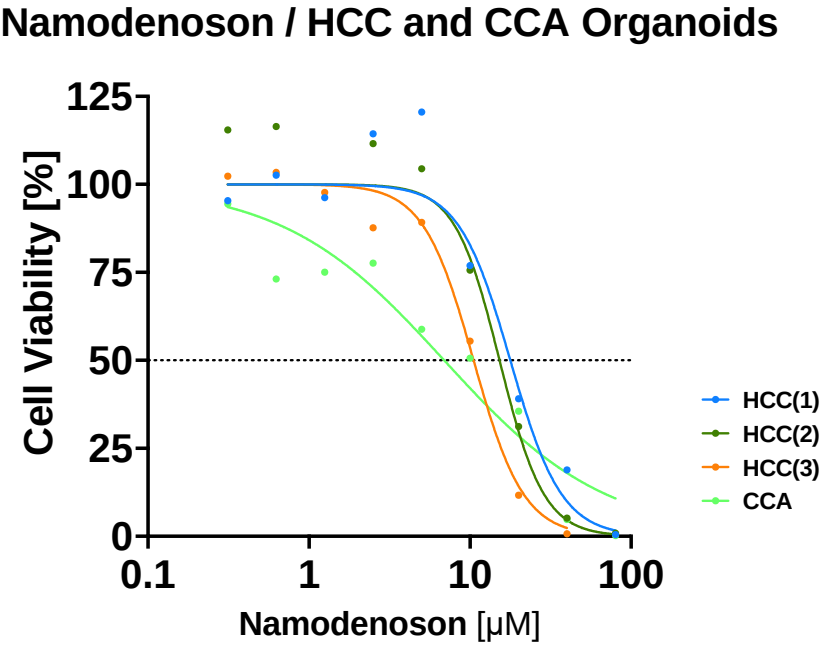

B)

IC50 Value Human HCC and CCA Organoids			
HCC (95% CI)		CCA (95% CI)	
HCC(1)	17.8 (12.2 – 27.2)	CCA	6.9 (3.3 – 13.9)
HCC(2)	15.2 (12.2 – 19.1)		
HCC(3)	10.5 (8.9 – 12.3)		

Figure 27 (A) Dose-dependent antiproliferative effect of Namodenoson in organoids derived from three HCC (HCC 1-3) and one CCA patients. Organoids were seeded for 48h. Thereafter rising concentrations (0, 0.3, 0.6, 1.3, 2.5, 5, 10, 20, 40, and 80 µM)) of Namo. were added for 4 days. Cell Viability was determined using the cell titer glow assay. The curves were automatically fitted using nonlinear regression with GraphPad Prism. Nonlinear regression was constrained to 100 for the top and 0 for the bottom. Thereafter IC50 values were calculated. The dashed line represents the IC50. The dots represent the average of at least four independent values gained for each treatment condition. (B) Calculated IC50 values of Namo. treatment.

We investigated three HCC organoids (Fig. 24 HCC 1 – 3) and one organoid derived from a patient diagnosed with CCA (Fig. 24, CCA). We first analyzed the organoids responses to the different HDACis. We therefore performed dose response studies and calculated the IC50 values as described above (Fig. 23 A/B).

A)

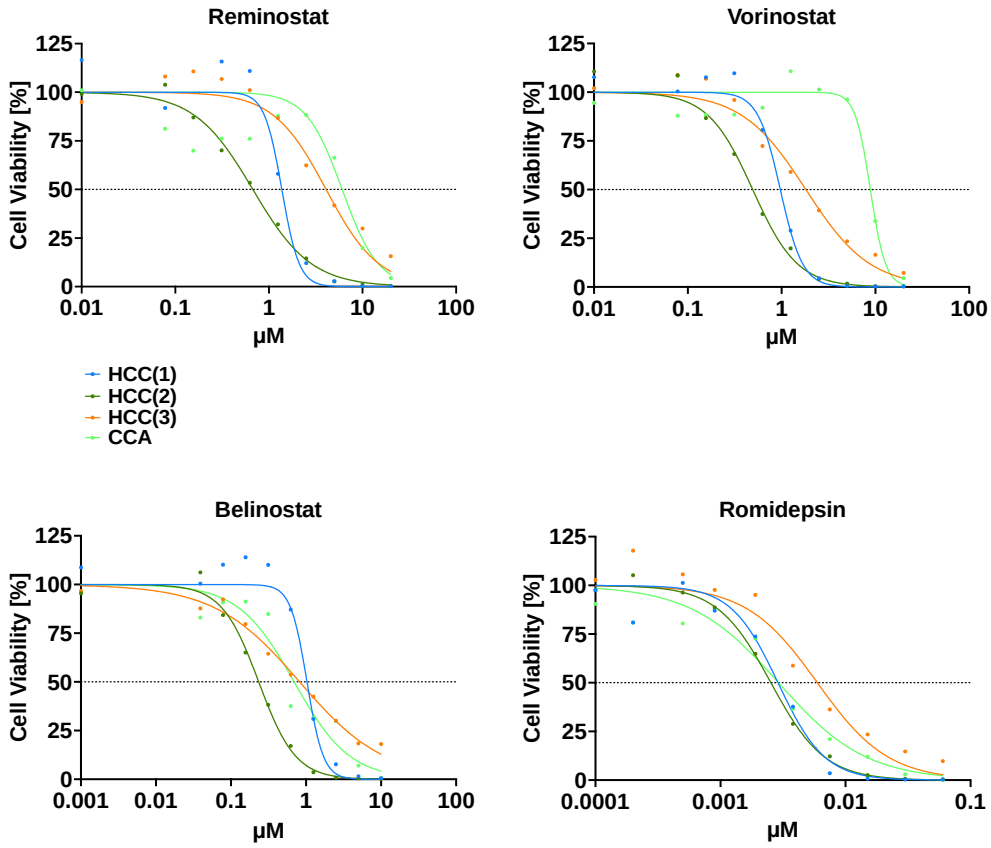

B)

IC50 Value (95% CI) Human HCC and CCA cell line				
Cells	**Resminostat (μM)**	**Vorinostat (μM)**	**Belinostat (μM)**	**Romidepsin (nM)**
HCC(1)	1.4 (1.1 – 1.8)	0.9 (0.8 – 1.2)	1.0 (0.8 – 1.2)	2.9 (2.1 – 3.8)
HCC(2)	0.7 (0.6 – 0.8)	0.5 (0.3 – 0.6)	0.2 (0.1 – 0.3)	2.5 (2.0 – 3.1)
HCC(3)	4.1 (3.2 – 5.5)	1.8 (1.6 – 2.1)	0.8 (0.6 – 1.1)	5.9 (4.7 – 7.6)
CCA	6.1 (4.0 – 7.9)	8.8 (7.3 – 10.6)	0.7 (0.5 – 1.0)	2.9 (1.8 – 4.4)

Figure 28 (A) Dose dependent antiproliferative effect of 3 organoids from HCC patients (HCC 1-3) and one organoid from a CCA patient. Organoid were seeded for 48h, and varying concentrations of the HDACs (20; 10; 5; 2,5; 1,2; 0,6; 0,3; 0,15; 0,07; 0 μM for Resminostat and Vorinostat, 10; 5; 2,5; 1,2; 0,6; 0,3; 0,15; 0,07; 0,03; 0 μM for Belinostat and 60; 30; 15; 7,5; 3,8; 1,9; 0,9; 0,5; 0,2; 0 nM for Romidepsin) were added for 4 days. Cell Viability was determined using the cell titer glow assay. The curves were automatically fitted using nonlinear regression with GraphPad Prism. Nonlinear regression was constrained to 100 for the top and 0 for the bottom. Thereafter IC50 values were calculated. The dashed line represents the IC50. The dots represent the average of at least four independent values gained for each treatment condition. (B) Calculated IC50 values of Namo. treatment

Interestingly, the IC50 values for all tested Organoids ranged from 6 – 20 µM. Comparing these IC50 range to that gained from the cell lines above, which ranged from 13 – 60 µM, these results suggest that the organoid might be more sensitive to Namodenoson treatment. We next looked at the sensitivity of the four tested organoids to the HDACis (Fig. 25 A/B).

We observed that the response to each tested HDACi was inconsistent throughout all tested organoids. The IC50 values ranged between 0.7 – 6.1 µM for Resminostat, 0.9 – 8.8 µM for Vorinostat, 0.2 – 1 µM for Belinostat and 2.5 – 2.9 nM for Romidepsin. To conclude, the organoids showed a dose dependent inhibition of cell viability when treated with Namodenoson or HDACi alone. Concentration ranges for following experiments were identified.

3.1.8. Namodenoson/HDACi co-treatment act synergistic or additive to reduce viability of patient derived HCC organoids

We then investigate the effect of combining HDACi to Namodenoson in patient derived HCC organoids. Briefly, five different concentrations of Namodenoson and six different concentrations of the HDACi were tested in a 5 x 6 matric. The concentrations chosen ranged around the average of the previously described IC50 values calculated for each drug used. The resulting 5 x 6 matrices were used to build synergy landscapes (Fig. 26) using the Zero interaction potency (ZIP) model and the “SynergyFinder” web-based program (142). Next, the the overall synergy score (∆-value) was determined for each cell line/treatment combination. According to the developer, drugs interaction is likely to be synergistic when the calculated score is > 10. For scores between 10 and -10, the interaction is likely to be additive and antagonistic interactions are considered for scores < -10.

We observed that all combination showed an average additive effect ranging from -0.15 for HCC(2) to 11.95 for HCC(3). Looking at the most synergistic area (yellow squares) our result showed that combining Namodenoson with Vorinostat was synergistic for all organoids, followed by a rather additive interactions in the combinations with Belinostat, Romidepsin and Resminostat. Of note, none of the combinations showed a threshold below -10 for likely antagonistic interactions. In

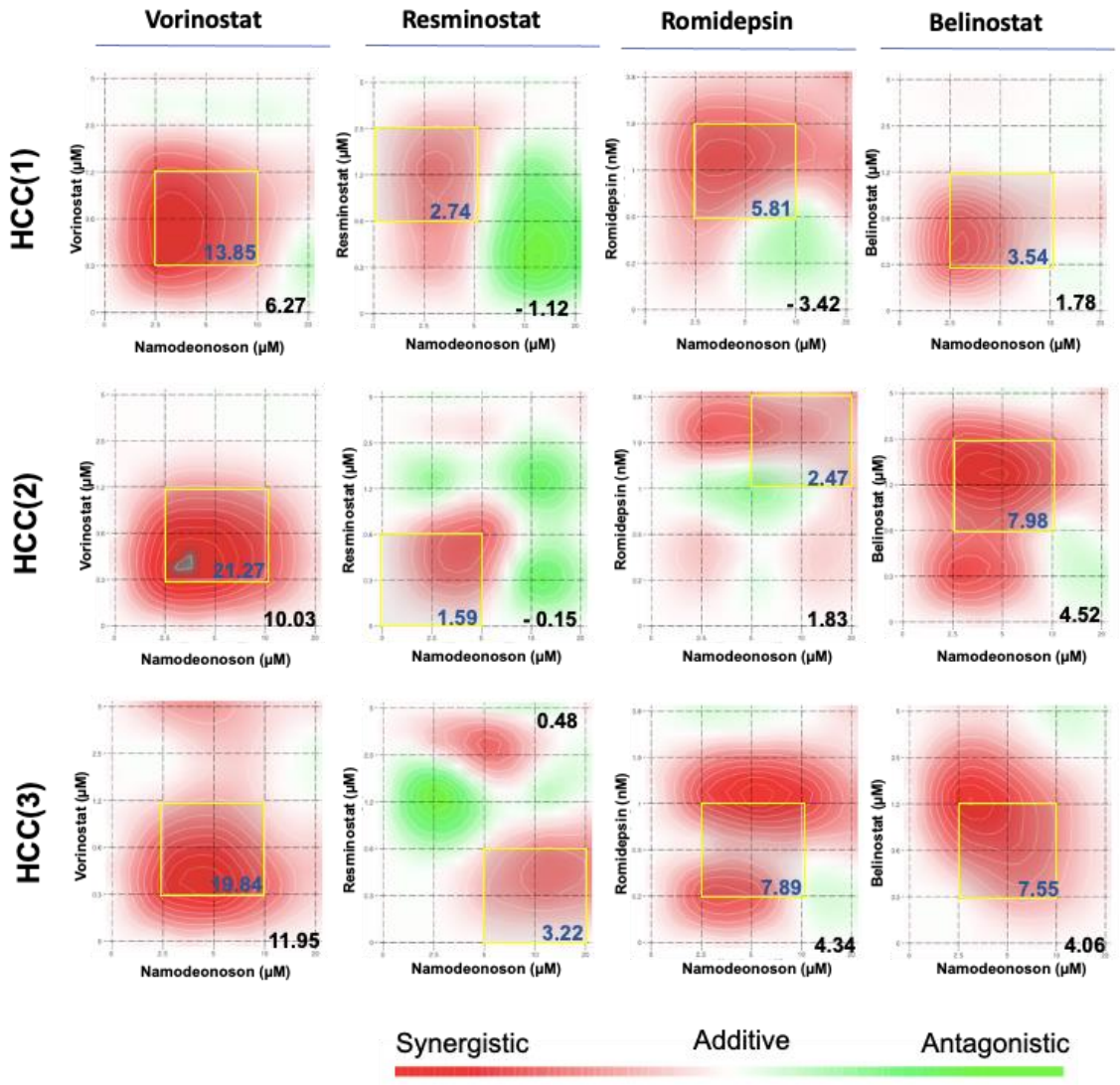

Figure 29 HCC organoids from three different patients (HCC 1- 3) were used to investigate the combination of Namodenoson with four different HDACi drugs Vorinostat, Resminostat, Romidepsin, and Belinostat. The interaction of this drug combination was investigated with SynergyFinder 2.0 to visualize and explore the drug synergy landscapes. Organoids were seeded in a 384 well plate for 48h and thereafter treated in a 5x6 matrix which comprised 5 different concentrations of Namodenoson (20, 10, 5. 2.5, 0 µM) and 6 different concentrations of the HDACis (Vorinostat, Resminostat and Belinostat with 5, 2.5, 1.25, 0.625, 0.312, 0 µM; Romidepsin with 3.8, 1.9, 0.95, 0.48, 0.24, 0 nM). After 6 days of treatment the tumor organoids´ viability was evaluated using the Cell Titer-Glow 3D cell viability assay. The resulting cell viability values of each 5 x 6 matrices were used to build and visualize synergy landscapes using the zero-interaction potency (ZIP) model. The average synergy score is shown in the right lower corner of each graph, the most synergistic area and the corresponding synergistic area score is shown within a yellow square in each graph. Scores > 10, the drug interactions are likely to be synergistic, 10 to -10, the interaction is likely to be additive, < -10, the interaction is likely to be antagonistic (https://synergyfinder.fimm.fi/synergy/synfin_docs/).

summary, we showed that combining HDAC inhibition and ADORA3 activation inhibited cell viability. Conclusively, our experiments employing human derived organoids further suggest combining an ADORA3 agonist with an HDAC inhibitor as a new option to target liver cancer.

3.2. Combined HDAC and AKT inhibition as novel therapeutic strategy against HCC and CCA

3.2.1. Dose dependent antiproliferative effect of AKT inhibitor MK2206 on HCC (HepG2, Huh7) and CCA (HUCCT1, SZ1) cell lines.

To investigate the effect of AKT inhibition, the dose dependent antiproliferative effect of AKT inhibitor MK2206 was studied in two HCC (HepG2, Huh7) and two CCA (HUCCT1, SZ1) cell lines.

A)

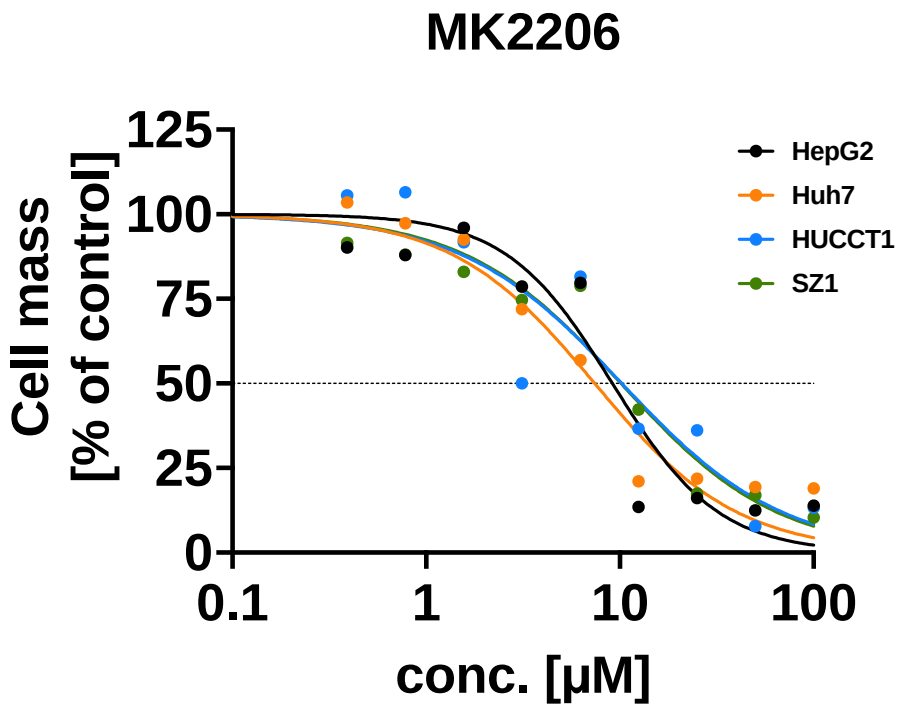

B)

IC50 Value MK2206 Treatment in HCC and CCA Cell lines			
HCC (95% CI)		CCA (95% CI)	
HepG2	9.1 (6.6 – 13.9)	HUCCT1	10.2 (6.0 – 17.5)
Huh7	7.4 (6.0 – 9.2)	SZ1	10.1 (7.3 – 13.9)

Figure 30. (A) represents a dose-dependent antiproliferative effect of MK2206 on HCC cells (HepG2, Huh7) and CCA cells (HUCCT1, SZ1). Briefly, cells were seeded overnight, and cultured in varying concentrations of MK2206 (0.39, 0.78, 1.56, 3.12, 6.25, 12.5, 25, 50, and 100 µM) for 72h. SRB assays were performed, the percentage of the cell mass as a surrogate marker for proliferation was determined. The curves were automatically fitted using nonlinear regression with GraphPad Prism. Nonlinear regression was constrained to 100 for the top and 0 for the bottom. Thereafter IC50 values were calculated. The dashed line represents the IC50. The dots represent the average of three independent replicates gained for each treatment condition. (B) Calculated IC50 values of MK2206 treatment.

Our results showed a dose-dependent reduction of cell mass in all 4 cell lines (Fig. 27A). As presented IC50 values were 9.1; 7.4; 10.2; 10.1 for Huh7, HepG2, HUCCT1 and SZ1 cells after 72 h of exposure (Fig. 27B).

Based on these results, and dose response as determined by IC50 values, a minimal-effective concentration of 5 µM MK2206, which lead to a cell mass reduction of about 20-30 %, in all cell lines, was chosen to be used for further studies.

3.2.2. AKTi/HDACi co-treatment increased anti-proliferative effect compared to the monotherapies in different HCC and CCA established cell lines

The next section aimed to investigate the antiproliferative effect of the AKTi/HDACi co-treatments compared to each monotreatment. We used the

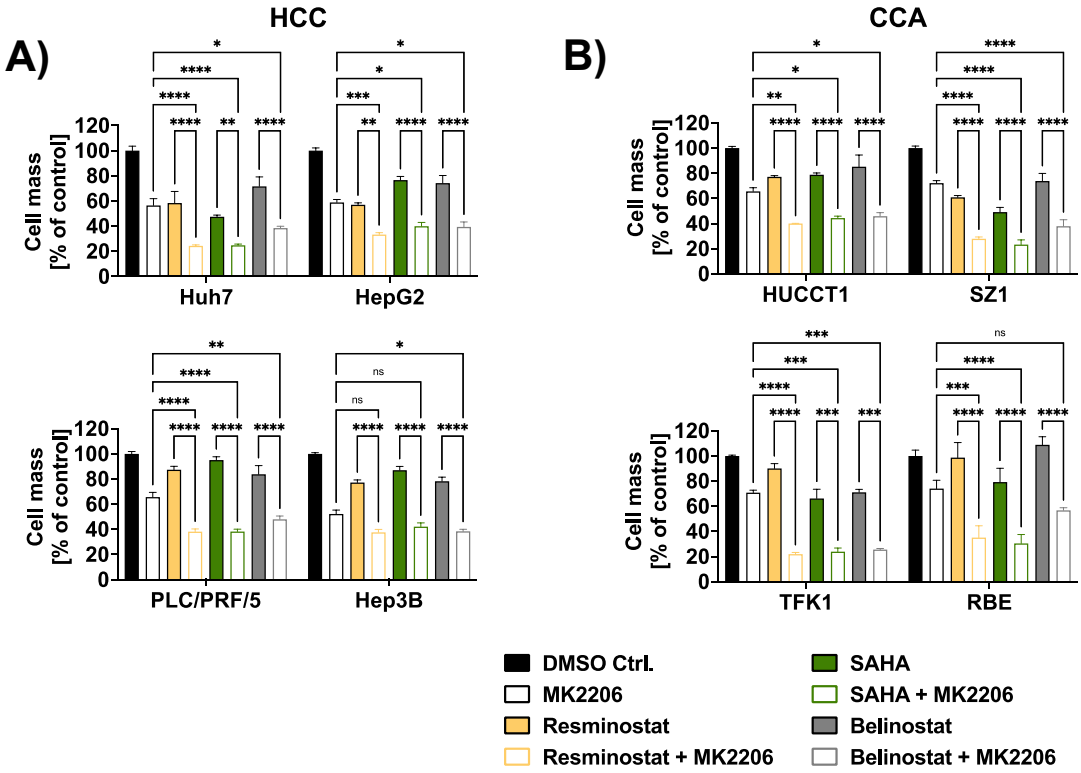

Figure 31 Presented is the combination effect of AKT inhibitor (AKTi) MK2206 with HDACis (Resminostat, Vorinostat, Belinostat) in four different HCC (Huh7, HepG2, PLC/PRF/5, Hep3B) and CCA cell lines (HUCCT1, SZ1, TFK1, RBE). Briefly, cells were seeded overnight and treated with 5 µM of MK2206 or HDACi (1 µM Resminostat (Res.), 1 µM Vorinostat (Vori.) or 0.25 µM Belinostat (Beli.)) alone or in combination as indicated, for 72 h. DMSO was used as control. SRB assays were performed, the percentage of the cell mass as a surrogate marker for proliferation was determined. Data represent standard error of the mean of three independent experiments. Statistical analysis was performed comparing the combination to the monotherapy with HDACis and the monotherapy with MK2206 to the AKTi/HDACi co-treatment, using 2way ANOVA with Turkey's multiple comparisons test (= p<0.05, ** = p<0.01, *** = p<0,001, **** = p<0,0001, ns= Not Significant).*

HDACis Resminostat (1 µM), Vori. (1 µM) and Belinostat (0.25 µM) and the AKTi MK2206 (5 µM) alone or in combinations as indicated. The concentrations chosen for the HDACis were adopted from our previous observations in section 7.1.6 We investigated the response of 4 different HCC (HepG2, Huh7, PLC/PRF/5, Hep3B) and 4 different CCA (HUCCT1, SZ1, TFK1, RBE)

established cell lines. Using SRB assays we compared the reduction in cell mass as a surrogate marker for proliferation.

In HCC cells lines Huh7, HepG2 and PLC/PRF/5, the combination reduced proliferation more effectively than each monotreatment. Statistical analysis showed that all comparisons were significant ($p<0.05$ to $p<0.0001$). Compared to the HDACis alone combining HDACis to AKTi in Hep3B cell resulted in a significant inhibition of proliferation. Compared to the monotherapy with MK2206 however, we observed that only the combination AKTi/Belinostat was significant ($p<0.05$) (Fig. 28A).

For all CCA cell lines, HUCCT1, SZ1, TFK1 and RBE analysis revealed a significant decrease in proliferation ($p<0.001$) when compared to the HDACis. Except for the combination with AKTi/Belinostat in RBE cells, the combination treatment was also shown to affect proliferation more significantly than MK2206 alone (Fig. 28B).

In summary figure 28 illustrate that AKTi/HDACi combination affected proliferation significantly compared to the treatment with HDACis alone. All AKTi/HDACi combinations improved the antiproliferative effect of the AKTi alone, albeit not significantly in all settings.

3.2.3. AKT inhibitors Ipatasertib and Perifosine show antiproliferative effects in the combination to different HDACis

We then assessed whether the significantly reduced proliferation observed with the AKTi/HDACi co-treatment was dependent on the AKT inhibitor used. Two different AKT inhibitors were tested. Both inhibitors Ipatasertib (NCT04177108) and Perifosine (NCT00590954, NCT00058214), were previously investigated in different clinical trials in the context of cancer treatment. We used HepG2 and HUCCT1 cell lines and performed SRB assays.

Looking at the treatment with Ipatasertib and Perifosine alone, our results showed that except for the treatment of HepG2 cells with Ipatasertib the cells showed similar sensitivity, with a reduction in cell mass of about 15 – 30 %. HepG2 cells were more sensitive to the monotreatment with Ipatasertib with about 50 % cell

mass reduction. Nevertheless, the combinations with the HDACis were still more effective than to the monotherapies.

As shown in Figure 29A statistical comparison of all AKTi/HDACi combinations to Perifosine alone indicated a significant reduced proliferation in HepG2 cells. The comparison to the HDACi alone was not found significant for the combinations Perifosine/Resminostat or Perifosine/Vorinostat. Perifosine/Belinostat was significant in HepG2 ($p<0.05$) and HUCCT1 ($p<0.0001$) cells compared to the treatment with Belinostat alone. HUCCT1 cells further showed a significant inhibition of proliferation with the Perifosine/Resminostat combination ($p<0.05$). Except for the Perifosine/Resminostat co-treatment HUCCT1 also showed significant inhibition of cell proliferation compared to Perifosine alone.

Using AKT inhibitor Ipatasertib, our results showed that all Ipatasertib/HDACis combinations were significant in both tested cell lines when compared to the monotherapy with the respective HDACi alone. Comparing the antiproliferative effect of the combinations to the treatment with Ipatasertib alone, we observed that except for the combination Ipatasertib/Resminostat in HepG2 cells, all other comparison were statistically significant (Fig. 29B).

To sum up, HDACis combined to Perifosine or Ipatasertib negatively affected proliferation more significantly than the monotherapies. Our results suggest that effects meditated through AKT inhibition in the combination are independent of the applied AKTi. Of note both AKTis Ipatasertib and Perifosine were not as effective as MK2206. Conclusively, these results support the assumption, that selective co-inhibition of AKT and HDAC might be a promising new target combination.

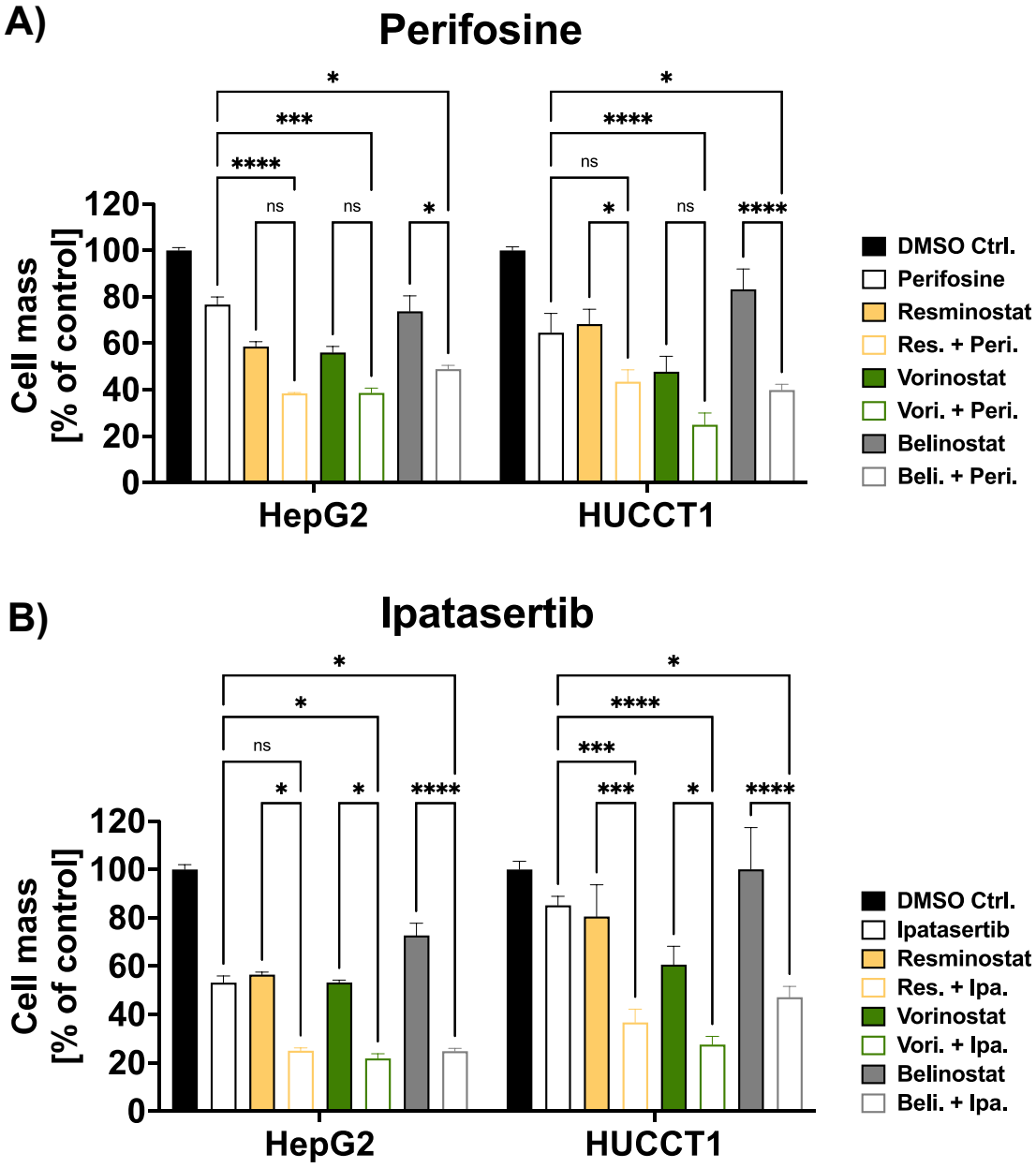

Figure 32 Shown are the combination effects of AKT inhibitors (AKTis) Perifosine (Peri.) (A) and Ipatasertib (Ipa.) (B) with HDACis (Resminostat, Vorinostat, Belinostat) in one selected HCC (HepG2) and CCA cell line (HUCCT1). Briefly, cells were seeded overnight and treated with 5 µM of the AKTi alone or in combination with 1 µM Resminostat (Res.), 1 µM Vorinostat (Vori.) or 0.25 µM Belinostat (Beli.). DMSO was used as control. SRB assays were performed, the percentage of the cell mass as a surrogate marker for proliferation was determined. Data represent standard error of the mean of three independent experiments. Statistical analysis was performed comparing the combination to the monotherapy with HDACis or the AKTis, using 2way ANOVA with Turkey's multiple comparisons test (= p <0.05; ** = p<0.01, *** = p<0,001, **** = p<0,0001, ns= Not Significant).*

3.2.4. MK2206 combined to HDACis act synergistic to mediate an antiproliferative effect

We next investigated whether the MK2206/HDACis combinations were synergistic. To cover different possible combinations, we chose four different concentrations of MK2206 and four different concentrations of the three already described HDACi compounds and investigated the potential additive or synergistic effect of the combination therapies (Fig. 30). The chosen concentrations ranged around the calculated IC_{50} values. The resulting 4 x 4 matrices were used to build synergy landscapes using the Zero interaction potency (ZIP) model with SynergyFinder 2.0 (141, 142). Briefly, the model takes into consideration, that two non-interacting drugs acquire changes in their potency (the amount of compound that is needed to produce a certain effect). In this model synergy is calculated by comparing the changes in potency of the dose-response curves between individual drugs and their combinations. Two HCC cell lines (HepG2, Huh7) and two CCA cell lines (HUCCT1, SZ1) were investigated.

As a result, both HCC cell lines HepG2 and Huh7 showed that, except for the combination with Vorinostat in Huh7 (synergy score: 8.5), all treatments were synergistic with an average synergy score between 10.9 (Huh7) and 23.3 (HepG2) for MK2206/Belinostat (Fig. 30A). Regarding CCA cell lines (Fig. 30B) HUCCT1 and SZ1, we observed that, except for the combination MK2206/Vorinostat in HUCCT1 cell (9.8), all combinations showed synergy values between 10.6 (HUCCT1) and 37.9 (SZ1), which indicate synergistic interactions.

Further, looking at the most synergistic area (yellow square) we observed synergistic interaction throughout all cell lines tested and independently of the HDACi used.

To sum up, we demonstrated synergistic interaction in 10 out of 12 comparisons. Regarding the most synergistic area 12/12 comparisons were synergistic.

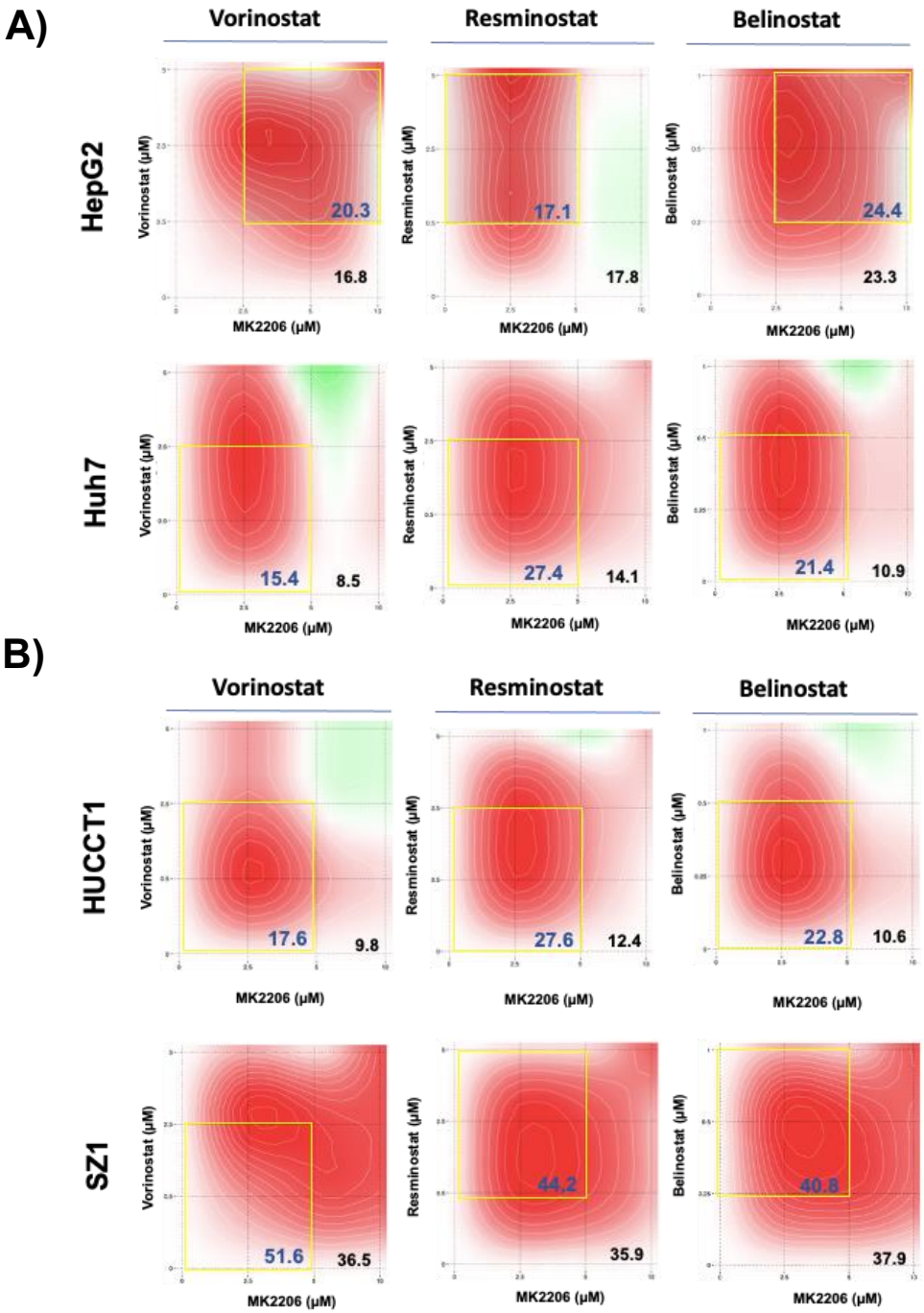

Figure 33 Shown is the analysis for synergistic interaction of the MK2206/HDACis combinations. HCC (HepG2, Huh7) (A) and CCA (HUCCT1, SZ1) (B) cell lines were used to investigate the combination of MK2206 with three different HDACi drugs Vorinostat, Resminostat, and Belinostat. We visualized and explored the MK2206/HDACis combinations using the web-based analytical package SynergyFinder 2.0 synergy landscapes. Cells were seeded overnight, thereafter treated in a 4 x 4 matric which comprised 4 different concentrations of MK2206 (10, 5, 2.5, 0 μM) and 4 different concentrations of the HDACis (Vorinostat and Resminostat with 5, 2.5, 0.5, 0 μM, and Belinostat with 1, 0.5, 0.25, 0 μM) for 72h. SRB assays were performed, the percentage of the cell mass as a surrogate marker for proliferation was determined. The 4 x 4 matrices were used to build and visualize synergy landscapes using the zero-interaction potency (ZIP) model. The average synergy score is shown in the right lower corner of each graph (black values), the most synergistic area and the corresponding synergistic area score is shown within a yellow square in each graph. For scores > 10, the drug interactions are likely to be synergistic, 10 to -10, the interaction is likely to be additive, < -10, the interaction is likely to be antagonistic (https://synergyfinder.fimm.fi/synergy/synfin_docs/).

3.2.5. MK2206/HDACi co-treatment inhibit migration in HCC (HepG2, Huh7) and CCA (HUCCT1, SZ1) cell lines

AKT or HDAC overexpression have been associated with an increased migration potential (48, 97, 169). We aimed to investigate on how the Akti/HDACis combinations alter migration in HCC (HepG2, Huh7) and CCA (HUCCT1, SZ1) cell lines.

We applied the wound healing (or scratch) assay in order to explore migration in HCC (Huh7 / HepG2) and CCA (HUCCT1 SZ1) cell lines after treatment with 5 µM MK2206, 1 µM Resminostat (Res.), 1 µM Vorinostat (Vori.), and 0.25 µM Belinostat (Beli.) alone or in combinations as indicated. Briefly, we generated an artificial gap in the middle of a confluent cell monolayer and tracked the movement of cells into this gap after treatment microscopically. Pictures were taken directly after treatment (0 h) or after 48 h of treatment. All cell lines were tested at the same time. HUCCT1 cells showed 100 % confluency in the DMSO control after 48 h. We therefore chose 48h as the maximal observation time for the experiment. The migration of cells was measured comparing the two timepoints.

For HCC cell lines HepG2 and Huh7, we observed that compared to MK2206 alone, migration was reduced but did not change significantly. Interestingly, comparing the combinations to the HDACis alone we found that except for the combination MK2206/Vorinostat in HepG2 cells, all combinations significantly reduced the migration potential of the cell lines (Fig. 31A).

HUCCT1 showed a significant reduction in migration independently of the comparison. SZ1 cells compared to that showed a significant reduced migration only when compared to the HDACi (Fig. 31B).

Interestingly the combinations MK2206/Resminostat and MK2206/Belinostat demonstrated a significant reduced migration potential in all tested cell lines compared to the respective HDACi alone.

To sum up, the results suggest, that the co-treatment significantly increased the inhibition of migration mediated through HDACis. Further even though the results indicated that AKTi MK2206 is a strong inhibitor of migration itself, the

combinations were still found to further decreased the migration potential albeit not significantly.

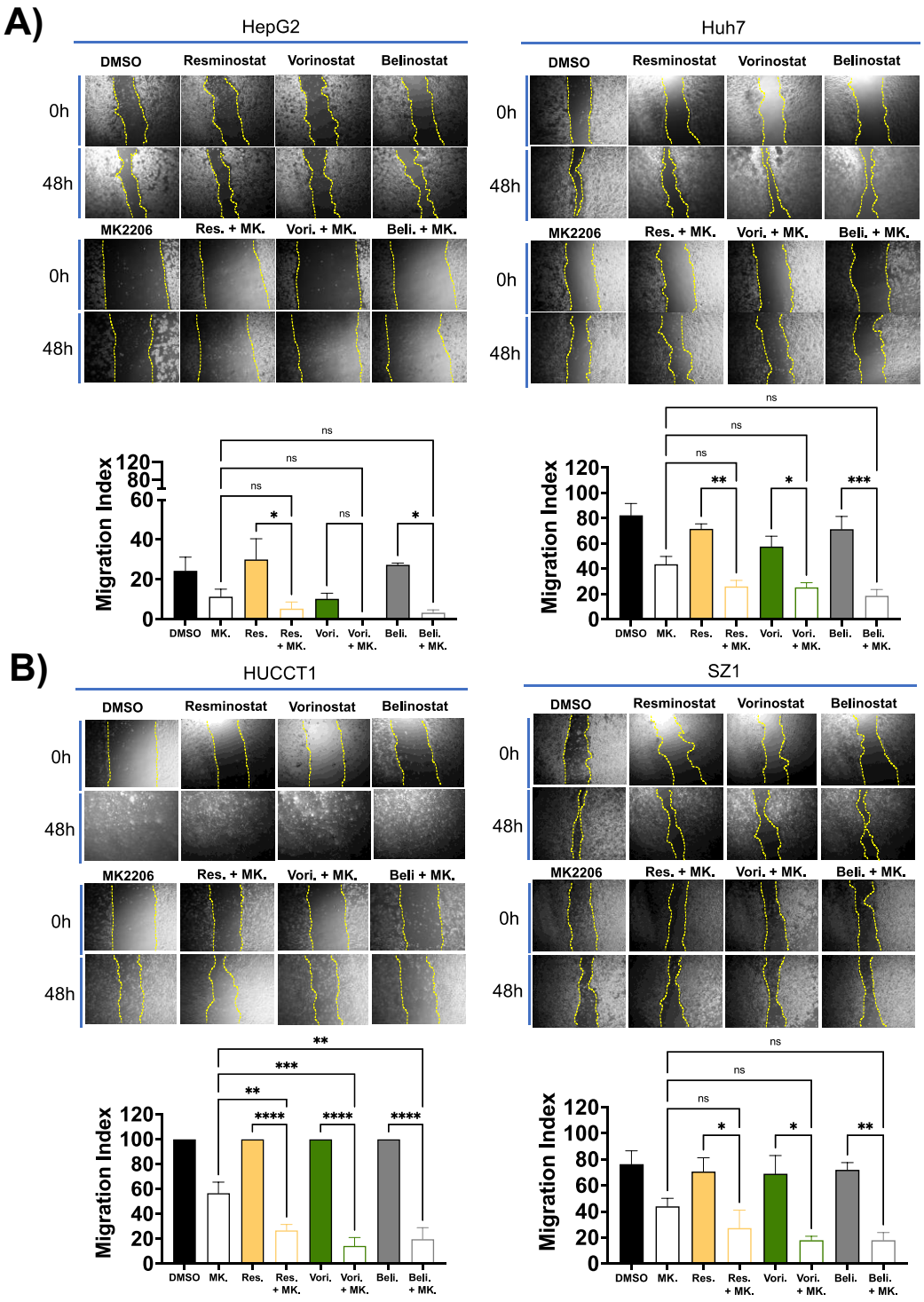

Figure 34 Presented is the wound healing / migration assay and its quantification. Briefly, HCC cell lines Huh7 / HepG2 (A) and CCA cell lines HUCCT1 / SZ1 (B) were seeded overnight to a confluent monolayer. A gap was generated in the middle of the monolayer. The cells were thereafter treated with 5 µM MK2206, 1 µM Resminostat (Res.), 1 µM Vorinostat (Vori.) and 0.25 µM Belinostat (Beli.) alone or in combinations as indicated. DMSO was used as vehicle control. The yellow dotted lines represent edges of the wound. Pictures were taken directly after treatment (0 h) and after 48 h of treatment using a light microscope (40× magnification). Shown are representative pictures. The migration index (the difference in the migrated area comparing ctrl 0 h to 48 h of incubation) was calculated. Three independent experiments were performed. Statistical analysis was performed, using GraphPad Prism and one-way ANOVA with Dunnett's multiple comparisons test. All treatment were compared to the monotherapy with HDACis or MK2206 (= p <0.05; ***

3.2.6. MK2206/HDACi co-treatment inhibit colony formation in HCC (HepG2, Huh7) and CCA (HUCCT1, SZ1) cell lines

We then assessed the long-term effect of the MK2206/HDACis combinations on the cells ability to proliferate and grow in colonies. The soft agar colony formation assay is a well-established method to determine this aspect of the tumorigenic potential of malignant cells. We used HCC cell lines HepG2 and Huh7 (Fig. 32A) and CCA cell lines HUCCT1 and SZ1 (Fig. 32B) and treated them with 5 µM MK2206, 1 µM Resminostat (Res.), 1 µM Vorinostat (Vori.), and 0.25 µM Belinostat (Beli.) alone or in combinations as indicated for a period of three weeks.

We observed that in HepG2 cells all combinations led to a reduction in colony formation compared to MK2206 or the respective HDACi alone. Huh7 cells showed similar results with the combination MK2206/Vorinostat. ($p<0.05 – 0.01$) The combination MK2206/Resminostat and MK2206/Belinostat showed significance only when compared to the HDACi alone (MK./Res. $P<0.001$) or to MK2206 (MK./Beli. $P<0.05$) Notably, colonies derived from Huh7 cells were not only decreased in their amount but were also found to be smaller as soon as MK2206 was added, which indicate a reduced ability of the cells to proliferate (Fig. 32A).

Except for the combination MK./Res. compared to Resminostat alone in SZ1 cells, combining MK2206 to different HDACis significantly inhibited colony formation in both CCA cell lines regardless of the comparison (Fig. 32B).

To sum up so far, we demonstrated that the AKTi/HDACi combination reduced the ability of HCC and CCA cells to migrate and beyond that we showed that the combination also reduced the cells' ability to proliferate and to grow as colonies.

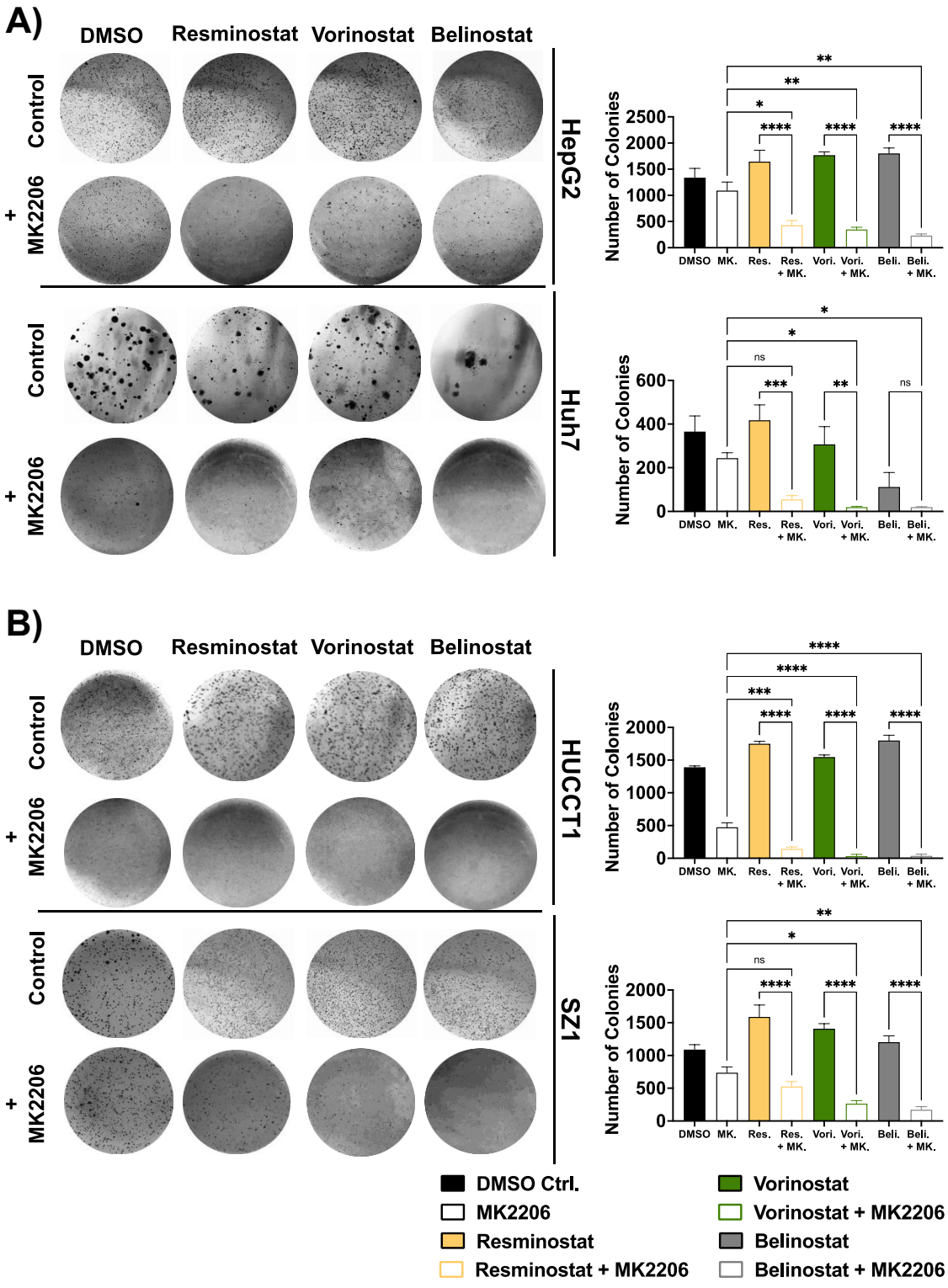

Figure 35 Shown is the colony formation assay and its quantification. HCC (Huh7 and HepG2) (A) and CCA (HUCCT1 and SZ1) (B) cell lines were seeded in a cell-agarose suspension that contained the desired treatment with 5 µM MK2206, 1 µM Resminostat (Res.), 1 µM Vorinostat (Vori) and 0.25 µM Belinostat (Beli.) alone or in combinations as indicated. Cells were then cultivated for 3 weeks to grow clones. After staining, pictures were taken manually (left) and the number of colonies was quantified using ImageJ software and plotted in bar graphs (right). Data represent three independent experiments. Statistical analysis comparing the combination to the monotherapy with HDACis or MK2206 was performed using Graphpad Prism and one-way ANOVA with Dunnett's multiple comparisons test (= p <0.05; ** = p<0.01, *** = p<0,001, **** = p<0,0001, ns= Not Significant).*

3.2.7. MK2206/HDACi co-treatment promote apoptosis in HCC (HepG2, Huh7) and CCA (HUCCT1, SZ1) cell lines.

Evading apoptosis is a cancer hallmark that has been associated to AKT overexpression (128, 170) or an aberrant expression of different HDACs (171, 172). To explore whether apoptosis play any role in the observed anti-tumor effects of the AKTi/HDACi cotreatment, selected hallmarks of the apoptotic cascade were investigated.

Firstly, we performed an Annexin V – FITC/PI stain in HCC (Fig. 33A) and CCA cells (Fig. 33B) to identify externalized phosphorylserine, a marker for apoptotic cells. Stained cells were thereafter analyzed by flow cytometry.

As results we observed that HepG2 cells appeared to be more sensitive to the procedure of sampling generation for the assay, which led to an overall increased number of dead cells in all three replicates. An average of 45 % of dead cells in the DMSO control and >90 % of dead cells in the combinations MK. + Res. and MK + Vori was observed.

Nevertheless, comparing the combinations to the treatment with MK2206 alone, the combinations induced apoptosis significantly. The number of apoptotic cells compared to the respective HDAC alone appeared to be higher, but those changes were not statistically significant.

In Huh7 the combination MK./Vori, and MK./Beli significantly increased the number of apoptotic cells ($p<0.05 – 0.01$) compared to the respective HDACi or to the AKTi. The combination MK./Res was not observed to change apoptosis significantly (Fig. 33A). Interestingly, in both CCA cell lines, all AKTi/HDACis combinations induced apoptosis significantly ($p<0.001$- p0.0001) in all comparisons (Fig. 33B).

Secondly, we explored the protein level of Poly (ADP-ribose) Polymerase (PARP) and its cleaved version. The cleavage of PARP is a useful marker to investigate apoptotic cell death (173). Western blot analysis was performed in HCC cell line (HepG2) and CCA cell line (HUCCT1) (Fig. 34). We assessed changes in apoptosis by comparing MK2206 or HDACi treatment to the combinations. Cleaved PARP expression was quantified to full PARP.

As a result, in both cell lines, we observed that all combinations increased the expression of cleaved PARP. However not all combinations were statistically significant. HepG2 cells showed a significant induction of apoptosis with the

combination MK./Vori. (p<0.05) and HUCCT1 cells with the combinations

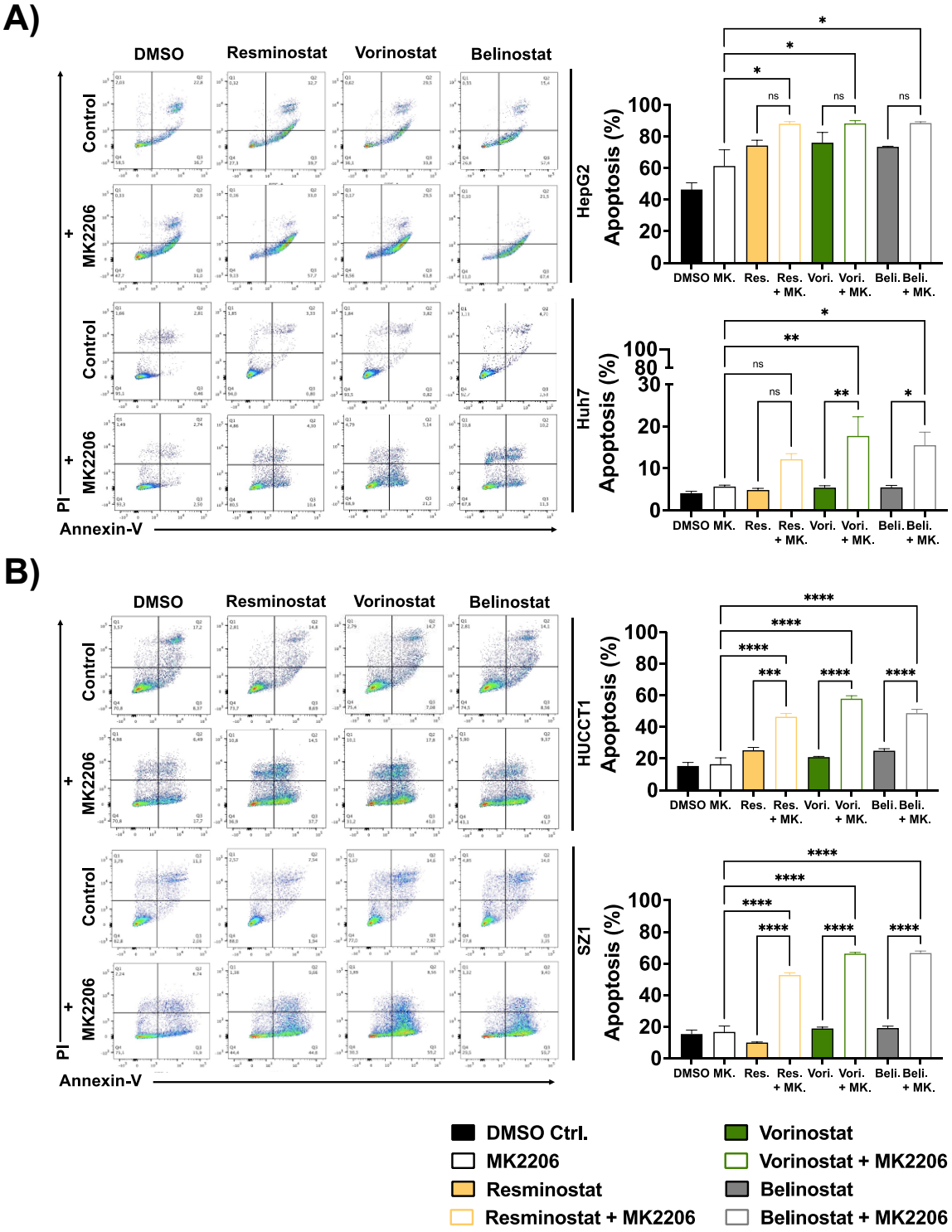

Figure 36 Shown is the analysis of apoptosis in HCC (Huh7, HepG2) (A) and CCA (HUCCT1, SZ1) cell lines (B) after treatment with 5 µM MK2206 (MK.), 1 µM Resminostat (Res.), 1 µM Vorinostat or 0.25 µM Belinostat (Beli.) alone or in combinations as indicated for 72 h. The level of apoptosis was measured by staining for annexin V and PI prior to cell sorting, using flow cytometry. Representative FACS measurements are presented (left). The annexin V positive early and late apoptotic cells (lower and upper right quadrant of each measurement) were quantified using the FlowJo™ v10.7 software and plotted in bar graphs (right). using GraphPad Prism V9. Data represent standard error of the mean of three independent experiments. Statistical analysis comparing the combination to the monotherapy with HDACis or MK2206 was performed using Graphpad Prism and the Dunnett's multiple comparisons test (= p <0.05; ** = p<0.01, *** = p<0,001, **** = p<0,0001, ns= Not Significant).*

MK./Vori (P<0.01) and MK./Beli (P<0.05). To conclude, the results indicated that combining AKTi to HDACi induced apoptosis in HCC and CCA cell lines but also showed that CCA cells reacted more sensitive to the co-treatment.

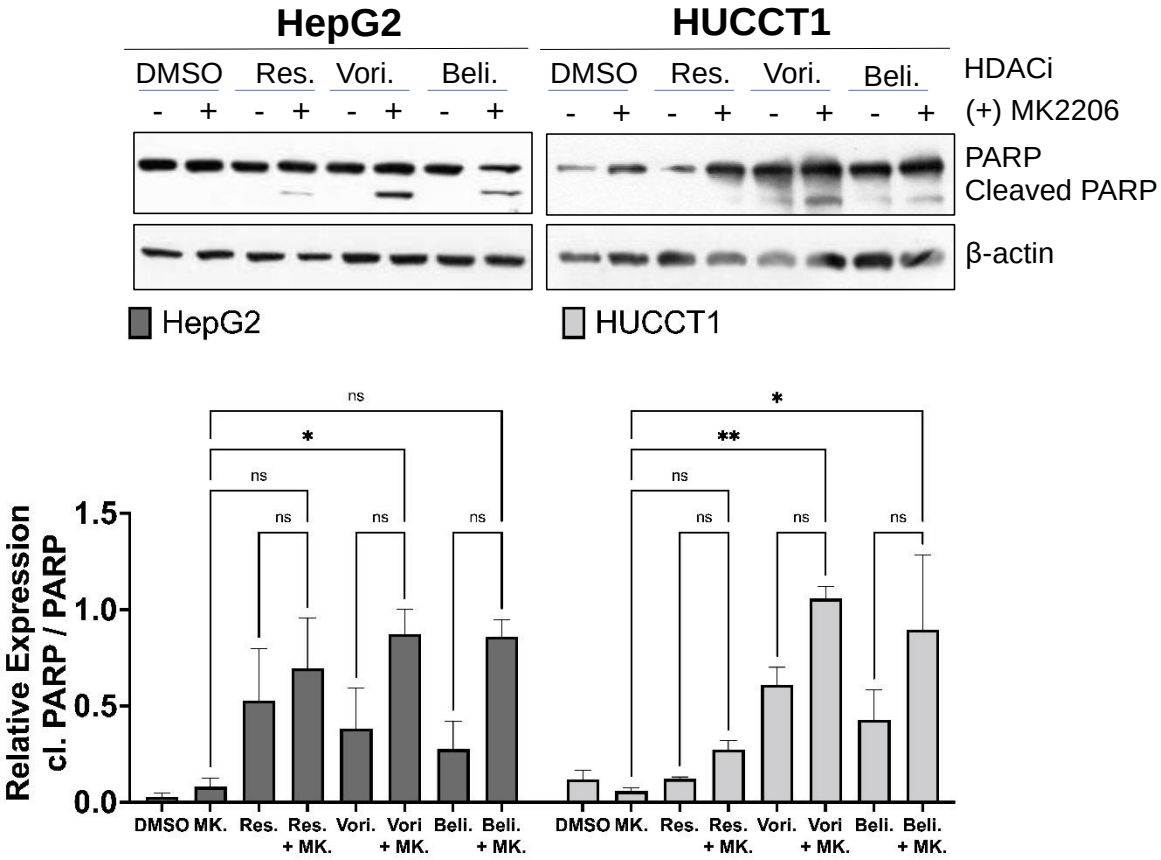

Figure 37. Shown is the western blot analysis and quantification of apoptotic marker Poly (ADP-ribose) Polymerase 1 (PARP) and cleaved PARP in HCC (HepG2) and CCA (HUCCT1) cells. Cells were seeded overnight and then treated with 5 µM MK2206 (MK.), 1 µM Resminostat (Res.), 1 µM Vorinostat or 0.25 µM Belinostat (Beli.) alone or in combinations as indicated. Protein extraction and western blot analysis was performed after 72 h of treatment. β-actin was used as loading control. Data represent standard error of the mean of three independent experiments. Statistical analysis was performed using 2 Way ANOVA and the Šídák's multiple comparisons test. Changes in apoptosis were assessed by comparing the combination to MK2206 or each respective HDACi (= p <0.05; ** = p<0.01, ns= Not Significant).*

3.2.8. MK2206/HDACi drug combinations alter the PI3K/AKT/mTOR pathway in HCC and CCA cell lines.

We next investigated the changes in the PI3K/AKT/mTOR pathway upon the combinations. Western blot analysis was performed in HCC (HepG2) and CCA (HUCCT1) cell line and we assessed 4 key signaling proteins of the pathway (AKT, mTOR, p70S6K and 4E-BP1). Analysis and quantification were performed comparing each combination to MK2206 or the respective HDACi alone, only significant changes are indicated as such.

Upon the addition of MK2206, we observed that AKT phosphorylation at S473 and T308 (Fig. 35 A/B, $pAKT^{308/473}$ / AKT) was inhibited in both cell lines, which is in line with the literature. This inhibition was not altered significantly in the combinations, suggesting that MK2206 way of action is sustained in the combination with the HDACi. Comparing the combinations to the respective HDACi we showed that $pAKT^{308}$ was significantly reduced with MK./Res. in HepG2 cells ($p<0.05$) and with MK./Beli. in HUCCT1 ($p<0.05$) cells. MK./Beli. significantly reduced $pAKT^{473}$ in HepG2($p<0.05$) and HUCCT1($p<0.05$) cells. Interestingly, we further observed that the treatment with MK2206 alone did not inhibit mTOR activation in both cell lines (Fig. 35 A/B, pmTOR / mTOR). In contrast to that, except for the treatment of HepG2 cells with the Mk./Res., combining MK2206 to HDACis decreases mTOR phosphorylation in both cell lines. In HUCCT1 cells we showed that MK./Res ($p<0.001$) and MK./Vori. ($p<0.05$) reduced P-mTOR significantly compared to the respective HDACi. Similarly, we did not observe a reduced expression of phosphorylated p70S6K (Fig. 35 A/B, P-p70S6K / β-actin) and 4E-BP1 (Fig. 35 A/B, p-4E-BP1 / β-actin) during MK2206 treatment alone. Interestingly, in HUCCT1 cells, MK./Beli. ($p<0.05$) inhibited P-4E-BP1 expression and MK./Vori. ($p<0.05$) as well as MK./Beli ($p<0.05$) also showed a significant reduction in P-p70S6K.

To sum up, these results indicate that inhibiting AKT may trigger an AKT-independent signaling, which diminish its effect on cancer cells, resulting in the need to combine it to other therapeutic targets. Secondly, the results imply that combining AKTi and HDACi may inhibit this alternative AKT-independent pathway and thus be a promising co-treatment approach. The quantification

further showed that, the combination with Belinostat followed by Vorinostat inhibited P-AKT, P-mTOR and its substrates more effectively than MK2206 combined to Resminostat.

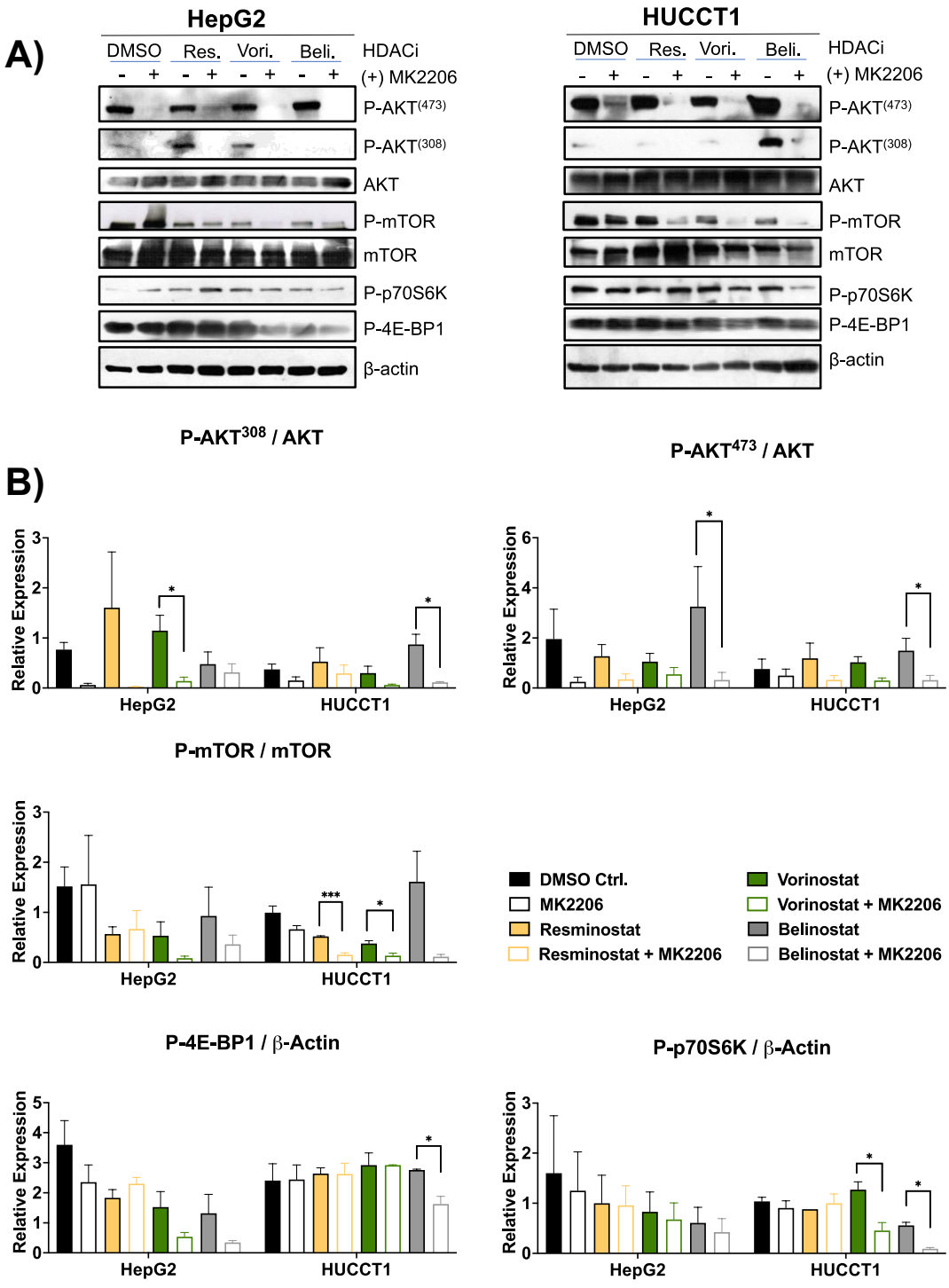

Figure 38 Shown is the western blot analysis and quantification of signaling proteins of the PI3K/AKT/mTOR pathway. Protein extraction and western blot analysis of phosphorylated(P) AKT (S473), P-AKT (T308), (pan-)AKT, P-mTOR, mTOR, P-p70S6K and P-4E-BP1) was performed after 72 h of treatment with 5 µM MK2206 (MK.), 1 µM Resminostat (Res.), 1 µM Vorinostat (Vori.) and 0.25 µM Belinostat (Beli.) alone or in combinations as indicated. DMSO was used as vehicle control. β-actin was used as loading control. Representative Western blots are shown in A and the quantification of three independent experiments is shown in B. Data represent standard error of the mean. Statistical analysis was performed using multiple t-test comparing the combination either to MK2206 or to the respective HDACi. Only significant differences are shown. (= p <0.05; *** = p<0,001).*

3.2.9. The PI3K/SGK1/mTOR pathway is inhibited during MK2206/HDACi co-treatment in HCC (HepG2) and CCA (HUCCT1) cells.

To find further evidence on alternative pathways that may be activated after AKT inhibition, we performed an RT^2 profiler PCR assay of the PI3K/AKT/mTOR pathway. We compared MK2206 treatment (5 µM) alone to the combination with Belinostat (5 µM MK + 0.25 µM Beli.). MK./Beli. was chosen because it constantly led to promising results in previous experiments. We aimed to identify genes in the PI3K/AKT/mTOR pathway that are commonly regulated in both cell lines when treated with the combinations compared to MK2206 alone.

We applied a threshold of $P<0.05$ and a log2 foldchange of <-1.5 or >1.5 as suggested by the vendor. The result showed that 12 out of the 84 genes were 1.5-fold up or down-regulation in HepG2 cells, with 8 genes up and 4 genes downregulated. Compared to that, 16 out of 84 genes were identified in HUCCT1 cells, with 13 up and 3 downregulated (Table 9). The results further indicate that MK./Beli. treatment significantly decreased serum- and glucocorticoid-regulated kinase 1 (SGK1) and p53 mRNA level (Log2 fold change HepG2/HUCCT1: -2.46/-2.07 (SGK1) -1.78/-2.5 (p53)) in both cell-lines (Table 10). Overall, these results implies that a common regulation upon the combination in both cell lines may include one or both genes.

We next investigated SGK1 and p53 protein expression after treatment with 5 µM MK2206 (MK.), 1 µM Resminostat (Res.), 1 µM Vorinostat (Vori.) and 0.25 µM Belinostat (Beli.) alone or in combinations as indicated (Fig. 36A). We then compared MK2206 treatment not only to the combination MK./Beli as it was performed for the RT^2 profiler PCR assay but also to MK./Res. and MK./Vori. (Fig. 36B).

Western blot analysis and quantification showed that in HepG2 cells, p53 expression was not significantly changed by any treatment. We observed a slight decrease in its expression upon MK./Beli. Further, in HUCCT1 cells, only the combination MK./Beli. significantly changed p53 expression (Fig. 36 A/B, p53 / β-actin). These results imply that changes in p53 expression is rather specific to the MK./Beli. treatment and not a general event occurring upon AKTi and HDACi treatment.

Results in HepG2 cells showed that MK2206 alone did not alter SGK1 expression and that upon the treatment with HDACi Vorinostat and Belinostat alone, SGK1 expression was increased, albeit not significantly. Interestingly, we observed that MK./Beli ($p<0.05$) and MK./Vori. ($p<0.05$) co-treatment significantly inhibited SGK1 expression.

In HUCCT1 the treatment with MK2206 or Resminostat alone did not changed SGK1 expression, while a slight decrease in its expression could be observed with Belinostat or Vorinostat alone. Similarly, to the observation in HepG2 cells the co-treatment MK./Beli. and MK./Vori. significantly changed SGK1 expression (Fig. 36 A/B, SGK1 / β-actin).

To conclude it seems as if MK2206 treatment does not directly trigger SGK1 expression. However, the co-treatment MK./Beli or MK./Vori reduced SGK1 expression significantly in both cell lines.

Table 9. Shown are the results of the mTOR signaling RT² Profiler PCR assay in HepG2 and HUCCT1 cells treated with 5 µM MK2206 alone or in combination with 0.25 µM Belinostat. Briefly, cells were seeded overnight, thereafter treated for 72 h. Cells were then harvested and total RNA was extracted and converted to cDNA. mTOR signaling cascade was investigated using the RT² Profiler PCR Array. Shown are the genes including p-values, that demonstrated a fold change of <-1.5 or > 1.5 in HepG2 and HUCCT1 cells when comparing MK2206 treatment to the combination (MK2206 and Belinostat). Positive and negative fold changes stand for up- or down-regulation, respectively. The measurement was repeated three times for each cell line and the analysis was performed using the manufacturer predesigned analysis platform for the array.

RT² Profiler PCR of the PI3K/AKT/mTOR pathway					
HepG2			**HUCCT1**		
Symbol	**Log2(FC)**	**p Value**	**Symbol**	**Log2(FC)**	**p Value**
IRS1	2,30	0,00002	**AKT1S1**	3,89	0,01554
RRAGC	2,18	0,00002	**ULK1**	3,02	0,00417
RRAGD	2,17	0,00000	**CHUK**	2,89	0,00004
RPS6KB1	2,04	0,00508	**STK11**	2,63	0,01451
RHOA	1,98	0,00043	**MAPK1**	2,45	0,00470
HIF1A	1,97	0,00041	**PRKAB2**	2,34	0,00081
PPP2R2B	1,96	0,00865	**RPS6KA5**	2,33	0,00214
EIF4E	1,63	0,01451	**PIK3CD**	2,07	0,00007
TP53	-1,78	0,00069	**PRKAA2**	2,00	0,00993
STRADB	-2,26	0,00643	**PRKCG**	1,97	0,00002
FKBP1A	-2,29	0,01157	**RPTOR**	1,89	0,00011

SGK1	-2,46	0,00428	**INSR**	1,75	0,00404
			DDIT4	1,71	0,00007
			CAB39	-1,70	0,00014
			SGK1	-2,07	0,00004
			TP53	-2,50	0,00013

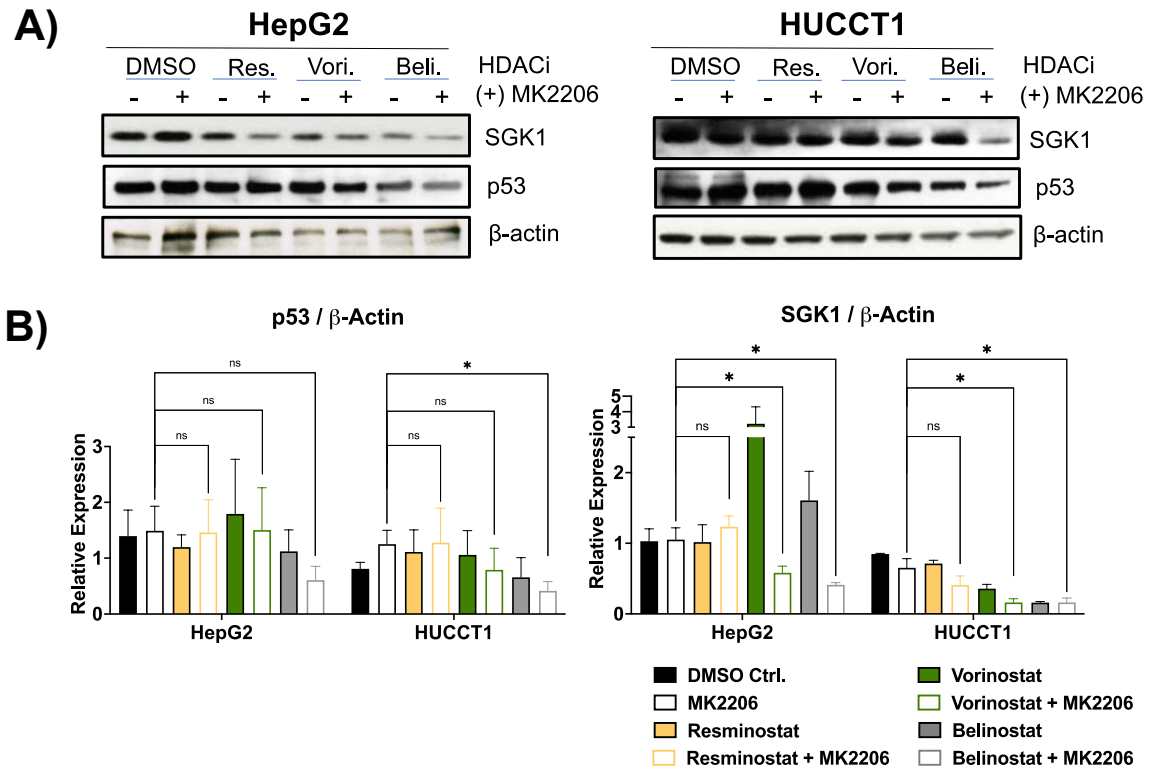

Figure 39. Western Blot analysis of p53 and SGK1 protein expression after 72 h of treatment with 5 µM MK2206 (MK.), 1 µM Resminostat (Res.), 1 µM Vorinostat (Vori.) and 0.25 µM Belinostat (Beli.) alone or in combinations as indicated. DMSO was used as vehicle control and β-actin was used as loading control. Representative western blots are shown in A and the quantification of three independent experiments is shown in B. Data represent standard error of the mean. Statistical analysis was performed using multiple t-test comparing MK2206 to the MK./HDACi combinations (= p <0.05; ns= Not Significant).*

3.2.10. MK2206/HDACi co-treatment inhibit cell growth and alters human derived HCC organoids morphology.

Finally, we investigated the combination of AKTi and HDACi in three patient-derived HCC organoids (PDOs). The organoids were seeded and treated with 5 µM MK2206 (MK.), 1 µM Resminostat (Res.), 1 µM Vorinostat (Vori.) and 0.25 µM Belinostat (Beli.) alone or in combinations as shown for 6 days. A qualitative analysis of growth and cell morphology was performed microscopically (Fig. 37).

As results, no clear difference could be observed when comparing the DMSO control to the treatment with MK2206 or the HDACi alone. In contrast to that, we observed that six days of co-treatment with MK./HDACi affected organoid HCC 1 – 3 growths when comparing the combinations to MK2206 alone or to the respective HDACi (Fig. 37). Microscopic analysis further indicated that PDOs co-treated with MK2206 and any of the HDACi not only inhibited their growth but also showed shrunk and dark cells, which implied dying or death cells (yellow arrows). Interestingly, all combinations showed comparable results throughout all organoids.

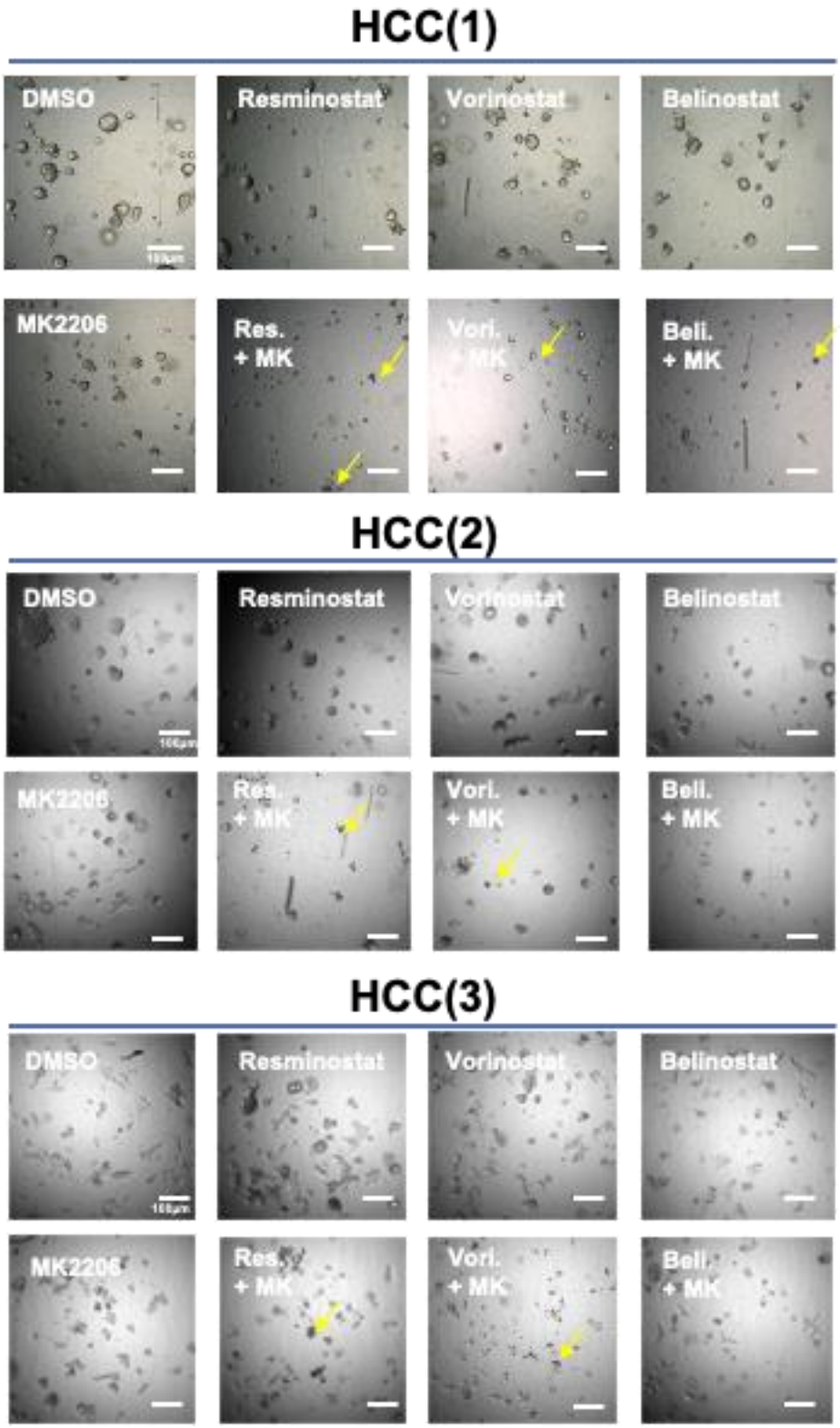

Figure 40 Shown are representative phase contrast images of tumor-derived organoids from three different patients, after treatment with 5 µM MK2206 (MK.), 1 µM Resminostat (Res.), 1 µM Vorinostat (Vori.) and 0.25 µM Belinostat (Beli.) alone or in combinations as shown. Briefly, organoids were seeded in Matrigel and incubated for two days before treatment for 6 days. DMSO was used as vehicle control. The Organoids were analyzed microscopically after treatment and pictures were taken. Images show cell type specific morphology & growth characteristics. Scale bar 100 µm.

3.2.11. MK2206/HDACi co-treatment act synergistic or additive to reduce viability in patient derived HCC organoids

We next aimed to see whether the MK2206/HDACis combinations were synergistic in PDOs. We seeded the organoids as previously described and combined 5 different concentrations of MK2206 to 6 different concentrations of each HDACi. The chosen concentrations ranged around the calculated IC_{50} values. The resulting 5 x 6 matrices were used to build synergy landscapes using the ZIP model the “SynergyFinder” software 2.0 (141, 142). The treatment matrices were then used to calculate the average synergy score (Fig. 38). Three PDOs were investigated

As a result, we observed that the average synergy score, ranged between 1.2 for MK./Res. in HCC (3) and 11.5 for MK./Vori. in HCC(2). Interestingly only the combination with MK./Vori. (synergy score: 11.5) and MK./Beli. (11.0) in HCC(2) showed synergistic interaction with synergy values above 10. All the remaining interactions rather additive with synergy values between 0 and 10.

Further, looking at the most synergistic area (yellow square) we observed that the combination MK./Vori. demonstrated significant interactions throughout all tested organoids. Following that the combination MK./Beli. showed synergistic interaction in 2 out of 3 organoids. No synergistic interactions were observed for MK./Res. Of note, none of or combination showed a threshold below -10 for likely antagonistic interactions. Conclusively, our experiments employing human derived organoids further suggest combining an AKTi with an HDACi as a new option to target liver cancer.

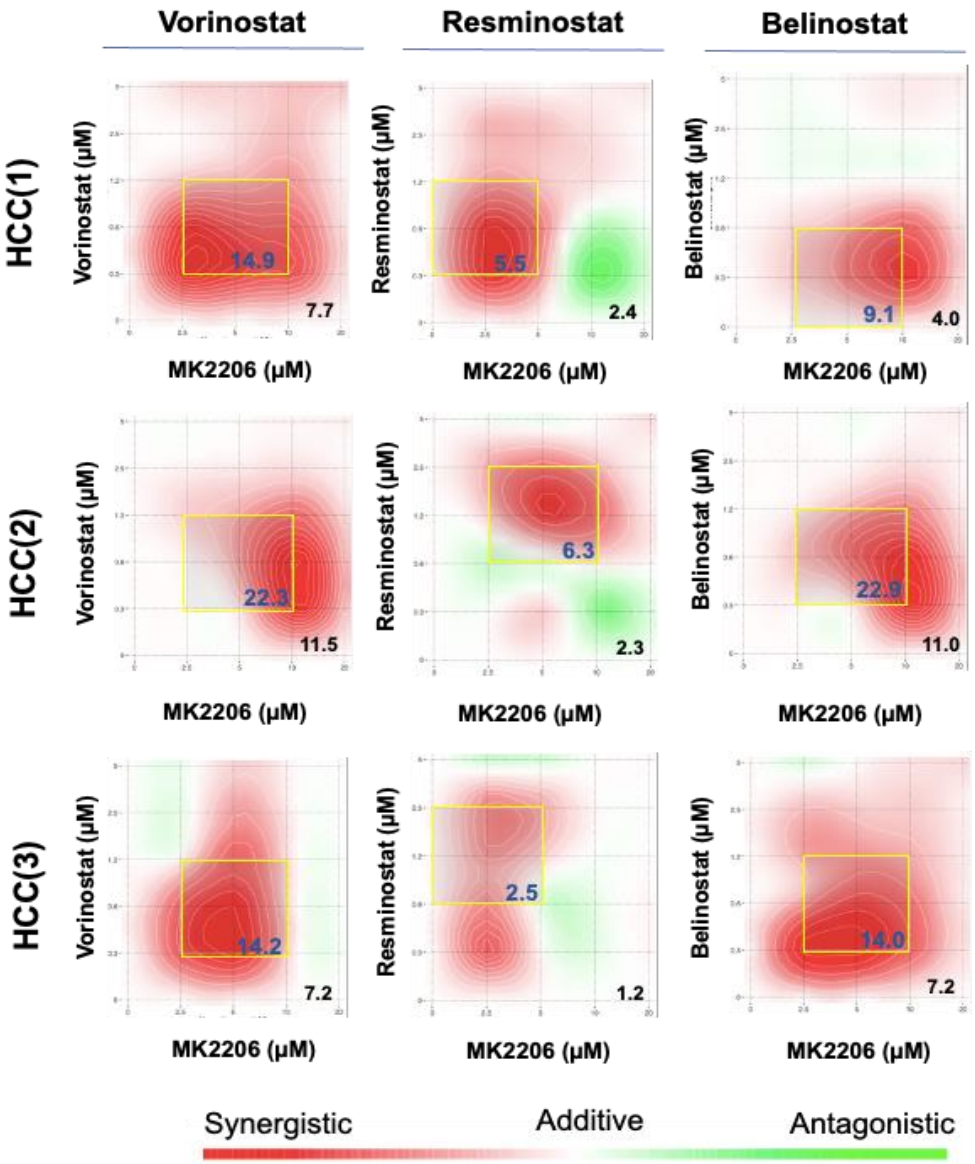

Figure 41 Shown is the analysis for synergistic interaction of the MK2206/HDACis combinations. Three HCC organoids (HCC 1-3) were used to investigate the combination of MK2206 with three different HDACi drugs Vorinostat, Resminostat, and Belinostat. We visualized and explored the MK2206/HDACis combinations using the web-based analytical package SynergyFinder 2.0 synergy landscapes. Organoids were seeded in a 384 well plate for 48h and thereafter treated with 5 different concentrations of MK2206 (20, 10, 5. 2.5, 0 µM) and 6 different concentrations of the HDACis (Vorinostat, Resminostat and Belinostat with 5, 2.5, 1.25, 0.625, 0.312, 0 µM). After 6 days of treatment the tumor organoids´ viability was evaluated using the Cell Titer-Glow 3D cell viability assay. The resulting cell viability values of each 5 x 6 matrices were used to build and visualize synergy landscapes using the zero-interaction potency (ZIP) model. The average synergy score is shown in the right lower corner of each graph (black values), the most synergistic area and the corresponding synergy score is shown within the yellow square in each graph. Scores > 10 indicate that the drug interactions are likely to be synergistic. Scores between 10 to -10, indicate that the interaction is likely to be additive and scores < -10, imply that the interaction is likely to be antagonistic (https://synergyfinder.fimm.fi/synergy/synfin_docs).

4. Discussion and outlook

HCC and CCA molecular heterogeneity pose severe challenges to the success of currently available systemic therapies. Addressing different molecular targets and finding novel therapeutic agents which could potentially augment the presently available options, with the overall goal of improving the survival of more patients with advanced HCC or CCA, was identified as a gap to be addressed. The presented study focused on three molecular targets, ADORA3 activation, direct AKT inhibition and HDAC inhibition and defined two major aims. Firstly, we aimed to explore role of ADORA3 in HCC and CCA. ADORA3 has been identified as a promising target in HCC but its role is still poorly understood. To date no investigations have addressed the importance of ADORA3 in CCA. Secondly, we aimed to investigate novel combination treatment approaches for the treatment of HCC and CCA. The following five objectives were investigated to address these aims.

4.1. Explore the role of ADORA3 in HCC and CCA by analyzing and comparing its expression in healthy vs. tumor tissue.

The importance of ADORA3 in inflammation and cancer onset/development has been reported over the last decade and has recently been reviewed by Pnina Fishman and Mazziota et al.(174, 175). In this context, Pnina Fishman and other studies further summarized the role of ADORA3 especially, as a potential target to treat cancer (77, 78, 86, 87, 176, 177). Interestingly ADORA3 pathophysiological activity in a variety of cancer types has repeatedly been corelated to its overexpression. High A3AR expression levels were reported in peripheral blood mononuclear cells (PBMCs) of patients with inflammatory diseases and cancer. Solid tumor cells, including breast, colon, small cell lung and pancreatic carcinoma, and melanoma, were reported to highly express ADORA3 compared to normal adjacent tissue cells (85, 90, 92, 93).

We are the first to illustrate a detailed comparison of ADORA3 expression in HCC, CCA, and normal liver tissues. Our investigations on ADORA3 expression showed that it is heterogeneously expressed in healthy liver, HCC and CCA

tissue. We showed a profound ADORA3 expression in normal liver tissue by immunohistochemistry, as well as by mRNA expression levels from an open-source database and own needle biopsy samples. Another important finding was that on the one hand, some tumor samples did not show to express the receptor at all and on the other hand, healthy tissue samples tended to have a higher receptor expression than previously assumed. Interestingly, this outcome is in contrary to previous studies and challenges the general assumption that ADORA3 is overexpressed in tumor tissues compared to healthy tissues (92, 178). The first and so far only phase II study with HCC included patients with liver cirrhosis CHILD B without any stratification concerning ADORA3 due to the hypothesis that a general overexpression of ADORA3 receptors is present in HCC (96). Compared to the reported phase II study by Stemmer et al. our observations rather suggest that a preselection of patients based on ADORA3 expression might be necessary to discriminate between responding and non-responding patients.

4.2. Investigate molecular mechanisms triggered after ADORA3 stimulation with the selective agonist Namodenoson

4.2.1. ADORA3 is ubiquitously expressed and its stimulation using Namodenoson trigger antiproliferative effects in HCC and CCA cell lines

ADORA3 agonist Namodenoson is a small water-insoluble, orally bioavailable compound that has been attributed to stimulate anticancer and anti-inflammatory effects on pathological liver cells alongside its hepatoprotective effects on normal liver (176). The stimulation of ADORA3 by Namodenoson has already reached clinical testing for non-alcoholic steatohepatitis (NASH) (95) and HCC (96, 179). Its mechanism of action in HCC as shown in preclinical studies so far, entails the modulation of key signaling proteins such as WNT/β-Catenin and NF-κB, as the foundation of drug efficacy. However, to select relevant patient groups in further clinical trials, more data are needed to characterize ADORA3 and cellular responses after receptor stimulation in liver cancer. To the best of our knowledge

the presented study is the first to investigate Namodenoson way of action in different CCA cell lines.

To further get more insight into the role of ADORA3 for cellular characteristics, we firstly aimed to look at ADORA3 expression in different HCC and CCA cell lines. HepG2, JHH1, and Huh7 are commonly used cell lines in studies on HCC (180). HUCCT1 and RBE have been reported to be derived from intrahepatic cholangiocarcinoma and TFK1 from an extrahepatic Cholangiocarcinoma (181) We observed clear albeit varying expression of ADORA3 in all tested cells. Interestingly ADORA3 expression seem to be the lowest in TFK1 cells, which are extrahepatic. The presented study further demonstrates a concentration dependent decrease in cell proliferation after ADORA3 stimulation with Namodenoson in all HCC and CCA cell lines, which is in line with the literature. Interestingly however, lower concentration of the drug appeared to rather enhance proliferation. This can be explained by the fact that, even though Namodenoson behaves as full agonist in most tissue (182) it was likewise observed that selective agonists only induce pro-apoptotic effects at higher micromolar concentrations while behaving as low efficacy partial agonist at lower concentrations (183, 184). Another assumption could be that Namodenoson albeit selective to ADORA3 could trigger its antiproliferative effect at higher concentration by activating receptor independent pathways. Our investigations on Namodenoson receptor dependency for antiproliferative effect, using a selective antagonist or RNAi technology, negate a receptor independent effect and rather support the assumption that receptor activation is a crucial starting point. In support with previous findings, this first results indicate that targeting ADORA3 in HCC is a promising approach to inhibit tumor progression. While preliminary the presented results also suggest that targeting ADORA3 in CCA, which has not been addressed before, might be effective to reduce tumor growth. Finally, we show that this antiproliferative effect depends directly on the receptor.

4.2.2. Namodenoson alters epigenetic modifiers.

A variety of mechanisms have been attributed to the mechanisms of action of Namodenoson on tumor cells. The main mechanisms that have been found were the deregulation of the NF-κB and the WNT/β-Catenin signal transduction pathways (77). However, none of the studies so far investigated whether triggering ADORA3 is directly responsible for these events or whether they are just bystander observations in the sense of a non-target influence of Namodenoson on tumor cells. At least for the antiproliferative effect we could demonstrate receptor-dependency as already discussed in section 8.2.1.

For a drug that is investigated in clinical trials the knowledge of Namodenoson influences on tumor cells is quite low. Therefore, we performed RNA-seq analysis of HepG2 cells treated with Namodenoson or DMSO control and assessed differential gene expression profiles after 24h and 36h of treatment. As a follow-up, we performed a gene set enrichment analysis to identify Namodenoson induced pathways. To the best of our knowledge, no data have been reported on gene profiling changes induced by Namodenoson in tumor cells. Interestingly, we observed a profound alteration in gene expression upon the treatment with Namodenoson within the first 24h. Numerous studies describing a tumor cell-dependent modification of the gene expression profile (GEP) after the addition of a receptor agonist exists (185-187). Those studies, however, focus on the drugs'-induced changes in transcription factors such as NFκB, which subsequently alter the GEP. Indeed, we observed an increased in transcription factor binding side after 24 h however, the gratitude of altered genes in our experiment, led us to hypothesize, that not only transcription factors may be induced by Namodenoson but also that chromatin remodeling events may be triggered by the treatment. A connection between ADORA3 activation and epigenetic remodeling events have not been described so far. To investigate further on our hypothesis, we performed a gene set enrichment analysis (GSEA) and found that 18 curated gene sets related to epigenetic remodeling events were significantly altered.
Interestingly the downregulation of those gene sets is associated with an increased transcriptional activity. Senese and colleagues showed that

downregulation of HDAC1 or HDAC1 combined with HDAC2 affected the transcription of specific target genes, that are involved in cell growth inhibition and an increased apoptosis (164). Based on the study performed by Pasini and colleagues the downregulation of SUZ12 targets implies an inactivation of SUZ12 with in turn is characterized by a global loss of H3K27 trimethylation (165). A decreased Methylation pattern is associated with an open chromatin status. Lu and colleagues associated the downregulation of EZH2 to a reduced methylation status of the vasohibin 1 (VASH1) expressing gene, which led to VASH1 reactivation and subsequently cancer cell growth inhibition (166).

The GSEA suggested that Namodenoson may impact the regulation of different HDACs, which we addressed by a qPCR and acetyl H3 expression analysis and confirmed. We demonstrate the downregulation of eleven HDACs and the changes in histone H3 acetylation upon the treatment with different concentrations of the Namodenoson. To sum it up, we could, for the first time, show evidence that ADORA3 activation with the agonist Namodenoson induces epigenetic remodeling events, including a downregulation of HDAC enzymes. In this context one can hypothesize that ADORA3 agonist Namodenoson acts as a drug that target epigenetic marks such as HDACs. Such drugs are also known as epidrugs (188). This would be a new attribute to the way of action for Namodenoson, that has not yet been described. Pharmacoepigenetic investigation and the importance of epidrugs in cancer treatment, is an emerging field especially towards precision medicine and when considering epigenetic alterations as the basis of individual variation in drug response. Epigenetic modifications acquired during lifetimes can be reversed. Drugs that regulate epigenetic changes associated with medical conditions are therefore promising therapeutic agents. In the case of Namodenoson the epigenetic profile of patients that would benefit from the treatment still need further investigation, however the presented study demonstrates preliminary evidence. Further we hypothesize that the clinical response of Namodenoson may be increased in a group of patients preselected based on the receptor expression and specific epigenetic marks.

4.3. Explore the potential benefit of simultaneous ADORA3 activation and HDAC inhibition as novel treatment strategy for HCC and CCA

4.3.1. Inhibition of HDACs and ADORA3 stimulation synergize to inhibit cell growth in HCC and CCA cells

Along with identifying the downregulation of HDAC enzymes upon Namodenoson treatment, we hypothesized whether a combination therapy of ADORA3 agonists and HDAC inhibitors might substantially enhance the effects of each monotherapy on liver cancer cells. This might be interesting for future clinical studies; therefore, we chose drugs that are already in clinical testing or are even approved for the treatment of other diseases for further experiments. We chose Vorinostat, Resminostat, Romidepsin and Belinostat and explored the HDAC inhibitors in combination with two different concentrations of Namodenoson in HCC and CCA cell lines. We demonstrate that all combinations enhance the antiproliferative effects of each drug alone in an additive or synergistic way. Interestingly, the combinations using Resminostat and Vorinostat were the most promising. Using Resminostat in a combination therapy has already been shown as effective. Streubel et al. (74) showed that combining Resminostat to Sorafenib triggered anti-proliferative effect and counteracted platelet-mediated pro-tumoral effects in HCC cells and Bitzer et al. showed that the combination with Resminostat was safe and that PFS was increased compared to the monotherapies (73). Gordon et al. investigated Vorinostat in the combination with Sorafenib and stated that even though the schedule and treatment strategy applied resulted in toxic and discouraging adverse effects the investigators underlined that the combination led to durable disease control (167).

The investigations so far showed that the combination effect can be reached by the treatment with different HDAC inhibitors, therefore it seemed to be an effect of this class of drugs and not just an observation of a certain drug combination. To further assess whether our observations could also be extended to other ADORA3 agonists, we chose the structurally similar (CF101) and the structurally different (MRS5698) agonists in our combination.

Notably, both agonists showed similar results. MRS5698 appeared to slightly affect proliferation more effectively. This could be explained by MRS5698 higher affinity and greater selectivity for ADORA3 compared to CF101 and Namodenoson (189). Using Namodenoson or any HDACi alone in the first place or combining Namodenoson to an HDACi to treat CCA has not been described yet. The presented study shows that CCA can likewise be targeted by combinations with Namodenoson and HDACi. HUCCT1 and RBE cells were observed to have a higher ADORA3 expression than TFK1 cells. We were the first to investigate the response of Namodenoson treatment in ADORA3 expressing CCA cells. However, since HUCCT1 and RBE cells are intrahepatic CCA derived cell lines, future research should further address the similarities and differences of ADORA3 stimulation with an agonist in extrahepatic derived CCA cells

Combinatorial therapies against HCC and CCA are the future treatment regimens widely recommended by experts (8, 190, 191). Here we describe a new approach that inhibits cell proliferation in vitro.

4.3.2. Inhibition of HDACs and ADORA3 stimulation synergize to inhibit cell growth in HCC patient-derived organoids

Ex-Vivo 3D Tumor organoid models enable the maintenance and culture of cells derived from patients and are generally considered as superior models compared to the established monolayer cell lines.

All investigated substances have already been at least part of clinical trials or have been approved for treating other diseases. The additive or synergistic inhibition of cell proliferation observed when ADORA3 agonists are combined to HDACis suggest that translating the combined therapy of ADORA3 activation and HDAC inhibition into clinical trials could be a promising approach. However, to further increase the evidence for such an approach, we investigated the effect of the combination therapy on patient-derived organoids. We used organoids from a previously generated cell bank (134), that were available without any further stratification. Interestingly, comparing the IC50 values of treated cell lines to the values of the tested organoids, we observed that organoids were more sensitive

to the agonist treatment, which could have different reasons. One reason could be that drug sensitivity of organoids strongly depend on its molecular profile, which is more preserved in organoid culture than in cell lines (192). Therefore, the organoids used may not have had the appropriate genetic profile to be effectively targeted. Secondly, organoid generation and propagation need many cofactors and other medium components that may influence the response to certain drugs (193). Moreover, the interplay between tumor microenvironment, extracellular factors, and drug response should not be neglected (194-196). The Synergy analysis of the combination demonstrated that all combinations were at least additive, which can be interpreted as predictive for the expected effect of the treatment in patients(196), and thus further supports the translation of the approach to a clinical setting. Bartfeld et al. described that organoid being the miniaturized avatar of a specific patient's organ, enable researcher to identify the ideal treatment for a particular patient (197). This approach is trendsetting and is currently applied in different settings. The APOLLO trial was the first study to offer organoid-assay-guided treatment. The investigators aimed to determine whether patients' derived organoid pretests, could help guide precision treatment for patients with colorectal cancer (CRC) and peritoneal metastases. This approach proved to be effective, feasible and reproduceable (198). Ooft et al. showed a correlation between drug treatment response from patient-derived organoids from biopsy samples and the patients' responses to the drug (199). Further a phase 3 clinical study is currently ongoing where the investigators explore whether chemotherapy regimens guided by organoid drug sensitivity test can improve the outcomes of advanced pancreatic cancer (NCT04931381). Of note the success rate of pretesting organoids to estimate the patient's response is closely related to the success rate for generating the respective tumor organoids. The success rate for generating CRC or Glioblastoma derived organoids lies at around 90 % and the rate for HCC and CCA is currently at about 26 % (134, 200, 201).

To sum up, our results hint toward a particular treatment benefit of our proposed therapy in a selected group of patients. However, due to the small cohort and the

challenges of organoid cultivation, further studies need to be conducted to solidify our assumptions.

4.4. Investigate the effect of an AKT/HDAC co-inhibition on three different hallmarks of cancer: sustained proliferation, evaded apoptosis, and promoted cell migration.

4.4.1. AKTi/HDACi co-treatment enhances antiproliferative effects compared to the monotherapies in different HCC and CCA-established cell lines.

The phosphatidylinositol 3-kinase (PI3K)/protein kinase B (AKT)/mTOR pathway has gained more and more interest as a therapeutic target since it is involved in different hallmarks of cancer (97, 109-116). Its hyper-activation in CCA and HCC due to activating mutations such as a mutation in PIK3CA, which among others occur in up to 50% of CCAs. Loss of PTEN has been reported to correlate with tumor aggressiveness, therapy resistance and poor prognosis (8, 98). Investigations with selective AKTi MK2206 have shown promising results in preclinical studies against CCA and HCC (127, 128). Several approaches have been made to clinically establish AKTi MK2206 in cancer monotreatment, however results were discouraging (120-125). Ahn and colleagues concluded that combinatorial treatments with other molecular targets might significantly influence therapy efficacy (129). Along with that a systematic literature review further showed that a series of reversible and irreversible genomic and epigenomic alterations are crucial for HCC and CCA development and progression (44, 51, 202-204). HDACs are upregulated in HCC and CCA (48, 49, 54, 55). Clinical studies applying HDACi have been considered promising, albeit none of the studies testing monotherapies with HDACi have extended a phase II trial as previously addressed in section 5.4.1. The combination of AKT inhibitor MK2206 and HDACis has been demonstrated effective in different models of solid tumors. Buglio et al. showed that patients with relapsed or refractory Lymphoma could benefit from the combination of MK2206 and HDACi Vorinostat. This combination was associated with an increased PARP cleavage and

induction of apoptosis (130). Further preclinical study in pancreatic cancer (131) and Prostate cancer (132) also showed promising results with the combination. Janku et al. reported in a case study that two patients with advanced HCC could benefit from the combinatorial therapy with the PI3K/AKT/mTOR inhibitor sirolimus and Vorinostat (133). To the best of our knowledge, there is no report on the efficacy of combining direct AKT inhibition and HDACis in HCC and CCA. The second part of this study aimed to investigate the antiproliferative effect of direct AKT inhibition in combination with HDAC inhibition and elucidate some of the molecular underpinnings of the combinatorial therapy. The study firstly demonstrates an enhanced and synergistic inhibition of cell proliferation in different HCC and CCA cell lines when combining MK2206 to different HDACis. The cell lines chosen for the experiments have been used in preclinical studies assessing drug response in HCC or CCA (180, 181, 205, 206). These first observations were in line with our expectations and reflect what is expected since both compounds are known for their antiproliferative effects. Regarding, the impact of the combination however, 10 out of 12 comparisons were observed to show highly synergistic interaction independently of the HDACi used. This first result support the assumption that inhibiting AKT and HDACs is a promising co-target approach. Using alternative AKT inhibitors (Ipatasertib, Perifosine) showed that the observed effect can be triggered by different AKT inhibitors and is not restricted to MK2206. Ipatasertib is an inhibitor, designed to target the different isoforms of AKT directly. It was recently approved as a highly potent drug against metastatic prostate cancer when combined with abiraterone (207). Perifosine targets the PH domain of AKT and was reported to be well tolerated in early clinical trials (208, 209). Discrepancies in their effectiveness can be attributed to the difference in their way of AKT inhibition and the pathways they trigger. Ipatasertib is agreed to be an ATP-competitive AKT inhibitor, whereas MK2206 and Perifosine are allosteric inhibitors. Perifosine and MK2206 have been shown to target different pathways alongside their AKT inhibition (210). In summary, the first findings demonstrate preliminary results on the short-term effect on cell proliferation of an AKT/HDAC co-inhibition. The presented study shows that proliferation is inhibited in an additive or synergistic manner.

4.4.2. The combination of AKTi and HDACi modulates hallmarks of cancer

The hallmarks of cancer comprise, among others, malignant proliferation, evasion of programmed cell death, as well as migration, invasion and metastasis (211). We aimed to investigate on whether combining AKTi and HDACi affected these hallmarks. The first hallmark analyzed was the migration and long term proliferation potential of HCC and CCA cells after the co-treatment. CCA and HCC can lead to metastasis, which are one reason for modest therapeutic effects or treatment failure (156-160). Cancer cells start to engage their metastatic journey by migration through natural barriers, such as the tumor stroma or basal membrane. One crucial feature of circulating tumor cells is their principal ability to gather and grow into colonies which leads to metastasis at distant sides from the primary tumor. AKT overexpression has been associated with an increased migration potential and sustained proliferation (90). AKT inhibition was shown to reduce these abilities (161). As demonstrated with our wound healing assay, most of the combinations showed significant inhibition of wound closure and cell migration when compared to the respective HDACi but not when compared to MK2206. Of note, HepG2 cells compared to all the other cell lines had the lowest migration potency, which has already been observed in other studies. the investigator addressed the difference. Nguyen et al. stated that the reduced migratory capability observed with HepG2 cells might be due to their high levels of E-cadherin, which is responsible for their epithelial phenotype. However, the likewise resumed that including HepG2 cells alongside with other cells would be representative in order to show the different HCC subtypes known in vivo (212, 213). Interestingly, Chen et al. found that overexpression of AKT1 enhanced HepG2 cell migration and invasion. In our study we demonstrate that inhibition of AKT alone inhibit HepG2 cell migration, which would be in line with previous observation (212). The presented study added up that the combination to HDACis increased the known effect. Moreover, including different cell type reflects the different results that my be observed in vivo.

Different signaling pathways such as JAK/STAT, HGF/c-Met and TGF-B and PI3K/AKT/mTOR (97, 114-116, 214-216) have been attributed to play a key function in HCC and CCA migration potential. The presented findings demonstrating that combining AKTi to HDACi does not significantly increase the effect of MK2206 alone, underline the crucial role of AKT and AKT-related pathways in migration and metastasis and indicate that the pathways additionally inhibited upon addition of HDACi may not be central in this context. Further, Zhang et al. as well as Noh et al. showed that HDACi mediated inhibition of migration in vitro is partly due to inhibition of the AKT pathway (217, 218). It can therefore be concluded that AKT inhibition has an effect on the migration potential of HCC and CCA cells in vitro, and that the combination to HDAC inhibitors supports the AKT mediated inhibition.

The second most important feature of a cancer cell is the ability to grow into colonies. In contrast to the differences, we observed for the migration assay, after performing the clonogenic assay we showed that long-term proliferation was significantly inhibited in almost all combinations compared to either monotherapy. Further CCA cells appeared to be more sensitive to the combinations than HCC cells in this context. These findings are central because the hints toward the most beneficial effect of the combination therapy, namely inhibiting proliferation and probably also overcoming resistance to each monotherapy. The presented study show that the combination inhibited proliferation on a short and on a long term. Hua et al. summarized that long term application of an AKT inhibitor enhances compensatory signaling pathways, such as the RAS/RAF/MEK/ERK or the SGK1/mTOR path, which confers resistance to AKT inhibition or sustain AKT independent activation of signaling molecules. The authors concluded that simultaneous inhibition of Akt and other compensatory pathways may improve each drug efficacy (219).

Induction of apoptosis is the principal mechanism by which MK2206 was described to induce cell death in HCC and CCA cells (127, 128). Therefore, we looked at the induction of apoptosis upon our treatment. Our result support previous findings and further show that the combinatorial treatment was successful where the monotherapies failed to show significance. We validated

this by looking at PARP cleavage as one marker for apoptosis. Of note, CCA cells showed an increase amount of apoptotic cells and a higher expression of cleaved PARP upon AKT and HDAC inhibition, which suggest that CCA might be more sensitive to the treatment.

To sum up, combining AKTi and HDACi trigger the extended inhibition of 3 significant hallmarks of cancer. The presented study shows that combining HDACi to AKTi supports AKT mediated inhibition of migration, which might be useful in the treatment of solid metastatic tumors. Of note 30 out of 50 clinical trials mentioned in the literature review section 5.4.3 evaluate the effect of MK2206 alone or in combinations in advanced, refractory, or metastatic tumors, which underline the applicability of the combinations under assessment. Further we show that the combination induced apoptosis and inhibited proliferation on a short- and long- term, which might help sustain a long-term response to the treatment and thus increase its overall efficacy.

4.5. Explore the molecular underpinning of AKT/HDAC co-inhibition

4.5.1. Combining AKTi and HDACi inhibits the AKT independent PI3K/SGK1/mTOR pathway.

Two phosphorylation events, one at S473 and the other at T308 are necessary for the full activation of AKT. In turn, Akt activates multiple downstream targets, most notably the mammalian target of rapamycin (mTOR) pathway. After AKT activation the primary mechanism by which AKT subsequently activates the mammalian target of rapamycin complex 1 (mTORC1) is by firstly phosphorylating and inhibiting the tuberous sclerosis complex 2 (TSC2) a GTPase activating protein (GAP) protein, allowing inactive Rheb-GDP to be GTP loaded which in turn results in mTORC1 activation. Activation of mTORC1 results in increased protein synthesis and cell survival by direct phosphorylation of its effectors, such as the ribosomal S6 kinase, 70 kDa, polypeptide (p70S6K), and 4E-BP1 (eIF4E-binding protein 1) that terminate binding to elongation factor eIF4E and relieve the block on translation (220). Experiments performed to

analyze the molecular underpinnings of AKTi/HDACi co-treatment first revealed that, as expected, upon MK2206 administration, AKT phosphorylation was inhibited at both of its activation sites S473 and T308. Looking at the downstream target of AKT, the results however showed no subsequent inhibition of mTOR upon MK2206 administration alone. In contrast to that, the combination with HDACi led to a subsequent reduction of mTOR activation and its substrates. Of note, even though the results indicate a reduction in mTOR signaling, not all combinations were statistically significant. This hints toward the need to inhibit a particular HDAC or a defined group of HDACs to achieve the best results. To do so more studies should be performed using more HDAC inhibitors, with the focus on determining the differences between those HDAC inhibitor in the presented context. This, however, would exceed the overall scope of the presented study. The incomplete inhibition of the PI3K/AKT/mTOR pathway by MK2206 however is a well-described phenomenon (221-223). One central explanation stated in all reported studies is that the incomplete inhibition may be due to the activation of compensatory pathways. Most interestingly, after performing an RT-Profiler PCR of the PI3K/AKT/mTOR pathway, we identified that the serum and glucocorticoid-regulated kinase 1 (SGK1) was significantly downregulated. The activation of SGK1 comparable to that of AKT, is mediated through phosphorylation by mTORC2 and PDK1 (224). Toska and colleagues, as well as Castel et al., demonstrated that SGK1 activation functions as an alternative to AKT and forms an AKT independent pathway to activate mTOR. It was described that tumor cells use the SGK1/mTOR path to invade AKT inhibition (225, 226). In glioblastoma, a correlation between HDAC inhibition and SGK1 inhibition has recently been postulated by Chen et al. (227). In their study, they observed that an HDAC-hybrid could inhibit SGK1 and glioma cell proliferation, invasion, and migration. SGK1 was shown to be overexpressed in HCC (228). The emerging importance of SKG1 in different hallmarks of tumor progression was recently reviewed by Sang et al. (229) and Cicenas et al.(230). They summarized that SKG1 upregulation plays a crucial role in apoptosis, proliferation, migration/invasion, metabolism, therapy resistance and autophagy in different cancer types. Further the stated that although several SGK1 inhibitors have paved the way for novel therapeutic

interventions in the future, the prospects for clinical application of these inhibitors in cancer therapy are vague, which means that more preclinical studies, especially on toxicity and safety, should be conducted, which might probably take another decade. The presented study shows that the combination of two already well studied compounds such as MK2206 and Belinostat significantly inhibited SGK1. This connection supports the use of the AKTi/HDACi combination as a possible treatment option in solid tumors an SGK1 overexpression might even be a first selection criteria in future trials.

In summary, as indicated in figure 39, we have elucidated one possible way of action of the AKTi/HDACi co-treatment.

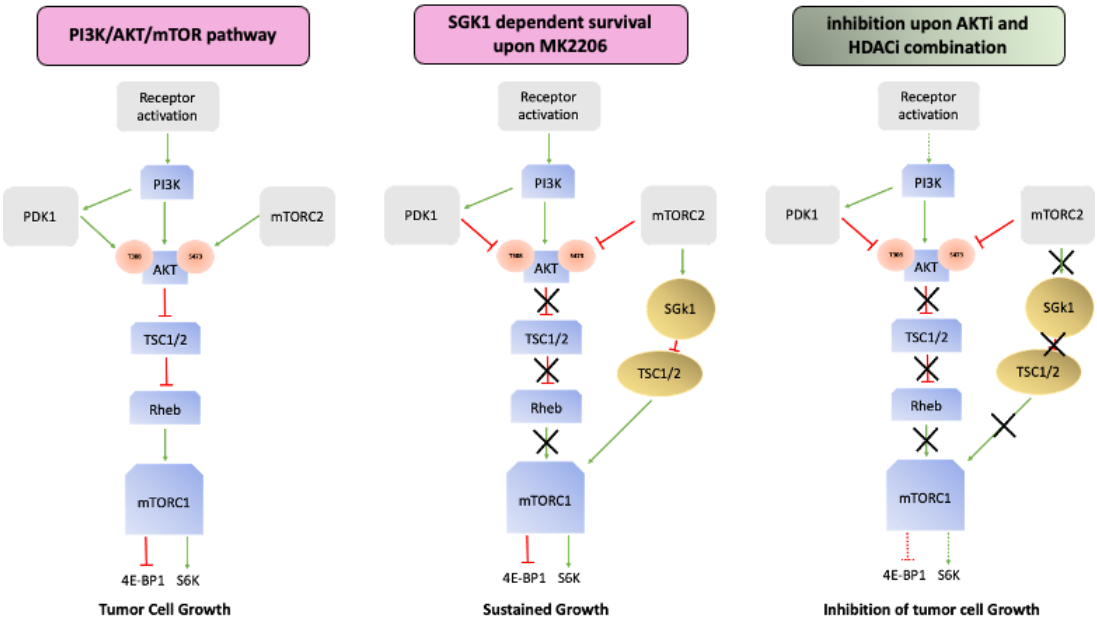

Figure 39. Proposed mechanism of action of AKT inhibition alone and simultaneous AKT/HDAC inhibition. PI3K dependent AKT phosphorylation at S473 and T308 lead to its activation subsequently to mTORC1 activation via tuberous sclerosis complex 2 (TSC2) and Rheb-GTP. mTORC1 further regulates its substrates 4E-BP1 and p70S6K (S6K), leading to tumor cell growth and proliferation (left panel). Upon MK2206 treatment (middle panel) compensatory mechanism via SGK1 is assumed, which sustain tumor growth via activated mTORC1 signaling. Combining AKTi and HDACi (right panel) blocks potential compensations, by inhibiting glucocorticoid-regulated kinase 1 (SGK1) and thus contributes to growth inhibition.

4.5.2. Patient-derived organoids support clinical translation of the combination AKTi and HDACi to treat liver cancer

Human Organoids provide unique opportunities to study human disease and complement animal models. They hold great promise but also limitations for use in medical research and the development of new treatments as discussed in

section 8.3.2. Nevertheless their benefits outweigh remaining challenges and therefore, they have already been utilized in the clinic, enabling personalized medicine for different diseases (231). Different studies imply that the outcome of drug application in organoid models is indicative for the response to be expected in the patient where the organoids are derived from. The antiproliferative effect of AKT and HDAC co-inhibition in HCC organoid showed an additive or even synergistic inhibition of cell proliferation. Interestingly, the combinations with HDACi Vorinostat showed the highest efficacy, regarding the most synergistic areas. Of note all tested drugs have been used in clinical trial or are already approved for other diseases. Vorinostat is approved for the treatment of cutaneous t-cell lymphoma. Regarding the use of MK2206 alone in clinical trials investigators have reported toxic effects with the concentrations used. The presented analysis on synergy using different concentrations of MK2206 and the respective HDACi showed that for all combinations additive or synergistic interaction would still be observed using lower concentrations of each drug.

CCA organoids could not be tested, which limits our discussion to HCC in this case. Nonetheless, due to our previous observations, we assume a comparable outcome for CCA. Looking at the colony formation assay or the migration assay even showed that HUCCT1 cells compared to all HCC cell lines appeared to be more sensitive to the treatments. We therefore hypothesized that co-inhibiting AKT and HDAC in CCA would likewise have antiproliferative effects on organoids. However, to conclusively validate the combinatorial approach in this context, further studies may be unavoidable.

To conclude our investigation on AKT and HDAC co-inhibition can be considered as a promising treatment regime. The presented study demonstrates first evidence that justify the application of the treatment in further preclinical studies or even in clinical trials.

4.6. Conclusion and Outlook

This thesis has revealed several important issues for the treatment of liver cancer. First, the role for ADORA3 stimulation in tumor cell proliferation has been examined in detail. Besides the observation, that receptor stimulation is indeed responsible for antiproliferative effects, the observation that a fraction of tumor cells do not express ADORA3 is an important finding. These results suggest that ADORA3 expression should at least be investigated in the tumor of each patient that enters clinical trials in which ADORA3 directed antitumor therapies are part of the treatment schedule. As a new mechanism of action, ADORA3 stimulation could be combined with epigenetic modulation in tumor cells, which was not known before. Finally, the results of this thesis suggest two new combination partners for HDAC inhibitors in liver cancer, namely ADORA3 agonists or AKT inhibitors. Our investigations used drugs that are either already approved for the treatment of other diseases or that have been applied in clinical trials. Therefore, besides a stimulation for further preclinical investigations our results could be the stimulus for translational clinical phase I/II trials in liver cancer. Taken together we have provided new perspectives in treating HCC and CCA, which are urgently needed.

5. References

1. Dasgupta P, Henshaw C, Youlden DR, Clark PJ, Aitken JF, Baade PD. Global Trends in Incidence Rates of Primary Adult Liver Cancers: A Systematic Review and Meta-Analysis. Front Oncol. 2020;10:171-.
2. Sung H, Ferlay J, Siegel RL, Laversanne M, Soerjomataram I, Jemal A, et al. Global Cancer Statistics 2020: GLOBOCAN Estimates of Incidence and Mortality Worldwide for 36 Cancers in 185 Countries. CA Cancer J Clin. 2021;71(3):209-49.
3. Lin L, Yan L, Liu Y, Qu C, Ni J, Li H. The Burden and Trends of Primary Liver Cancer Caused by Specific Etiologies from 1990 to 2017 at the Global, Regional, National, Age, and Sex Level Results from the Global Burden of Disease Study 2017. Liver Cancer. 2020;9(5):563-82.
4. Torre LA, Bray F, Siegel RL, Ferlay J, Lortet-Tieulent J, Jemal A. Global cancer statistics, 2012. CA Cancer J Clin. 2015;65(2):87-108.
5. Valery PC, Laversanne M, Clark PJ, Petrick JL, McGlynn KA, Bray F. Projections of primary liver cancer to 2030 in 30 countries worldwide. Hepatology. 2018;67(2):600-11.
6. Nagtegaal ID, Odze RD, Klimstra D, Paradis V, Rugge M, Schirmacher P, et al. The 2019 WHO classification of tumours of the digestive system. Histopathology. 2020;76(2):182-8.
7. Lee JS, Heo J, Libbrecht L, Chu IS, Kaposi-Novak P, Calvisi DF, et al. A novel prognostic subtype of human hepatocellular carcinoma derived from hepatic progenitor cells. Nat Med. 2006;12(4):410-6.
8. Banales JM, Marin JJG, Lamarca A, Rodrigues PM, Khan SA, Roberts LR, et al. Cholangiocarcinoma 2020: the next horizon in mechanisms and management. Nature Reviews Gastroenterology & Hepatology. 2020;17(9):557-88.
9. Sia D, Villanueva A, Friedman SL, Llovet JM. Liver Cancer Cell of Origin, Molecular Class, and Effects on Patient Prognosis. Gastroenterology. 2017;152(4):745-61.
10. Sharma D, Subbarao G, Saxena R. Hepatoblastoma. Semin Diagn Pathol. 2017;34(2):192-200.
11. Llovet JM, Kelley RK, Villanueva A, Singal AG, Pikarsky E, Roayaie S, et al. Hepatocellular carcinoma. Nat Rev Dis Primers. 2021;7(1):6.
12. WHO. Cancer Research: A Summary of Problems, Risk Factors, Diagnosis and Treatment 2021 [.
13. Chou YT, Li CH, Sun ZJ, Shen WC, Yang YC, Lu FH, et al. A Positive Relationship between Betel Nut Chewing and Significant Liver Fibrosis in NAFLD Subjects, but Not in Non-NAFLD Ones. Nutrients. 2021;13(3).
14. Ueno Y, Nagata S, Tsutsumi T, Hasegawa A, Watanabe MF, Park HD, et al. Detection of microcystins, a blue-green algal hepatotoxin, in drinking water sampled in Haimen and Fusui, endemic areas of primary liver cancer in China, by highly sensitive immunoassay. Carcinogenesis. 1996;17(6):1317-21.

15. Craig AJ, von Felden J, Garcia-Lezana T, Sarcognato S, Villanueva A. Tumour evolution in hepatocellular carcinoma. Nat Rev Gastroenterol Hepatol. 2020;17(3):139-52.

16. Dimitroulis D, Damaskos C, Valsami S, Davakis S, Garmpis N, Spartalis E, et al. From diagnosis to treatment of hepatocellular carcinoma: An epidemic problem for both developed and developing world. World J Gastroenterol. 2017;23(29):5282-94.

17. Llovet JM, Zucman-Rossi J, Pikarsky E, Sangro B, Schwartz M, Sherman M, et al. Hepatocellular carcinoma. Nat Rev Dis Primers. 2016;2:16018.

18. Llovet JM, Montal R, Sia D, Finn RS. Molecular therapies and precision medicine for hepatocellular carcinoma. Nat Rev Clin Oncol. 2018;15(10):599-616.

19. Abou-Alfa GK, Schwartz L, Ricci S, Amadori D, Santoro A, Figer A, et al. Phase II study of sorafenib in patients with advanced hepatocellular carcinoma. J Clin Oncol. 2006;24(26):4293-300.

20. Weis SM, Cheresh DA. Tumor angiogenesis: molecular pathways and therapeutic targets. Nat Med. 2011;17(11):1359-70.

21. Donisi C, Puzzoni M, Ziranu P, Lai E, Mariani S, Saba G, et al. Immune Checkpoint Inhibitors in the Treatment of HCC. Front Oncol. 2020;10:601240.

22. Finn RS, Qin S, Ikeda M, Galle PR, Ducreux M, Kim TY, et al. Atezolizumab plus Bevacizumab in Unresectable Hepatocellular Carcinoma. N Engl J Med. 2020;382(20):1894-905.

23. Bertuccio P, Malvezzi M, Carioli G, Hashim D, Boffetta P, El-Serag HB, et al. Global trends in mortality from intrahepatic and extrahepatic cholangiocarcinoma. J Hepatol. 2019;71(1):104-14.

24. Khan SA, Tavolari S, Brandi G. Cholangiocarcinoma: Epidemiology and risk factors. Liver Int. 2019;39 Suppl 1:19-31.

25. Razumilava N, Gores GJ. Cholangiocarcinoma. Lancet. 2014;383(9935):2168-79.

26. Labib PL, Goodchild G, Pereira SP. Molecular Pathogenesis of Cholangiocarcinoma. BMC Cancer. 2019;19(1):185.

27. Moazzami B, Majidzadeh AK, Dooghaie-Moghadam A, Eslami P, Razavi-Khorasani N, Iravani S, et al. Cholangiocarcinoma: State of the Art. J Gastrointest Cancer. 2020;51(3):774-81.

28. Darwish Murad S, Kim WR, Harnois DM, Douglas DD, Burton J, Kulik LM, et al. Efficacy of neoadjuvant chemoradiation, followed by liver transplantation, for perihilar cholangiocarcinoma at 12 US centers. Gastroenterology. 2012;143(1):88-98.e3; quiz e14.

29. Darwish Murad S, Kim WR, Therneau T, Gores GJ, Rosen CB, Martenson JA, et al. Predictors of pretransplant dropout and posttransplant recurrence in patients with perihilar cholangiocarcinoma. Hepatology. 2012;56(3):972-81.

30. Mantel HT, Westerkamp AC, Adam R, Bennet WF, Seehofer D, Settmacher U, et al. Strict Selection Alone of Patients Undergoing Liver Transplantation for Hilar Cholangiocarcinoma Is Associated with Improved Survival. PLoS One. 2016;11(6):e0156127.

31. Valle J, Wasan H, Palmer DH, Cunningham D, Anthoney A, Maraveyas A, et al. Cisplatin plus gemcitabine versus gemcitabine for biliary tract cancer. N Engl J Med. 2010;362(14):1273-81.

32. Lamarca A, Palmer DH, Wasan HS, Ross PJ, Ma YT, Arora A, et al. Second-line FOLFOX chemotherapy versus active symptom control for advanced biliary tract cancer (ABC-06): a phase 3, open-label, randomised, controlled trial. Lancet Oncol. 2021;22(5):690-701.

33. Abou-Alfa GK, Sahai V, Hollebecque A, Vaccaro G, Melisi D, Al-Rajabi R, et al. Pemigatinib for previously treated, locally advanced or metastatic cholangiocarcinoma: a multicentre, open-label, phase 2 study. The Lancet Oncology. 2020;21(5):671-84.

34. Hoy SM. Pemigatinib: First Approval. Drugs. 2020;80(9):923-9.

35. Javle M, Roychowdhury S, Kelley RK, Sadeghi S, Macarulla T, Weiss KH, et al. Infigratinib (BGJ398) in previously treated patients with advanced or metastatic cholangiocarcinoma with FGFR2 fusions or rearrangements: mature results from a multicentre, open-label, single-arm, phase 2 study. Lancet Gastroenterol Hepatol. 2021;6(10):803-15.

36. Boilève A, Hilmi M, Gougis P, Cohen R, Rousseau B, Blanc J-F, et al. Triplet combination of durvalumab, tremelimumab, and paclitaxel in biliary tract carcinomas: Safety run-in results of the randomized IMMUNOBIL PRODIGE 57 phase II trial. European Journal of Cancer. 2021;143:55-63.

37. Churi CR, Shroff R, Wang Y, Rashid A, Kang HC, Weatherly J, et al. Mutation profiling in cholangiocarcinoma: prognostic and therapeutic implications. PLoS One. 2014;9(12):e115383.

38. Schulze K, Nault JC, Villanueva A. Genetic profiling of hepatocellular carcinoma using next-generation sequencing. J Hepatol. 2016;65(5):1031-42.

39. Huang A, Yang XR, Chung WY, Dennison AR, Zhou J. Targeted therapy for hepatocellular carcinoma. Signal Transduct Target Ther. 2020;5(1):146.

40. Abou-Alfa GK, Chan SL, Kudo M, Lau G, Kelley RK, Furuse J, et al. Phase 3 randomized, open-label, multicenter study of tremelimumab (T) and durvalumab (D) as first-line therapy in patients (pts) with unresectable hepatocellular carcinoma (uHCC): HIMALAYA. Journal of Clinical Oncology. 2022;40(4_suppl):379-.

41. Wu C-J, Lee P-C, Hung Y-W, Lee C-J, Chi C-T, Lee IC, et al. Lenvatinib plus pembrolizumab for systemic therapy-naïve and -experienced unresectable hepatocellular carcinoma. Cancer Immunology, Immunotherapy. 2022.

42. Zhao Z, Shilatifard A. Epigenetic modifications of histones in cancer. Genome Biology. 2019;20(1):245.

43. Fujisawa T, Filippakopoulos P. Functions of bromodomain-containing proteins and their roles in homeostasis and cancer. Nature Reviews Molecular Cell Biology. 2017;18(4):246-62.

44. Fernandez-Barrena MG, Arechederra M, Colyn L, Berasain C, Avila MA. Epigenetics in hepatocellular carcinoma development and therapy: The tip of the iceberg. JHEP Rep. 2020;2(6):100167.

45. Singh BN, Zhang G, Hwa YL, Li J, Dowdy SC, Jiang SW. Nonhistone protein acetylation as cancer therapy targets. Expert Rev Anticancer Ther. 2010;10(6):935-54.

46. Liu SS, Wu F, Jin YM, Chang WQ, Xu TM. HDAC11: a rising star in epigenetics. Biomed Pharmacother. 2020;131:110607.

47. Bayo J, Fiore EJ, Dominguez LM, Real A, Malvicini M, Rizzo M, et al. A comprehensive study of epigenetic alterations in hepatocellular carcinoma identifies potential therapeutic targets. Journal of Hepatology. 2019;71(1):78-90.

48. Freese K, Seitz T, Dietrich P, Lee SML, Thasler WE, Bosserhoff A, et al. Histone Deacetylase Expressions in Hepatocellular Carcinoma and Functional Effects of Histone Deacetylase Inhibitors on Liver Cancer Cells In Vitro. Cancers (Basel). 2019;11(10).

49. Wu J, Du C, Lv Z, Ding C, Cheng J, Xie H, et al. The up-regulation of histone deacetylase 8 promotes proliferation and inhibits apoptosis in hepatocellular carcinoma. Dig Dis Sci. 2013;58(12):3545-53.

50. Bi L, Ren Y, Feng M, Meng P, Wang Q, Chen W, et al. HDAC11 Regulates Glycolysis through the LKB1/AMPK Signaling Pathway to Maintain Hepatocellular Carcinoma Stemness. Cancer Res. 2021;81(8):2015-28.

51. O'Rourke CJ, Lafuente-Barquero J, Andersen JB. Epigenome Remodeling in Cholangiocarcinoma. Trends Cancer. 2019;5(6):335-50.

52. Serra RW, Fang M, Park SM, Hutchinson L, Green MR. A KRAS-directed transcriptional silencing pathway that mediates the CpG island methylator phenotype. Elife. 2014;3:e02313.

53. Zhu J, Sammons MA, Donahue G, Dou Z, Vedadi M, Getlik M, et al. Gain-of-function p53 mutants co-opt chromatin pathways to drive cancer growth. Nature. 2015;525(7568):206-11.

54. Morine Y, Shimada M, Iwahashi S, Utsunomiya T, Imura S, Ikemoto T, et al. Role of histone deacetylase expression in intrahepatic cholangiocarcinoma. Surgery. 2012;151(3):412-9.

55. Mastoraki A, Schizas D, Charalampakis N, Naar L, Ioannidi M, Tsilimigras D, et al. Contribution of Histone Deacetylases in Prognosis and Therapeutic Management of Cholangiocarcinoma. Mol Diagn Ther. 2020;24(2):175-84.

56. Malone CF, Emerson C, Ingraham R, Barbosa W, Guerra S, Yoon H, et al. mTOR and HDAC Inhibitors Converge on the TXNIP/Thioredoxin Pathway to Cause Catastrophic Oxidative Stress and Regression of RAS-Driven Tumors. Cancer Discov. 2017;7(12):1450-63.

57. Paillas S, Then CK, Kilgas S, Ruan JL, Thompson J, Elliott A, et al. The Histone Deacetylase Inhibitor Romidepsin Spares Normal Tissues While Acting as an Effective Radiosensitizer in Bladder Tumors in Vivo. Int J Radiat Oncol Biol Phys. 2020;107(1):212-21.

58. Connolly RM, Laille E, Vaishampayan U, Chung V, Kelly K, Dowlati A, et al. Phase I and Pharmacokinetic Study of Romidepsin in Patients with Cancer and Hepatic Dysfunction: A National Cancer Institute Organ Dysfunction Working Group Study. Clin Cancer Res. 2020;26(20):5329-37.

59. Takebe N, Beumer JH, Kummar S, Kiesel BF, Dowlati A, O'Sullivan Coyne G, et al. A phase I pharmacokinetic study of belinostat in patients with advanced cancers and varying degrees of liver dysfunction. British Journal of Clinical Pharmacology. 2019;85(11):2499-511.

60. Fukutomi A, Hatake K, Matsui K, Sakajiri S, Hirashima T, Tanii H, et al. A phase I study of oral panobinostat (LBH589) in Japanese patients with advanced solid tumors. Invest New Drugs. 2012;30(3):1096-106.

61. Jones SF, Bendell JC, Infante JR, Spigel DR, Thompson DS, Yardley DA, et al. A phase I study of panobinostat in combination with gemcitabine in the treatment of solid tumors. Clin Adv Hematol Oncol. 2011;9(3):225-30.

62. Blumenschein GR, Jr., Kies MS, Papadimitrakopoulou VA, Lu C, Kumar AJ, Ricker JL, et al. Phase II trial of the histone deacetylase inhibitor vorinostat (Zolinza, suberoylanilide hydroxamic acid, SAHA) in patients with recurrent and/or metastatic head and neck cancer. Invest New Drugs. 2008;26(1):81-7.

63. Giaccone G, Rajan A, Berman A, Kelly RJ, Szabo E, Lopez-Chavez A, et al. Phase II study of belinostat in patients with recurrent or refractory advanced thymic epithelial tumors. J Clin Oncol. 2011;29(15):2052-9.

64. Hainsworth JD, Infante JR, Spigel DR, Arrowsmith ER, Boccia RV, Burris HA. A phase II trial of panobinostat, a histone deacetylase inhibitor, in the treatment of patients with refractory metastatic renal cell carcinoma. Cancer Invest. 2011;29(7):451-5.

65. Haigentz M, Jr., Kim M, Sarta C, Lin J, Keresztes RS, Culliney B, et al. Phase II trial of the histone deacetylase inhibitor romidepsin in patients with recurrent/metastatic head and neck cancer. Oral Oncol. 2012;48(12):1281-8.

66. Di Fazio P, Schneider-Stock R, Neureiter D, Okamoto K, Wissniowski T, Gahr S, et al. The pan-deacetylase inhibitor panobinostat inhibits growth of hepatocellular carcinoma models by alternative pathways of apoptosis. Cell Oncol. 2010;32(4):285-300.

67. Gahr S, Mayr C, Kiesslich T, Illig R, Neureiter D, Alinger B, et al. The pan-deacetylase inhibitor panobinostat affects angiogenesis in hepatocellular carcinoma models via modulation of CTGF expression. Int J Oncol. 2015;47(3):963-70.

68. Yeo W, Chung HC, Chan SL, Wang LZ, Lim R, Picus J, et al. Epigenetic therapy using belinostat for patients with unresectable hepatocellular carcinoma: a multicenter phase I/II study with biomarker and pharmacokinetic analysis of tumors from patients in the Mayo Phase II Consortium and the Cancer Therapeutics Research Group. J Clin Oncol. 2012;30(27):3361-7.

69. Asgar MA, Senawong G, Sripa B, Senawong T. Synergistic anticancer effects of cisplatin and histone deacetylase inhibitors (SAHA and TSA) on cholangiocarcinoma cell lines. Int J Oncol. 2016;48(1):409-20.

70. Baradari V, Höpfner M, Huether A, Schuppan D, Scherübl H. Histone deacetylase inhibitor MS-275 alone or combined with bortezomib or sorafenib exhibits strong antiproliferative action in human cholangiocarcinoma cells. World J Gastroenterol. 2007;13(33):4458-66.

71. Yin Y, Zhang M, Dorfman RG, Li Y, Zhao Z, Pan Y, et al. Histone deacetylase 3 overexpression in human cholangiocarcinoma and promotion of cell growth via apoptosis inhibition. Cell Death Dis. 2017;8(6):e2856.

72. Dizon DS, Blessing JA, Penson RT, Drake RD, Walker JL, Johnston CM, et al. A phase II evaluation of belinostat and carboplatin in the treatment of recurrent or persistent platinum-resistant ovarian, fallopian tube, or primary peritoneal carcinoma: a Gynecologic Oncology Group study. Gynecol Oncol. 2012;125(2):367-71.

73. Bitzer M, Horger M, Giannini EG, Ganten TM, Worns MA, Siveke JT, et al. Resminostat plus sorafenib as second-line therapy of advanced hepatocellular carcinoma - The SHELTER study. J Hepatol. 2016;65(2):280-8.

74. Streubel G, Schrepfer S, Kallus H, Parnitzke U, Wulff T, Hermann F, et al. Histone deacetylase inhibitor resminostat in combination with sorafenib counteracts platelet-mediated pro-tumoral effects in hepatocellular carcinoma. Scientific Reports. 2021;11(1):9587.

75. Zhang G, Park MA, Mitchell C, Hamed H, Rahmani M, Martin AP, et al. Vorinostat and sorafenib synergistically kill tumor cells via FLIP suppression and CD95 activation. Clin Cancer Res. 2008;14(17):5385-99.

76. Lachenmayer A, Toffanin S, Cabellos L, Alsinet C, Hoshida Y, Villanueva A, et al. Combination therapy for hepatocellular carcinoma: additive preclinical efficacy of the HDAC inhibitor panobinostat with sorafenib. J Hepatol. 2012;56(6):1343-50.

77. Borea PA, Gessi S, Merighi S, Vincenzi F, Varani K. Pharmacology of Adenosine Receptors: The State of the Art. Physiol Rev. 2018;98(3):1591-625.

78. Gorain B, Choudhury H, Yee GS, Bhattamisra SK. Adenosine Receptors as Novel Targets for the Treatment of Various Cancers. Curr Pharm Des. 2019;25(26):2828-41.

79. Borea PA, Gessi S, Merighi S, Varani K. Adenosine as a Multi-Signalling Guardian Angel in Human Diseases: When, Where and How Does it Exert its Protective Effects? Trends Pharmacol Sci. 2016;37(6):419-34.

80. Wang P, Jia J, Zhang D. Purinergic signalling in liver diseases: Pathological functions and therapeutic opportunities. JHEP Rep. 2020;2(6):100165.

81. Kazemi MH, Raoofi Mohseni S, Hojjat-Farsangi M, Anvari E, Ghalamfarsa G, Mohammadi H, et al. Adenosine and adenosine receptors in the immunopathogenesis and treatment of cancer. J Cell Physiol. 2018;233(3):2032-57.

82. Boison D, Yegutkin GG. Adenosine Metabolism: Emerging Concepts for Cancer Therapy. Cancer Cell. 2019;36(6):582-96.

83. Merighi S, Benini A, Mirandola P, Gessi S, Varani K, Leung E, et al. A3 adenosine receptor activation inhibits cell proliferation via phosphatidylinositol 3-kinase/Akt-dependent inhibition of the extracellular signal-regulated kinase 1/2 phosphorylation in A375 human melanoma cells. J Biol Chem. 2005;280(20):19516-26.

84. Borea PA, Varani K, Vincenzi F, Baraldi PG, Tabrizi MA, Merighi S, et al. The A3 adenosine receptor: history and perspectives. Pharmacol Rev. 2015;67(1):74-102.

85. Bar-Yehuda S, Stemmer SM, Madi L, Castel D, Ochaion A, Cohen S, et al. The A3 adenosine receptor agonist CF102 induces apoptosis of hepatocellular carcinoma via de-regulation of the Wnt and NF-kappaB signal transduction pathways. Int J Oncol. 2008;33(2):287-95.

86. Mailavaram RP, Al-Attraqchi OHA, Kar S, Ghosh S. Current Status in the Design and Development of Agonists and Antagonists of Adenosine A3 Receptor as Potential Therapeutic Agents. Curr Pharm Des. 2019;25(25):2772-87.

87. Merighi S, Battistello E, Giacomelli L, Varani K, Vincenzi F, Borea PA, et al. Targeting A3 and A2A adenosine receptors in the fight against cancer. Expert Opin Ther Targets. 2019;23(8):669-78.

88. Cheong SL, Federico S, Venkatesan G, Mandel AL, Shao YM, Moro S, et al. The A3 adenosine receptor as multifaceted therapeutic target: pharmacology, medicinal chemistry, and in silico approaches. Med Res Rev. 2013;33(2):235-335.

89. Bar-Yehuda S, Barer F, Volfsson L, Fishman P. Resistance of muscle to tumor metastases: a role for a3 adenosine receptor agonists. Neoplasia. 2001;3(2):125-31.

90. Varani K, Maniero S, Vincenzi F, Targa M, Stefanelli A, Maniscalco P, et al. A(3) receptors are overexpressed in pleura from patients with mesothelioma and reduce cell growth via Akt/nuclear factor-kappaB pathway. Am J Respir Crit Care Med. 2011;183(4):522-30.

91. Morello S, Petrella A, Festa M, Popolo A, Monaco M, Vuttariello E, et al. Cl-IB-MECA inhibits human thyroid cancer cell proliferation independently of A3 adenosine receptor activation. Cancer Biol Ther. 2008;7(2):278-84.

92. Madi L, Ochaion A, Rath-Wolfson L, Bar-Yehuda S, Erlanger A, Ohana G, et al. The A3 adenosine receptor is highly expressed in tumor versus normal cells: potential target for tumor growth inhibition. Clin Cancer Res. 2004;10(13):4472-9.

93. Gessi S, Cattabriga E, Avitabile A, Gafa R, Lanza G, Cavazzini L, et al. Elevated expression of A3 adenosine receptors in human colorectal cancer is reflected in peripheral blood cells. Clin Cancer Res. 2004;10(17):5895-901.

94. Ohana G, Cohen S, Rath-Wolfson L, Fishman P. A3 adenosine receptor agonist, CF102, protects against hepatic ischemia/reperfusion injury following partial hepatectomy. Mol Med Rep. 2016;14(5):4335-41.

95. Safadi R, Braun M, Francis A, Milgrom Y, Massarwa M, Hakimian D, et al. Randomised clinical trial: A phase 2 double-blind study of namodenoson in non-alcoholic fatty liver disease and steatohepatitis. Aliment Pharmacol Ther. 2021;54(11-12):1405-15.

96. Stemmer SM, Manojlovic NS, Marinca MV, Petrov P, Cherciu N, Ganea D, et al. Namodenoson in Advanced Hepatocellular Carcinoma and Child-Pugh B Cirrhosis: Randomized Placebo-Controlled Clinical Trial. Cancers (Basel). 2021;13(2).

97. Yothaisong S, Dokduang H, Techasen A, Namwat N, Yongvanit P, Bhudhisawasdi V, et al. Increased activation of PI3K/AKT signaling pathway is associated with cholangiocarcinoma metastasis and PI3K/mTOR inhibition presents a possible therapeutic strategy. Tumour Biol. 2013;34(6):3637-48.

98. Mroweh M, Roth G, Decaens T, Marche PN, Lerat H, Macek Jílková Z. Targeting Akt in Hepatocellular Carcinoma and Its Tumor Microenvironment. Int J Mol Sci. 2021;22(4).

99. Boyault S, Rickman DS, de Reynies A, Balabaud C, Rebouissou S, Jeannot E, et al. Transcriptome classification of HCC is related to gene alterations and to new therapeutic targets. Hepatology. 2007;45(1):42-52.

100. Zhou L, Huang Y, Li J, Wang Z. The mTOR pathway is associated with the poor prognosis of human hepatocellular carcinoma. Med Oncol. 2010;27(2):255-61.

101. Dimri M, Satyanarayana A. Molecular Signaling Pathways and Therapeutic Targets in Hepatocellular Carcinoma. Cancers (Basel). 2020;12(2).

102. Chen C, Wang G. Mechanisms of hepatocellular carcinoma and challenges and opportunities for molecular targeted therapy. World J Hepatol. 2015;7(15):1964-70.

103. Whittaker S, Marais R, Zhu AX. The role of signaling pathways in the development and treatment of hepatocellular carcinoma. Oncogene. 2010;29(36):4989-5005.

104. Kunter I, Erdal E, Nart D, Yilmaz F, Karademir S, Sagol O, et al. Active form of AKT controls cell proliferation and response to apoptosis in hepatocellular carcinoma. Oncol Rep. 2014;31(2):573-80.

105. Dokduang H, Juntana S, Techasen A, Namwat N, Yongvanit P, Khuntikeo N, et al. Survey of activated kinase proteins reveals potential targets for cholangiocarcinoma treatment. Tumour biology : the journal of the International Society for Oncodevelopmental Biology and Medicine. 2013;34.

106. Bozic I, Reiter JG, Allen B, Antal T, Chatterjee K, Shah P, et al. Evolutionary dynamics of cancer in response to targeted combination therapy. Elife. 2013;2:e00747.

107. Hu TH, Huang CC, Lin PR, Chang HW, Ger LP, Lin YW, et al. Expression and prognostic role of tumor suppressor gene PTEN/MMAC1/TEP1 in hepatocellular carcinoma. Cancer. 2003;97(8):1929-40.

108. Yeung Y, Lau DK, Chionh F, Tran H, Tse JWT, Weickhardt AJ, et al. K-Ras mutation and amplification status is predictive of resistance and high basal pAKT is predictive of sensitivity to everolimus in biliary tract cancer cell lines. Molecular oncology. 2017;11(9):1130-42.

109. Baserga R, Morrione A. Differentiation and malignant transformation: two roads diverged in a wood. J Cell Biochem. 1999;Suppl 32-33:68-75.

110. Dian MJ, Li J, Zhang XL, Li ZJ, Zhou Y, Zhou W, et al. MST4 negatively regulates the EMT, invasion and metastasis of HCC cells by inactivating PI3K/AKT/Snail1 axis. J Cancer. 2021;12(15):4463-77.

111. Zhangyuan G, Wang F, Zhang H, Jiang R, Tao X, Yu D, et al. VersicanV1 promotes proliferation and metastasis of hepatocellular carcinoma through the activation of EGFR-PI3K-AKT pathway. Oncogene. 2020;39(6):1213-30.

112. Zhou S, Qu KL, Li JA, Chen SL, Zhang YG, Zhu C, et al. YY1 activates EMI2 and promotes the progression of cholangiocarcinoma through the PI3K/Akt signaling axis. Cancer Cell Int. 2021;21(1):699.

113. Hao X, Zhang Y, Lu Y, Han G, Rong D, Sun G, et al. STK39 enhances the progression of Cholangiocarcinoma via PI3K/AKT pathway. iScience. 2021;24(11):103223.

114. Dong J, Zhai B, Sun W, Hu F, Cheng H, Xu J. Activation of phosphatidylinositol 3-kinase/AKT/snail signaling pathway contributes to epithelial-mesenchymal transition-induced multi-drug resistance to sorafenib in hepatocellular carcinoma cells. PLoS One. 2017;12(9):e0185088.

115. Chen KF, Chen HL, Tai WT, Feng WC, Hsu CH, Chen PJ, et al. Activation of phosphatidylinositol 3-kinase/Akt signaling pathway mediates acquired resistance to sorafenib in hepatocellular carcinoma cells. J Pharmacol Exp Ther. 2011;337(1):155-61.

116. Liang S, Guo H, Ma K, Li X, Wu D, Wang Y, et al. A PLCB1-PI3K-AKT Signaling Axis Activates EMT to Promote Cholangiocarcinoma Progression. Cancer Res. 2021;81(23):5889-903.

117. Efeyan A, Sabatini DM. mTOR and cancer: many loops in one pathway. Curr Opin Cell Biol. 2010;22(2):169-76.

118. Sun SY, Rosenberg LM, Wang X, Zhou Z, Yue P, Fu H, et al. Activation of Akt and eIF4E survival pathways by rapamycin-mediated mammalian target of rapamycin inhibition. Cancer Res. 2005;65(16):7052-8.

119. Song M, Bode AM, Dong Z, Lee M-H. AKT as a Therapeutic Target for Cancer. Cancer Research. 2019;79(6):1019-31.

120. Konopleva MY, Walter RB, Faderl SH, Jabbour EJ, Zeng Z, Borthakur G, et al. Preclinical and early clinical evaluation of the oral AKT inhibitor, MK-2206, for the treatment of acute myelogenous leukemia. Clin Cancer Res. 2014;20(8):2226-35.

121. Ma BB, Goh BC, Lim WT, Hui EP, Tan EH, Lopes Gde L, et al. Multicenter phase II study of the AKT inhibitor MK-2206 in recurrent or metastatic nasopharyngeal carcinoma from patients in the mayo phase II consortium and the cancer therapeutics research group (MC1079). Invest New Drugs. 2015;33(4):985-91.

122. Ramanathan RK, McDonough SL, Kennecke HF, Iqbal S, Baranda JC, Seery TE, et al. Phase 2 study of MK-2206, an allosteric inhibitor of AKT, as second-line therapy for advanced gastric and gastroesophageal junction cancer: A SWOG cooperative group trial (S1005). Cancer. 2015;121(13):2193-7.

123. Xing Y, Lin NU, Maurer MA, Chen H, Mahvash A, Sahin A, et al. Phase II trial of AKT inhibitor MK-2206 in patients with advanced breast cancer who have tumors with PIK3CA or AKT mutations, and/or PTEN loss/PTEN mutation. Breast Cancer Res. 2019;21(1):78.

124. Doi T, Tamura K, Tanabe Y, Yonemori K, Yoshino T, Fuse N, et al. Phase 1 pharmacokinetic study of the oral pan-AKT inhibitor MK-2206 in Japanese patients with advanced solid tumors. Cancer Chemother Pharmacol. 2015;76(2):409-16.

125. Oki Y, Fanale MA, Romaguera JE, Fayad L, Fowler N, Copeland ARM, et al. Phase II Study of an AKT Inhibitor MK2206 in Patients with Relapsed or Refractory Lymphoma. Blood. 2014;124(21):3093-.

126. Fraveto A, Cardinale V, Bragazzi MC, Giuliante F, De Rose AM, Grazi GL, et al. Sensitivity of Human Intrahepatic Cholangiocarcinoma Subtypes to Chemotherapeutics and Molecular Targeted Agents: A Study on Primary Cell Cultures. PLoS One. 2015;10(11):e0142124.

127. Wilson JM, Kunnimalaiyaan S, Gamblin TC, Kunnimalaiyaan M. MK2206 inhibits hepatocellular carcinoma cellular proliferation via induction of apoptosis and cell cycle arrest. J Surg Res. 2014;191(2):280-5.

128. Wilson JM, Kunnimalaiyaan S, Kunnimalaiyaan M, Gamblin TC. Inhibition of the AKT pathway in cholangiocarcinoma by MK2206 reduces cellular viability via induction of apoptosis. Cancer Cell Int. 2015;15(1):13-.

129. Ahn DH, Li J, Wei L, Doyle A, Marshall JL, Schaaf LJ, et al. Results of an abbreviated phase-II study with the Akt Inhibitor MK-2206 in Patients with Advanced Biliary Cancer. Scientific reports. 2015;5:12122-.

130. Buglio D, Lemoine M, Estrella J, Neelapu SS, Davis RE, Doyle L, et al. The Allosteric AKT Inhibitor MK-2206 Demonstrates Potent Antiproliferative Activity in Lymphoma Cells and Synergizes with the HDAC Inhibitor Vorinostat. Blood. 2011;118(21):3729-.

131. Ischenko I, Petrenko O, Hayman MJ. A MEK/PI3K/HDAC inhibitor combination therapy for KRAS mutant pancreatic cancer cells. Oncotarget. 2015;6(18):15814-27.

132. Ellis L, Ku SY, Ramakrishnan S, Lasorsa E, Azabdaftari G, Godoy A, et al. Combinatorial antitumor effect of HDAC and the PI3K-Akt-mTOR pathway inhibition in a Pten defecient model of prostate cancer. Oncotarget. 2013;4(12):2225-36.

133. Janku F, Kaseb AO, Tsimberidou AM, Wolff RA, Kurzrock R. Identification of novel therapeutic targets in the PI3K/AKT/mTOR pathway in hepatocellular carcinoma using targeted next generation sequencing. Oncotarget. 2014;5(10):3012-22.

134. Nuciforo S, Fofana I, Matter MS, Blumer T, Calabrese D, Boldanova T, et al. Organoid Models of Human Liver Cancers Derived from Tumor Needle Biopsies. Cell Rep. 2018;24(5):1363-76.

135. Tao YF, Pang L, Du XJ, Sun LC, Hu SY, Lu J, et al. Differential mRNA expression levels of human histone-modifying enzymes in normal karyotype B cell pediatric acute lymphoblastic leukemia. Int J Mol Sci. 2013;14(2):3376-94.

136. Xiao PF, Tao YF, Hu SY, Cao L, Lu J, Wang J, et al. mRNA expression profiling of histone modifying enzymes in pediatric acute monoblastic leukemia. Pharmazie. 2017;72(3):177-86.

137. Skehan P, Storeng R, Scudiero D, Monks A, McMahon J, Vistica D, et al. New colorimetric cytotoxicity assay for anticancer-drug screening. J Natl Cancer Inst. 1990;82(13):1107-12.

138. Livak KJ, Schmittgen TD. Analysis of relative gene expression data using real-time quantitative PCR and the 2(-Delta Delta C(T)) Method. Methods. 2001;25(4):402-8.

139. Higuchi R, Fockler C, Dollinger G, Watson R. Kinetic PCR analysis: real-time monitoring of DNA amplification reactions. Biotechnology (N Y). 1993;11(9):1026-30.

140. Berenbaum MC. What is synergy? Pharmacol Rev. 1989;41(2):93-141.

141. Ianevski A, He L, Aittokallio T, Tang J. SynergyFinder: a web application for analyzing drug combination dose-response matrix data. Bioinformatics. 2017;33(15):2413-5.

142. Ianevski A, Giri AK, Aittokallio T. SynergyFinder 2.0: visual analytics of multi-drug combination synergies. Nucleic Acids Res. 2020;48(W1):W488-W93.

143. Ianevski A, He L, Aittokallio T, Tang J. SynergyFinder: a web application for analyzing drug combination dose–response matrix data. Bioinformatics. 2017;33(15):2413-5.

144. Yadav B, Wennerberg K, Aittokallio T, Tang J. Searching for Drug Synergy in Complex Dose-Response Landscapes Using an Interaction Potency Model. Computational and structural biotechnology journal. 2015;13:504-13.

145. Bosmuller H, Pfefferle V, Bittar Z, Scheble V, Horger M, Sipos B, et al. Microvessel density and angiogenesis in primary hepatic malignancies: Differential expression of CD31 and VEGFR-2 in hepatocellular carcinoma and intrahepatic cholangiocarcinoma. Pathol Res Pract. 2018;214(8):1136-41.

146. Mamanova L, Turner DJ. Low-bias, strand-specific transcriptome Illumina sequencing by on-flowcell reverse transcription (FRT-seq). Nature Protocols. 2011;6(11):1736-47.

147. Ewels P, Magnusson M, Lundin S, Käller M. MultiQC: summarize analysis results for multiple tools and samples in a single report. Bioinformatics (Oxford, England). 2016;32(19):3047-8.

148. Andrews S. FastQC: A Quality Control Tool for High Throughput Sequence Data. Available online at: http://wwwbioinformaticsbabrahamacuk/projects/fastqc/. 2010.

149. Krueger F. Trim Galore: A Wrapper Tool Around Cutadapt and Fastqc to Consistently Apply Quality and Adapter Trimming to Fastq Files, with Some Extra Functionality for Mspi-Digested Rrbs-Type (Reduced Representation Bisufite-Seq) Libraries. URL Http://Www Bioinformatics Babraham Ac Uk/Projects/Trim_galore/(Date of Access: 28/04/2016). 2012.

150. Dobin A, Davis CA, Schlesinger F, Drenkow J, Zaleski C, Jha S, et al. STAR: ultrafast universal RNA-seq aligner. Bioinformatics. 2013;29(1):15-21.

151. Wang L, Wang S, Li W. RSeQC: quality control of RNA-seq experiments. Bioinformatics. 2012;28(16):2184-5.

152. Liao Y, Smyth GK, Shi W. featureCounts: an efficient general purpose program for assigning sequence reads to genomic features. Bioinformatics. 2014;30(7):923-30.

153. Love M, Anders S, Huber W, editors. Differential analysis of count data@ the DESeq 2 package2014.

154. Korotkevich G, Sukhov V, Budin N, Shpak B, Artyomov MN, Sergushichev A. Fast gene set enrichment analysis. bioRxiv. 2021:060012.

155. Liberzon A, Birger C, Thorvaldsdóttir H, Ghandi M, Mesirov JP, Tamayo P. The Molecular Signatures Database (MSigDB) hallmark gene set collection. Cell Syst. 2015;1(6):417-25.

156. Reimand J, Arak T, Adler P, Kolberg L, Reisberg S, Peterson H, et al. g:Profiler—a web server for functional interpretation of gene lists (2016 update). Nucleic Acids Research. 2016;44(W1):W83-W9.

157. Reimand J, Kull M, Peterson H, Hansen J, Vilo J. g:Profiler--a web-based toolset for functional profiling of gene lists from large-scale experiments. Nucleic Acids Res. 2007;35(Web Server issue):W193-200.

158. Collado-Torres L, Nellore A, Kammers K, Ellis SE, Taub MA, Hansen KD, et al. Reproducible RNA-seq analysis using recount2. Nat Biotechnol. 2017;35(4):319-21.

159. Benjamini Y, Hochberg Y. Controlling the False Discovery Rate - a Practical and Powerful Approach to Multiple Testing. J R Stat Soc B. 1995;57(1):289-300.

160. Li H-D. GTFtools: a Python package for analyzing various modes of gene models. bioRxiv. 2018:263517.

161. Bar-Yehuda S, Stemmer SM, Madi L, Castel D, Ochaion A, Cohen S, et al. The A3 adenosine receptor agonist CF102 induces apoptosis of hepatocellular carcinoma via de-regulation of the Wnt and NF-κB signal transduction pathways. Int J Oncol. 2008;33(2):287-95.

162. Vichai V, Kirtikara K. Sulforhodamine B colorimetric assay for cytotoxicity screening. Nat Protoc. 2006;1(3):1112-6.

163. Subramanian A, Tamayo P, Mootha VK, Mukherjee S, Ebert BL, Gillette MA, et al. Gene set enrichment analysis: A knowledge-based approach for interpreting genome-wide expression profiles. Proceedings of the National Academy of Sciences. 2005;102(43):15545.

164. Senese S, Zaragoza K, Minardi S, Muradore I, Ronzoni S, Passafaro A, et al. Role for histone deacetylase 1 in human tumor cell proliferation. Mol Cell Biol. 2007;27(13):4784-95.

165. Pasini D, Bracken AP, Hansen JB, Capillo M, Helin K. The polycomb group protein Suz12 is required for embryonic stem cell differentiation. Mol Cell Biol. 2007;27(10):3769-79.

166. Lu C, Han HD, Mangala LS, Ali-Fehmi R, Newton CS, Ozbun L, et al. Regulation of tumor angiogenesis by EZH2. Cancer Cell. 2010;18(2):185-97.

167. Gordon SW, McGuire WP, 3rd, Shafer DA, Sterling RK, Lee HM, Matherly SC, et al. Phase I Study of Sorafenib and Vorinostat in Advanced Hepatocellular Carcinoma. Am J Clin Oncol. 2019;42(8):649-54.

168. Afaloniati H, Angelopoulou K, Giakoustidis A, Hardas A, Pseftogas A, Makedou K, et al. HDAC1/2 Inhibitor Romidepsin Suppresses DEN-Induced Hepatocellular Carcinogenesis in Mice. Onco Targets Ther. 2020;13:5575-88.

169. Wang JH, Lee EJ, Ji M, Park SM. HDAC inhibitors, trichostatin A and valproic acid, increase E-cadherin and vimentin expression but inhibit migration and invasion of cholangiocarcinoma cells. Oncol Rep. 2018;40(1):346-54.

170. Wang Z, Cui X, Hao G, He J. Aberrant expression of PI3K/AKT signaling is involved in apoptosis resistance of hepatocellular carcinoma. Open Life Sci. 2021;16(1):1037-44.

171. Pant K, Peixoto E, Richard S, Gradilone SA. Role of Histone Deacetylases in Carcinogenesis: Potential Role in Cholangiocarcinoma. Cells. 2020;9(3):780.

172. Garmpis N, Damaskos C, Garmpi A, Georgakopoulou VE, Sarantis P, Antoniou EA, et al. Histone Deacetylase Inhibitors in the Treatment of Hepatocellular Carcinoma: Current Evidence and Future Opportunities. J Pers Med. 2021;11(3):223.

173. Duriez PJ, Shah GM. Cleavage of poly(ADP-ribose) polymerase: a sensitive parameter to study cell death. Biochem Cell Biol. 1997;75(4):337-49.

174. Fishman P. Drugs Targeting the A3 Adenosine Receptor: Human Clinical Study Data. Molecules. 2022;27(12):3680.

175. Mazziotta C, Rotondo JC, Lanzillotti C, Campione G, Martini F, Tognon M. Cancer biology and molecular genetics of A3 adenosine receptor. Oncogene. 2022;41(3):301-8.

176. Fishman P, Bar-Yehuda S, Liang BT, Jacobson KA. Pharmacological and therapeutic effects of A3 adenosine receptor agonists. Drug Discov Today. 2012;17(7-8):359-66.

177. Gessi S, Merighi S, Varani K, Leung E, Mac Lennan S, Borea PA. The A3 adenosine receptor: an enigmatic player in cell biology. Pharmacol Ther. 2008;117(1):123-40.

178. Madi L, Cohen S, Ochayin A, Bar-Yehuda S, Barer F, Fishman P. Overexpression of A3 adenosine receptor in peripheral blood mononuclear cells in rheumatoid arthritis: involvement of nuclear factor-kappaB in mediating receptor level. J Rheumatol. 2007;34(1):20-6.

179. Stemmer SM, Benjaminov O, Medalia G, Ciuraru NB, Silverman MH, Bar-Yehuda S, et al. CF102 for the treatment of hepatocellular carcinoma: a phase I/II, open-label, dose-escalation study. Oncologist. 2013;18(1):25-6.

180. Hirschfield H, Bian CB, Higashi T, Nakagawa S, Zeleke TZ, Nair VD, et al. In vitro modeling of hepatocellular carcinoma molecular subtypes for anti-cancer drug assessment. Exp Mol Med. 2018;50(1):e419.

181. Vicent S, Lieshout R, Saborowski A, Verstegen MMA, Raggi C, Recalcati S, et al. Experimental models to unravel the molecular pathogenesis, cell of origin and stem cell properties of cholangiocarcinoma. Liver Int. 2019;39 Suppl 1:79-97.

182. Jacobson KA, Kim HS, Ravi G, Kim S-K, Lee K, Chen A, et al. Engineering of A3 adenosine and P2Y nucleotide receptors and their ligands. Drug Development Research. 2003;58(4):330-9.

183. Gao Z-G, Jacobson KA. Translocation of arrestin induced by human A(3) adenosine receptor ligands in an engineered cell line: comparison with G protein-dependent pathways. Pharmacol Res. 2008;57(4):303-11.

184. Marwein S, Mishra B, De UC, Acharya PC. Recent Progress of Adenosine Receptor Modulators in the Development of Anticancer Chemotherapeutic Agents. Curr Pharm Des. 2019;25(26):2842-58.

185. Cariello NF, Romach EH, Colton HM, Ni H, Yoon L, Falls JG, et al. Gene Expression Profiling of the PPAR-alpha Agonist Ciprofibrate in the Cynomolgus Monkey Liver. Toxicological Sciences. 2005;88(1):250-64.

186. Coral S, Covre A, Jmg Nicolay H, Parisi G, Rizzo A, Colizzi F, et al. Epigenetic remodelling of gene expression profiles of neoplastic and normal tissues:

immunotherapeutic implications. British Journal of Cancer. 2012;107(7):1116-24.

187. Derocq J-M, Jbilo O, Bouaboula M, Ségui M, Clère C, Casellas P. Genomic and Functional Changes Induced by the Activation of the Peripheral Cannabinoid Receptor CB2 in the Promyelocytic Cells HL-60: POSSIBLE INVOLVEMENT OF THE CB2 RECEPTOR IN CELL DIFFERENTIATION*. Journal of Biological Chemistry. 2000;275(21):15621-8.

188. Miranda Furtado CL, Dos Santos Luciano MC, Silva Santos RD, Furtado GP, Moraes MO, Pessoa C. Epidrugs: targeting epigenetic marks in cancer treatment. Epigenetics. 2019;14(12):1164-76.

189. Jacobson KA, Tosh DK, Jain S, Gao Z-G. Historical and Current Adenosine Receptor Agonists in Preclinical and Clinical Development. Frontiers in Cellular Neuroscience. 2019;13.

190. Roderburg C, Özdirik B, Wree A, Demir M, Tacke F. Systemic treatment of hepatocellular carcinoma: from sorafenib to combination therapies. Hepatic Oncology. 2020;7(2):HEP20.

191. Romero D. Combination set to transform HCC therapy. Nature Reviews Clinical Oncology. 2020;17(7):389-.

192. Porter RJ, Murray GI, McLean MH. Current concepts in tumour-derived organoids. British Journal of Cancer. 2020;123(8):1209-18.

193. Wang H, Brown PC, Chow ECY, Ewart L, Ferguson SS, Fitzpatrick S, et al. 3D cell culture models: Drug pharmacokinetics, safety assessment, and regulatory consideration. Clinical and Translational Science. 2021;14(5):1659-80.

194. van de Wetering M, Francies Hayley E, Francis Joshua M, Bounova G, Iorio F, Pronk A, et al. Prospective Derivation of a Living Organoid Biobank of Colorectal Cancer Patients. Cell. 2015;161(4):933-45.

195. Weeber F, Ooft SN, Dijkstra KK, Voest EE. Tumor Organoids as a Pre-clinical Cancer Model for Drug Discovery. Cell Chemical Biology. 2017;24(9):1092-100.

196. Wensink GE, Elias SG, Mullenders J, Koopman M, Boj SF, Kranenburg OW, et al. Patient-derived organoids as a predictive biomarker for treatment response in cancer patients. npj Precision Oncology. 2021;5(1):30.

197. Bartfeld S, Clevers H. Stem cell-derived organoids and their application for medical research and patient treatment. Journal of Molecular Medicine. 2017;95(7):729-38.

198. Narasimhan V, Wright JA, Churchill M, Wang T, Rosati R, Lannagan TRM, et al. Medium-throughput Drug Screening of Patient-derived Organoids from Colorectal Peritoneal Metastases to Direct Personalized Therapy. Clinical Cancer Research. 2020;26(14):3662-70.

199. Ooft SN, Weeber F, Dijkstra KK, McLean CM, Kaing S, van Werkhoven E, et al. Patient-derived organoids can predict response to chemotherapy in metastatic colorectal cancer patients. Science Translational Medicine. 2019;11(513):eaay2574.

200. Klein E, Hau A-C, Oudin A, Golebiewska A, Niclou SP. Glioblastoma Organoids: Pre-Clinical Applications and Challenges in the Context of Immunotherapy. Front Oncol. 2020;10(2755).

201. Zhang R, Guo T, Ji L, Yin Y, Feng S, Lu W, et al. Development and Application of Patient-Derived Cancer Organoidsin Clinical Management of Gastrointestinal Cancer: A State-of-the-Art Review. Front Oncol. 2021;11.

202. Herath NI, Leggett BA, MacDonald GA. Review of genetic and epigenetic alterations in hepatocarcinogenesis. J Gastroenterol Hepatol. 2006;21(1 Pt 1):15-21.

203. Mann DA. Epigenetics in liver disease. Hepatology. 2014;60(4):1418-25.

204. Morel D, Jeffery D, Aspeslagh S, Almouzni G, Postel-Vinay S. Combining epigenetic drugs with other therapies for solid tumours - past lessons and future promise. Nat Rev Clin Oncol. 2020;17(2):91-107.

205. El Khatib M, Bozko P, Palagani V, Malek NP, Wilkens L, Plentz RR. Activation of Notch signaling is required for cholangiocarcinoma progression and is enhanced by inactivation of p53 in vivo. PLoS One. 2013;8(10):e77433.

206. Gui L, Zhang S, Xu Y, Zhang H, Zhu Y, Kong L. UBE2S promotes cell chemoresistance through PTEN-AKT signaling in hepatocellular carcinoma. Cell Death Discovery. 2021;7(1):357.

207. Sweeney C, Bracarda S, Sternberg CN, Chi KN, Olmos D, Sandhu S, et al. Ipatasertib plus abiraterone and prednisolone in metastatic castration-resistant prostate cancer (IPATential150): a multicentre, randomised, double-blind, phase 3 trial. The Lancet. 2021;398(10295):131-42.

208. Kaley TJ, Panageas KS, Pentsova EI, Mellinghoff IK, Nolan C, Gavrilovic I, et al. Phase I clinical trial of temsirolimus and perifosine for recurrent glioblastoma. Annals of Clinical and Translational Neurology. 2020;7(4):429-36.

209. Kushner BH, Cheung NV, Modak S, Becher OJ, Basu EM, Roberts SS, et al. A phase I/Ib trial targeting the Pi3k/Akt pathway using perifosine: Long-term progression-free survival of patients with resistant neuroblastoma. Int J Cancer. 2017;140(2):480-4.

210. Liu R, Liu D, Xing M. The Akt inhibitor MK2206 synergizes, but perifosine antagonizes, the BRAF(V600E) inhibitor PLX4032 and the MEK1/2 inhibitor AZD6244 in the inhibition of thyroid cancer cells. J Clin Endocrinol Metab. 2012;97(2):E173-E82.

211. Hanahan D, Weinberg RA. Hallmarks of cancer: the next generation. Cell. 2011;144(5):646-74.

212. Chen L, Kang QH, Chen Y, Zhang YH, Li Q, Xie SQ, et al. Distinct roles of Akt1 in regulating proliferation, migration and invasion in HepG2 and HCT 116 cells. Oncol Rep. 2014;31(2):737-44.

213. Nguyen RY, Xiao H, Gong X, Arroyo A, Cabral AT, Fischer TT, et al. Cytoskeletal dynamics regulates stromal invasion behavior of distinct liver cancer subtypes. Communications Biology. 2022;5(1):202.

214. Leelawat K, Leelawat S, Tepaksorn P, Rattanasinganchan P, Leungchaweng A, Tohtong R, et al. Involvement of c-Met/hepatocyte growth factor pathway in cholangiocarcinoma cell invasion and its therapeutic inhibition with small interfering RNA specific for c-Met. J Surg Res. 2006;136(1):78-84.

215. Puthdee N, Sriswasdi S, Pisitkun T, Ratanasirintrawoot S, Israsena N, Tangkijvanich P. The LIN28B/TGF-β/TGFBI feedback loop promotes cell

migration and tumour initiation potential in cholangiocarcinoma. Cancer Gene Therapy. 2022;29(5):445-55.

216. Wang H, Rao B, Lou J, Li J, Liu Z, Li A, et al. The Function of the HGF/c-Met Axis in Hepatocellular Carcinoma. Front Cell Dev Biol. 2020;8:55.

217. Noh JH, Bae HJ, Eun JW, Shen Q, Park SJ, Kim HS, et al. HDAC2 Provides a Critical Support to Malignant Progression of Hepatocellular Carcinoma through Feedback Control of mTORC1 and AKT. Cancer Research. 2014;74(6):1728-38.

218. Zhang P, Zhu X, Wu Y, Hu R, Li D, Du J, et al. Histone deacetylase inhibitors reduce WB-F344 oval cell viability and migration capability by suppressing AKT/mTOR signaling in vitro. Archives of Biochemistry and Biophysics. 2016;590:1-9.

219. Hua H, Zhang H, Chen J, Wang J, Liu J, Jiang Y. Targeting Akt in cancer for precision therapy. Journal of Hematology & Oncology. 2021;14(1):128.

220. Manning BD, Toker A. AKT/PKB Signaling: Navigating the Network. Cell. 2017;169(3):381-405.

221. Butler DE, Marlein C, Walker HF, Frame FM, Mann VM, Simms MS, et al. Inhibition of the PI3K/AKT/mTOR pathway activates autophagy and compensatory Ras/Raf/MEK/ERK signalling in prostate cancer. Oncotarget. 2017;8(34):56698-713.

222. Cao Z, Liao Q, Su M, Huang K, Jin J, Cao D. AKT and ERK dual inhibitors: The way forward? Cancer Letters. 2019;459:30-40.

223. Zhai B, Zhang X, Sun B, Cao L, Zhao L, Li J, et al. MK2206 overcomes the resistance of human liver cancer stem cells to sorafenib by inhibition of pAkt and upregulation of pERK. Tumor Biology. 2016;37(6):8047-55.

224. García-Martínez JM, Alessi DR. mTOR complex 2 (mTORC2) controls hydrophobic motif phosphorylation and activation of serum- and glucocorticoid-induced protein kinase 1 (SGK1). Biochem J. 2008;416(3):375-85.

225. Castel P, Ellis H, Bago R, Toska E, Razavi P, Carmona FJ, et al. PDK1-SGK1 Signaling Sustains AKT-Independent mTORC1 Activation and Confers Resistance to PI3Kα Inhibition. Cancer Cell. 2016;30(2):229-42.

226. Toska E, Castel P, Chhangawala S, Arruabarrena-Aristorena A, Chan C, Hristidis VC, et al. PI3K Inhibition Activates SGK1 via a Feedback Loop to Promote Chromatin-Based Regulation of ER-Dependent Gene Expression. Cell Reports. 2019;27(1):294-306.e5.

227. Chen J, Luo B, Wen S, Pi R. Discovery of a novel rhein-SAHA hybrid as a multi-targeted anti-glioblastoma drug. Investigational New Drugs. 2020;38(3):755-64.

228. Chung EJ, Sung YK, Farooq M, Kim Y, Im S, Tak WY, et al. Gene expression profile analysis in human hepatocellular carcinoma by cDNA microarray. Mol Cells. 2002;14(3):382-7.

229. Sang Y, Kong P, Zhang S, Zhang L, Cao Y, Duan X, et al. SGK1 in Human Cancer: Emerging Roles and Mechanisms. Front Oncol. 2020;10:608722.

230. Cicenas J, Meskinyte-Kausiliene E, Jukna V, Rimkus A, Simkus J, Soderholm D. SGK1 in Cancer: Biomarker and Drug Target. Cancers (Basel). 2022;14(10).

231. Zhou Z, Cong L, Cong X. Patient-Derived Organoids in Precision Medicine: Drug Screening, Organoid-on-a-Chip and Living Organoid Biobank. Front Oncol. 2021;11.

6. Appendix

6.1. List of Figures

6.2. List of Tables

6.3. Summary of Abbreviations

%	Procent	DNMT	DNA methyltransferase
µl	Microliter	**DTT**	Dithiothreitol
5mc	5-methylcytosine	**BSA**	Bovine serum albumin
AC	adenyl cyclase	**ctrl.**	Control
ADORA1	Adenosine receptor 1	**DMEM**	Dulbecco's modified Eagle Medium
ADORA2A	Adenosine receptor 2A	**eCCA**	extrahepatic cholangiocarcinoma
ADORA2B	Adenosine receptor 2B	**ECL**	Electrochemiluminescence
ADORA3	Adenosine receptor 3	**ECOG**	Eastern Cooperative Oncology Group score
ADP	Adenosine diphosphate	**EDTA**	Ethylenediaminetetraacetic acid
AFP	Alpha fetoprotein	**ENT**	Equilibrative nucleoside transporter
AKT	Protein kinase B	**FDA**	Food and drug administration
AKTi	Protein kinase B inhibitor	**FGF**	Fibroblast growth factor
AMP	Adenosinemonophosphate	**FGFR2**	Fibroblast growth factor receptor 2
ASDR	Age standardizes death rate	**Fig.**	Figure
ATCC	American type culture collection	**FOLFOX**	Folonic acid, fluorouracil and oxaliplatin
ATP	Adenosine triphosphate	**FOXE3**	Forkhead Box E3
BET	Bromodomain and extra terminal domain	**GF**	Growth Factor
DE	Differetially Expresed	**GSEA**	Gene Set Enrichment Analysis
BRD	Bromodomain	**GPCR**	G-protein coupled receptor
cAMP	cyclic AMP	**GSK**	glycogen synthase kinase
CCND1	Cyclin D1	**H**	Histone
CDKL2	Cyclin dependent kinase like 2	**h**	hour
CDKN2A	Cyclin-dependent kinase inhibitor 2A	**HBV**	Hepatitis-B-Virus oder Virushepatitis B
cDNA	complementary DNA	**HGF**	hepatocyte growth factor
CNT	concentrative nucleoside transporter	**HNF1A**	Hepatocyte nuclear factor 1 homeobox A
COX2	Cyclo-oxygenase-2	**HRP**	Horseradish peroxidase
CP	Child-Pugh	**iCCA**	intrahepatic cholangiocarcinoma
CTLA-4	T-lymphocyte protein 4	**IDH1/2**	isocitrate dehydrogenase 1/2
CTNNB1	Catenin Beta 1	**IGF**	Insulin-like growth factor
dCCA	distal cholangiocarcinoma	**JAK**	Janus Kinase
IKK	IkappaB kinase;	**KMT2**	Lysine methyltranferase 2
DMSO	Dimethylsulfoxid	**mM**	millimolar
ERK-1/2	extracellular signalregulatedkinase ½	**mTOR**	mammalian target of rapamycin
G	gram	**mTORC1/2**	mammalian target of rapamycin complex 1/2
DE	Differential Expression	Mg	Milligram
DNA	Desoxyribonucleic acid	miRNA	Micro RNA
ml	Milliliter	**RNAi**	RNA interference
mM	Millimolar	**RPS6K**	Ribosomal Protein S6 kinase
mRNA	messenger RNA	**RTK**	Receptor tyrosine kinase
Myc	Proto-Oncogene	**RTKi**	Receptor tyrosine kinase inhibitor
Namo.	Namodenoson	**S / Ser**	Serine

NAFLD	Nonalcoholic fatty liver desease		
NASH	Nonalcoholic steatohepatitis	**SAH**	S-adenosylhomocysteine
NF-κB	nuclear factor kappa of activated B-cells	**SGK1**	Serum/Glucocorticoid Regulated Kinase 1
nM	nanomolar	**siRNA**	small interfering RNA
p53/TP53	Tumorsuppressor gen p53	**SRB**	Sulforhodamin B
PBS	phosphate buffered saline	**SIRT**	Sirtuin
PI3K	Phosphatidylinositol-3-Kinase	**SOX2**	SRY-Box transcription factor 2
PIK3CA	phosphatidylinositol-4,5-bisphosphate 3-kinase	**STAT**	Signal transducer ad activators of transcription
PTEN	phosphatase and tensin homolog	**SVR**	sustained virologic response
RNA	Ribonucleic acid	**T / Thr**	threonine
Ng	nanogram	**TACE**	transarterielle Chemoembolisation
OS	overall survival	**TBS**	Tris-buffered saline
		TPM	Transcript per Million
PBS	phosphate buffered saline	**TBST**	Tris-bufered saline with Tween20
pCCA	peripheral cholangiocarcinoma	**TCA**	trichloro-acid
PCR	Polymerase chain reaction	**CCA**	Cholangiocellular carcinoma
PD-L1	Programmed cell death 1 ligand 1	**TCGA**	The Cancer Genome Atlas
PDGF	platelet derived growth factor	**TERT**	Telomerase reverse transcriptase
PDK1	phosphoinositide-dependent kinase 1	**TGF**	Transforming growth factor
PDT	photodynamic therapy	**TFBS**	Transcription factor binding sites
PFS	Progression free survival		
PH	Pleckstrin homology		
PHLPP2	PH domain leucine-rich-repeat-containing protein phosphatase 2A		
PKA	Protein kinase A		
PLC	phospholipase C		
PLC	Primary Liver Cancer		
PLD	phospholipase D		
PP2A	Phosphatases like protein phosphatase 2A		
PVDF	Polyvinylidene difluoride		
qPCR	quantitative PCR		
RAF	Rapidly Accelerated Fibrosarcoma		
RAS	Rat Sarcoma		
RB1	Retinoblastoma (transcriptional Corepressor 1)		

6.4. Acknowledgements

The presented work would not have been possible without the help and support of many people around me:

First and foremost, I would like to thank Prof. Dr. Michael Bitzer for giving me the opportunity to join his lab and work on this project. Thank you, a lot, for your scientific supervision, your support, patience, and your guidance throughout the last years. Thanks as well for the time dedicated for correcting the manuscript.

I wish to acknowledge Prof. Dr. Alfred Nordheim for accepting the supervision of this work and for the time dedicated for correcting the manuscript and for all invaluable advice during our committee meetings.

I thank Dr. Daniel Dauch for his co-supervision on this project. Thank you for the expertise you shared with me.

I would like to thank Christine Geisler for the help in the lab and for making me master this challenging path of my scientific career with a friend.

A special thanks to Inga Leske for the help in the lab.

I deeply thank all members of the Bitzer lab, the Lauer lab, the Malek lab and the former Plentz lab for their technical and personal assistance. A special thanks to Dr. Bozko. Thank you for all the discussions in the hallway.

Especially I want to express my deepest gratitude to Prof. Dr. Markus Heim for allowing me to be part of his lab and to learn all I know about organoids. I am thankful for Dr. Sandro Nuciforo and the Heim lab for their support and the friendly atmosphere during my time in Basel.

I am thankful to all collaborators for the great teamwork.

I thank my Parents for their tireless fight for their children. Pour papa sans toi je ne saurais jamais arrivé ou je suis aujourd'hui. Mama tu nous a laissé partir pour un meilleur avenir.

I am grateful for my parents in law Heidi and Winni. Thank you for your support in the last years. To all my family and friends, thank you for keeping me grounded during the good and bad times.

Finally, I am immensely grateful for my husband Philip. Philip this work is also dedicated to you. Thank you for your unlimited support and your constant encouragement. You are the best partner and friend I could have wished for through all the difficulties and during this entire process.

6.5. Submissions / Publications

Submitted Manuscript:

Louise Kaldjob-Heinrich, Sandro Nuciforo, Steffen Lemke, Aaron Stahl, Stefan Czemmel, Sepideh Babaei, Irene Gonzalez-Menendez, Nisar P. Malek, Veit Scheble, Sven Nahnsen, Manfred Claassen, Markus Templin, Hans Bösmüller, Markus Heim, Daniel Dauch, Michael Bitzer: ADENOSINE RECEPTOR 3 STIMULATION IN LIVER CANCER MODULATES EPIGENETIC MECHANISMS AND ENHANCES ANTITUMOR EFFECTS OF HISTONE DEACETYLASE INHIBITORS
(2022)

6.6. Selbstständigkeitserklärung

Ich, Louise Gaelle Kaldjob-Heinrich, geboren am 09.10.1988 in Duala, Kamerun erkläre hiermit, dass ich:

- die eingereichte Dissertation selbstständig und ohne Benutzung unerlaubte Hilfsmittel angefertigt habe.
- Außer den im Schrifttumsverzeichnis angegebenen Quellen und Hilfsmittel keine weiteren benutzt und alle Stellen, die aus dem Schrifttum ganz oder annährend entnommen sind, als solche kenntlich gemacht und einzeln unter Angabe der Quelle gekennzeichnet habe.
- keine entgeltliche Hilfe von Vermittlungs- bzw. Beratungsdiensten in Anspruch genommen habe.
- die Arbeit noch keine andere Stelle im In- noch im Ausland in gleicher oder ähnlicher Form zur Prüfung vorgelegt habe.